ARL-TR-7337 ● JULY 2015

US Army Research Laboratory

Simulation Analysis of a Strip Dipole Excited Electromagnetic Band-Gap (EBG) Structure

by Seth A McCormick and William O Coburn

NOTICES

Disclaimers

The findings in this report are not to be construed as an official Department of the Army position unless so designated by other authorized documents.

Citation of manufacturer's or trade names does not constitute an official endorsement or approval of the use thereof.

Destroy this report when it is no longer needed. Do not return it to the originator.

ARL-TR-7337 ● JULY 2015

US Army Research Laboratory

Simulation Analysis of a Strip Dipole Excited Electromagnetic Band-Gap (EBG) Structure

by Seth A McCormick and William O Coburn
Sensors and Electron Devices Directorate, ARL

REPORT DOCUMENTATION PAGE

Form Approved
OMB No. 0704-0188

1. REPORT DATE *(DD-MM-YYYY)*	2. REPORT TYPE	3. DATES COVERED (From - To)
July 2015	Final	11/2014 – 4/2015

4. TITLE AND SUBTITLE
Simulation Analysis of a Strip Dipole Excited Electromagnetic Band-Gap (EBG) Structure

5a. CONTRACT NUMBER

5b. GRANT NUMBER

5c. PROGRAM ELEMENT NUMBER

6. AUTHOR(S)
Seth A McCormick and William O Coburn

5d. PROJECT NUMBER
R.0010490.24

5e. TASK NUMBER

5f. WORK UNIT NUMBER

7. PERFORMING ORGANIZATION NAME(S) AND ADDRESS(ES)
US Army Research Laboratory
ATTN: RDRL-SER-M
2800 Powder Mill Road
Adelphi, MD 20783-1138

8. PERFORMING ORGANIZATION REPORT NUMBER
ARL-TR-7337

9. SPONSORING/MONITORING AGENCY NAME(S) AND ADDRESS(ES)

10. SPONSOR/MONITOR'S ACRONYM(S)

11. SPONSOR/MONITOR'S REPORT NUMBER(S)

12. DISTRIBUTION/AVAILABILITY STATEMENT
Approved for public release; distribution unlimited.

13. SUPPLEMENTARY NOTES

14. ABSTRACT
The design of an Electromagnetic Band-Gap (EBG) for a particular antenna application is described and investigated in detail through simulation. The typical design parameters, analytical models, and numerical methods for EBG design are summarized. Discussion is provided on interpretation of the EBG reflection coefficient phase for antenna applications and on the range of the EBG bandwidth. It is determined for antenna applications that the reflection phase and current design methods may be misleading. Instead, it is opinioned and shown that the phase of the scattered near fields at the EBG surface is more applicable to characterizing the EBG for antenna applications. A new set of design parameters is presented that will allow an engineer to design an EBG with relative accuracy. The impact of a dielectric substrate, vias, and number of unit cells is also demonstrated.

15. SUBJECT TERMS
electromagnetic band gap, strip dipole, reflection phase, vias, near fields, bandwidth, EBG analysis, EBG design procedure

16. SECURITY CLASSIFICATION OF:			17. LIMITATION OF ABSTRACT	18. NUMBER OF PAGES	19a. NAME OF RESPONSIBLE PERSON
a. REPORT	b. ABSTRACT	c. THIS PAGE	UU	138	Seth A McCormick
Unclassified	Unclassified	Unclassified			19b. TELEPHONE NUMBER (Include area code) (301) 394-2706

Standard Form 298 (Rev. 8/98)
Prescribed by ANSI Std. Z39.18

Contents

List of Figures

List of Tables

INTENTIONALLY LEFT BLANK.

1. Introduction

The electromagnetic band-gap (EBG) structure is a type of grounded textured surface ". . .that prohibit the propagation of electromagnetic waves in a certain frequency band for certain arrival angles and polarization. . .". (Volakis 2007) EBG structures have attractive features in transmission with application to frequency selective surfaces (FSS) and in reflection with application for high-impedance surfaces (HIS) where the fields are reflected in-phase. The in-phase reflection property of the EBG structure is often used to create low-profile antennas with improved gain and in some cases, bandwidth. Another typical antenna application involves reducing coupling between antenna elements such as patch arrays by mitigating surface waves. The EBG structure is typically designed using either predefined parameters found in the literature or through the use of an analytical method such as a circuit model (CM) or transmission line model (TLM) and in some other cases through optimization software. Image Theory (IT) can also be used to analytically or numerically calculate the source antenna impedance (typically a dipole) and the radiation pattern of the source antenna and its image. The EBG structure is often modeled numerically by assuming an infinite structure through periodic boundary conditions (PBC) and excited with a plane wave for either normal or off axis incidence. Whether designed analytically or numerically, an EBG is characterized primarily by the phase of the reflection coefficient, φ, which also defines the operational bandwidth of the EBG structure.

What bounds the EBG bandwidth appears in the literature to be debatable as there have been found at least 3 different bandwidth ranges: $\varphi = 0° \pm 90°$, (Sievenpiper et al. 1999) $0° \pm 45°$, (Hansen 2002) and $90° \pm 45°$. (Volakis 2007; Yang and Rahmat-Samii 2003). It is also debatable as to whether or not vias are necessary for an EBG structure. From the literature, via usage depends on the EBG surface impedance since when positive (inductive) only transverse magnetic (TM) surface waves are supported and when negative (capacitive) only transverse electric (TE) surface waves are supported (McMichael et al. 2013). So for antenna applications the use of vias in EBG construction will depend on the type of antenna considered as the antenna may or may not excite TM surface waves on the EBG surface. While vias are most likely found in microelectronic circuits as either interconnects between layered printed circuit boards or as a means to attenuate surface waves that propagate along a dielectric boundary, for antenna structures (and EBGs in particular) vias are often used for the latter method but introduce increased costs and greater construction difficulty. For this report, which investigates EBG excitation by a thin strip dipole, no TM surface modes exist so vias should not be required; nevertheless, the impact of including vias will be investigated.

The goal of this technical report is to summarize typical EBG design methods and to take a more comprehensive look into how an EBG effects the performance of a particular antenna, in this case a resonant thin strip dipole, so as to offer a more complete characterization of an EBG for a specific antenna application rather than just relying on φ. The CM, TLM, IT and PBC methods are summarized to maintain consistency with what has already been done by other authors while additional analysis through simulated near field (NF) results for the electric field (E-field) at the EBG surface and through simulated excitation using a thin strip dipole near the EBG surface will offer a more in depth look into the EBG effect on a specific antenna. The end result will offer a more insightful characterization of the EBG structure for excitation by a strip dipole and conclude with a design procedure that does not rely solely upon numerical solutions and optimizations.

This report first summarizes in Section 2, the typical analytical and numerical models that are used in EBG design. Then in Section 3, using the EBG parameters referenced in the antenna engineering handbook (Volakis 2007) (whose source material can be found in Yang and Rahmat-Samii [2003] the simulation software FEKO (www.feko.info), using the method of moments (MoM), is validated as an accurate full-wave simulation tool for EBG design. Following up in Section 4, another EBG, which does not possess vias or a dielectric substrate and still functions as desired, is studied both analytically and numerically. The simulated impact that this EBG has on a strip dipole's performance is presented in detail to highlight key effects that are not accounted for in typical EBG analytical or numerical models. Section 5 highlights the application and accuracy of the analytical and numerical models from Section 2 for antenna applications, comments on the operational bandwidth of an EBG for a specific antenna application including comparing the bandwidth estimations from the numerical and analytical models, and then presents antenna specific physical parameters for EBG design. The goal is to allow the antenna engineer to design an EBG for a specific antenna while only having to simulate the antenna-EBG structure, instead of approximating the EBG characteristics, which are often not sufficient for antennas.

In Section 6, a design example for a strip dipole excited EBG structure for the Wi-Fi band 802.11g/n centered at 2.437 GHz is presented to demonstrate the antenna specific EBG design parameters. The effect of including a dielectric substrate and vias on the strip dipole's performance in the presence of the EBG is also investigated. This technical report concludes with a detailed summary highlighting the major points on modeling methods, EBG effects on the strip dipole, design procedure, physical design parameters, and effects from dielectric substrates and vias.

2. Analytical and Numerical Models for EBG Design

In this section, the current popular analytical and numerical models for EBG design are summarized, and an additional numerical method that simulates an antenna dependent finite EBG is introduced. Typical EBG analytical models are approximate but allow rapid initial design and some insight into the critical EBG design parameters. The commonly used numerical model can be more accurate for complex structures but requires an infinitely periodic 2-D structure. Optimization techniques for a finite structure are popular, but a simple method to find a first order approximate design is still desired. Regardless, the typical analytical and numerical models offer only general insight into the most basic EBG features, which may be fine for most applications, but for antenna applications, a model that offers specific insight for a given antenna geometry is required (antenna dependent model).

2.1 The Circuit Model Approach

The first analytical approach is the circuit model that is constructed from the viewpoint of induced current flow on the EBG surface using either a plane wave or antenna as the source. The CM models the EBG surface as a frequency dependent reactive impedance in the form of an LC tank circuit that represent unit cells. The CM for an EBG unit cell that does not contain vias consists of a parallel combination of a gap capacitance between the patches, C_g, shunt capacitance between the parallel plates of the unit cell, C_s, and shunt inductance between the parallel plates of the unit cell, L_s. The CM for an EBG that does contain vias is a parallel combination of a gap capacitance between patches and shunt inductance between the parallel plates (Fig. 1). It is worth noting that there can be found, in the literature, variations for approximating the gap capacitance, while the equation for the shunt inductance is still the same regardless if vias are included or not.

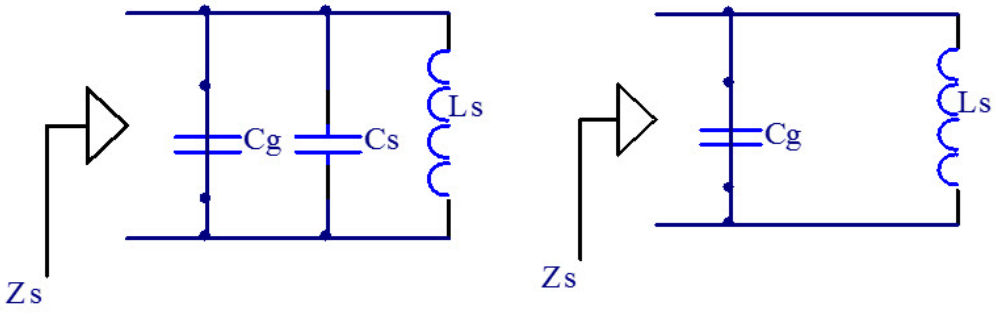

Fig. 1 The EBG circuit model without vias (left) and with vias (right)

Determining where the inductance comes from is simple. When considering 2 parallel conducting plates, the inductance between the plates is solved directly

from the magnetic flux, Ψ_m, and flux linkage, Λ. Because the geometry results in only 1 turn, the flux and flux linkage are equal, $N = 1$, making the inductance easily calculated (Fig. 2a). With the inclusion of a gap to split the top conducting plate into smaller plates, only the unit cells of the EBG can be considered analogous to the parallel conducting plates. The gap width causes a small mismatch in size between the 2 plates, but if the gap width is much smaller than the patch width, the inductance between the unit cell plates is approximately the same as the 2 parallel plates. When a via is included in the EBG unit cell, an induced current that flows through the via creates a magnetic field between the plates (Fig. 2b). When a via is not included, a displacement current exists between the plates that creates the magnetic field, per Ampere's Law (Fig. 2c).

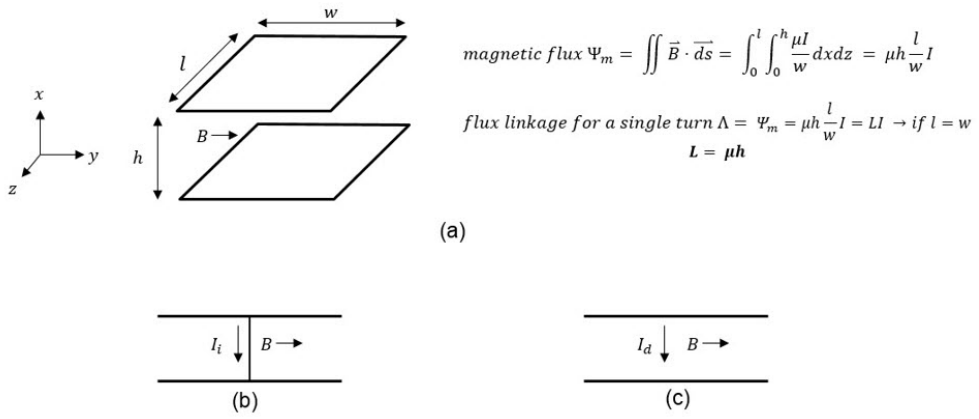

Fig. 2 a) The inductance between 2 parallel rectangular conducting plates. b) The EBG unit cell with via. Induced current, I_i, through the via creates a magnetic field between the plates per Ampere's Law. c) The EBG unit cell without via. Displacement current, I_d, between the plates creates a magnetic field per Ampere's Law.

As said, the inductance in both cases is solved in the same manner as the parallel plate example (Sievenpiper et al. 1999; Hayt and Buck 2006).

$$L_s = \mu_0 \mu_r h \, . \tag{1}$$

Where *h* is the thickness of the EBG unit cell and the relative permeability, $\mu_r = 1$, since only dielectric substrates are considered in this report. Note that because the patterned EBG surface is backed by a ground plane, this thickness, *h*, is a critical design parameter. The shunt capacitance, C_s, is approximated using the well-known equation for the capacitance between 2 parallel conducting plates, and the gap capacitance, C_g, can be approximated using the also well-known 2-wire method (Hayt and Buck 2006).

$$C_s = \frac{\varepsilon_0 \varepsilon_r A}{h}. \quad (2)$$

$$C_g = \frac{2\pi\varepsilon_0 \varepsilon_{eff} W}{\cosh^{-1}\frac{g}{a}}. \quad (3)$$

The variable A is the patch area; W is the patch width; g is the gap between patches; $\varepsilon_{eff} = \frac{\varepsilon_r+1}{2}$ is the effective permittivity for a substrate having relative permittivity, ε_r; and a is the effective radius that is defined as one-half the thickness of the patch (0.02 mm for 1 oz copper). The EBG surface impedance, Z_s, and reflection coefficient (which describes the impedance mismatch between the surface impedance and free space impedance), Γ, can be calculated using Eqs. 4 and 5 (Palreddy and Zaghloul 2013).

$$Z_s = \frac{j\omega L_s}{1-\left(\frac{\omega}{\omega_0}\right)^2}. \quad (4)$$

$$\Gamma = \frac{Z_s - \eta_0}{Z_s + \eta_0}. \quad (5)$$

Where η_0 is the intrinsic impedance of free space and is equal to 120π. The resonant frequency, ω_0, that corresponds to the zero-phase crossing in φ can be calculated for either an EBG with vias (Eq. 6) or an EBG without vias (Eq. 7). Including the vias in the EBG simply shorts the shunt capacitance in the CM.

$$\omega_0 = \frac{1}{\sqrt{L_s(C_g + C_s)}}. \quad (6)$$

$$\omega_0 = \frac{1}{\sqrt{L_s C_g}}. \quad (7)$$

The gap capacitance, C_g, can also be approximated from the E-fields within the EBG gaps (field-gap) using Eq. 8 (Azad and Ali 2008). An advantage to Eq. 8 over Eq. 3 is that Eq. 8 does not require an approximation of the patch thickness when simulations use zero thickness perfect electric conductors (PEC); however, both equations are inaccurate and unstable under the conditions of extremely thin-gaps as the inverse hyperbolic cosine function grows very large (Eq. 8) or very small (Eq. 3). Equation 8 will give a larger value for the gap capacitance than Eq. 3.

$$C_g = \frac{W\varepsilon_0(1+\varepsilon_r)}{\pi}\cosh^{-1}\frac{W+g}{g} \quad (8)$$

The CM is the preferred analytical model for EBG design as it is simple and can be used to determine the dimensions for the patches, gap, and thickness while it can also easily estimate the operational bandwidth of the EBG. However, using a circuit model for any structure assumes that the elements that make up the lumped capacitances and inductances are much smaller than a wavelength so that the circuit does not radiate, and in the case of the shunt inductance and shunt capacitance, both equations assume that the fields are entirely contained within the unit cell. A particular issue with the inductance is that the equation is derived assuming a constant and uniform current distribution on the parallel plates of the unit cell, but for antenna applications, the current distribution in any 1 unit cell (much less the EBG as a whole) is not necessarily constant and uniform. The circuit model also assumes that the structure is uniform and semi-infinite, which is also not true in practice.

These simplifications will reduce the accuracy of the analytical model, but it will not prevent a good first start using the CM to characterize the EBG *reflection-phase*. Even with the simplification of an electromagnetically complicated structure by the CM, the greatest advantage is that this analytical model can give a reasonable estimation on the EBG operational bandwidth assuming it is an impedance bandwidth and using well-known equations. At normal incidence, the 3-dB impedance bandwidth occurs when $Z_s = \eta_0 = 120\pi$ (free space impedance) or:

$$\omega^2 = \frac{1}{LC} + \frac{1}{2\eta_0^2 C^2} \pm \frac{1}{\eta_0 C}\sqrt{\frac{1}{LC} + \frac{1}{4\eta_0^2 C^2}}, \tag{9}$$

which can be simplified for typical geometries that have inductances that are a few orders of magnitude larger than the capacitances (causing the second order terms to be very small and negligible)

$$\omega = \omega_0\sqrt{1 \pm \frac{Z_0}{\eta_0}}, \tag{10}$$

where $Z_0\left(= \sqrt{\frac{L}{C}}\right)$ is the characteristic impedance of the LC circuit, ω_0 can be calculated using Eq. 7, and $C = C_g$. It can be further expanded as Z_0 is usually significantly smaller than η_0.

$$\omega = \omega_0\left(1 \pm \frac{1}{2}\frac{Z_0}{\eta_0}\right). \tag{11}$$

Therefore, the 3-dB impedance bandwidth of an EBG can be estimated by:

$$\Delta\omega = \omega_0 \frac{Z_0}{\eta_0}. \tag{12}$$

2.2 The Transmission Line Approach (TLM)

The second analytical approach is the TLM, which computes the EBG impedance from the perspective of an electromagnetic field incident on the EBG surface at some angle θ from the normal. This particular TLM can be found in (Luukkonen et al. 2008), where a 2-wire transmission line matched to free space is terminated by the EBG. The input impedance to the EBG structure, Z_{in}, is a parallel combination of the EBG grid impedance attributed to the textured surface, $Z_{g'}$, and the impedance of a shorted length of transmission line, Z_s, created by the metal-backed dielectric slab, see Fig. 3.

$$Z_{in}^{-1} = Z_{g'}^{-1} + Z_s^{-1}, \tag{13}$$

$Z_{g'}$ and Z_s can be calculated for either a TE or TM-polarized field that is incident at some angle θ from the surface normal.

$$z_{g'}^{TM} = -j\frac{\eta_{eff}}{2\alpha} \tag{14a}$$

$$z_{g'}^{TE} = -j\frac{\eta_{eff}}{2\alpha}\frac{1}{\left(1-\frac{k_0^2\ (\sin\theta)^2}{k_{eff}^2\quad 2}\right)}, \tag{14b}$$

$$\overline{\overline{Z_s}} = j\omega\mu\frac{\tan(\beta h)}{\beta}\left(\overline{\overline{I_t}} - \frac{\boldsymbol{k_t k_t}}{k^2}\right). \tag{15}$$

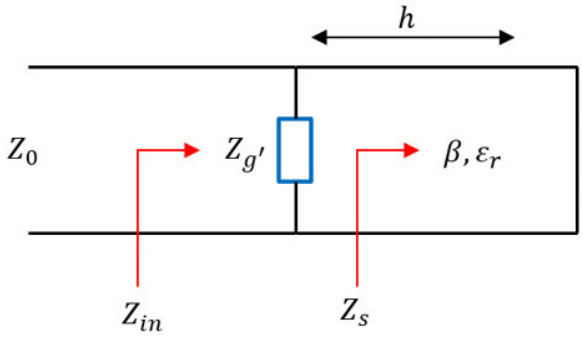

Fig. 3 The transmission line model for an array of patches on top of a metal-backed dielectric slab

Here, the surface impedance Z_s is written in dyadic form, which can be split into 2 separate impedances for the TM and TE cases. The variable η_{eff} is the intrinsic impedance with respect to the effective permittivity, k_{eff} is the effective wave number that accounts for the effect of the substrate on the grid impedance, $\beta = \sqrt{k^2 - k_t^2}$, k_t is the tangential component of the wave number attributed to the incident wave, and k $(= k_0\sqrt{\varepsilon_r})$ is the wave number in the dielectric. The grid parameter, α, in Eqs. 14a and 14b, is dimensionless and can be calculated with the following equation:

$$\alpha = \frac{k_{eff}D}{\pi} \ln\left(\frac{1}{\sin\frac{\pi g}{2D}}\right). \tag{16}$$

The grid parameter characterizes the physical features of the EBG surface and is dependent upon the substrate thickness, *h*, the unit cell periodicity $D = W + g$, and the gap width, *g*. Using Eqs. 13, 14a, and 15, the EBG input impedance for a TM-polarized incident field is found by:

$$Z_{in}^{TM} = \frac{j\omega\mu\frac{\tan(\beta h)}{\beta}(\cos\theta_2)^2}{1-2k_{eff}\alpha\frac{\tan(\beta h)}{\beta}(\cos\theta_2)^2}, \tag{17}$$

and the EBG input impedance for a TE-polarized incident field using Eqs. 13, 14b, and 15 is:

$$Z_{in}^{TE} = \frac{j\omega\mu\frac{\tan(\beta h)}{\beta}}{1-2k_{eff}\alpha\frac{\tan(\beta h)}{\beta}\left(1-\frac{1}{\varepsilon_r+1}(\sin\theta)^2\right)}. \tag{18}$$

The angle θ_2 can be calculated using Snell's law of refraction and the angle of incidence: $\theta_2 = \sin^{-1}\left(\frac{\sin\theta}{\sqrt{\varepsilon_r}}\right)$. The impedance mismatch to free space (reflection coefficient) at the EBG surface can be computed using Eq. 5, 17 or 18, and the

following equations for the free space impedance with incident angle and mode dependency.

$$Z_0^{TM} = \eta_0 \cos\theta \tag{19a}$$

$$Z_0^{TE} = \frac{\eta_0}{\cos\theta}\,. \tag{19b}$$

When considering normal incidence, which will be the focus of this report, the EBG input impedance for both TE and TM-polarized incident fields, Z_{in}, reduces to:

$$Z_{in} = \frac{j\omega\mu_0\frac{\tan(\beta h)}{\beta}}{1-2k_{eff}\alpha\frac{\tan(\beta h)}{\beta}}\,. \tag{20}$$

The TLM can be considered a more accurate representation for the input impedance of a semi-infinite EBG structure. Surface illumination by an electromagnetic wave would be more analogous to a TLM rather than a circuit model; however, the TLM does not account for any mutual coupling that can occur between representative loads (much like the circuit model), and it does not account for any scattering or edge effects that could have an appreciable impact on an antenna's performance (again much like the circuit model). In fact, under small argument conditions, the TLM and CM for all intents and purposes produce the same results.

Under small argument conditions, where the EBG thickness is small and the gap width is much smaller than the unit cell periodicity, the numerator in Eq. 20 reduces to $j\omega\mu_0 h$ and with some simplification, the denominator reduces to $1-\omega^2\left(\frac{D(1+\varepsilon_r)\varepsilon_0}{\pi}\ln\left(\frac{2D}{\pi g}\right)\right)(\mu_0 h)$. Comparing the simplified Eq. 20 with Eqs. 1, 7, and 8 substituted into Eq. 4 shows that both equations are nearly the same.

$$Z_{in} = \frac{j\omega\mu_0 h}{1-\omega^2\left(\frac{D(1+\varepsilon_r)\varepsilon_0}{\pi}\ln\left(\frac{2D}{\pi g}\right)\right)(\mu_0 h)} \approx \frac{j\omega\mu_0 h}{1-\omega^2\left(\frac{W\varepsilon_0(1+\varepsilon_r)}{\pi}\cosh^{-1}\frac{W+g}{g}\right)(\mu_0 h)} \tag{21}$$

Because of the small argument conditions, the unit cell periodicity, D, and the patch width, W, are effectively the same, but the 2 equations differ with the factor of $\frac{2}{\pi}$ in the argument of the natural logarithm for the TLM and the inclusion of an inverse hyperbolic cosine function instead of a logarithmic function in the CM (which will grow faster than the natural logarithm). The similarity between models under small argument conditions is only seen for the case where vias are included. Also, under the small argument conditions, estimating the EBG operational bandwidth with the TLM is estimated the same way as it is done with the CM. When not using small argument conditions and vias, however, a numerical software package must be used to solve the transcendental equation to determine the bandwidth from the TLM based on the desired φ.

2.3 Image Theory Approximation

The last analytical model is image theory, which can be used to represent the EBG structure by an image dipole in the NF of a source dipole (Hansen 2002), see Fig. 4. This model assumes an infinite plane and that the ground plane does not support surface waves. Based on the mutual impedance between the source dipole and its image, an optimum phase difference can be determined to provide the best impedance match to a given feed line impedance (McMichael et al. 2013). The source dipole and its image radiate as a 2 element array so that when in-phase the peak gain is broadside. For radiation into the upper half space at angle θ from broadside, the phase of the image depends on the separation distance according to,

$$\varphi = kd\cos(90 - \theta)\,, \tag{22}$$

where the electrical separation distance, *kd*, would also account for the EBG thickness. With $\frac{\lambda}{2}$ spacing, the array radiates in the end-fire direction when $\varphi = 180°$ (just as for a PEC surface at $\frac{\lambda}{4}$), but for small separation, the progressive phase shift would be adjusted accordingly. In free space with an EBG thickness of $\frac{\lambda}{10}$ the separation distance is $\frac{\lambda}{5}$ so the image dipole should have a phase difference of $\varphi = 72°$ to radiate in the end-fire (upward) direction. This is the phase of the EBG reflection coefficient only for thin EBG structures since the ground plane is at some distance from the source dipole. When the dipole height above the EBG surface is small and the EBG is thick, the reflection coefficient phase could still be near 0° corresponding to the image dipole contribution being in phase at the source position.

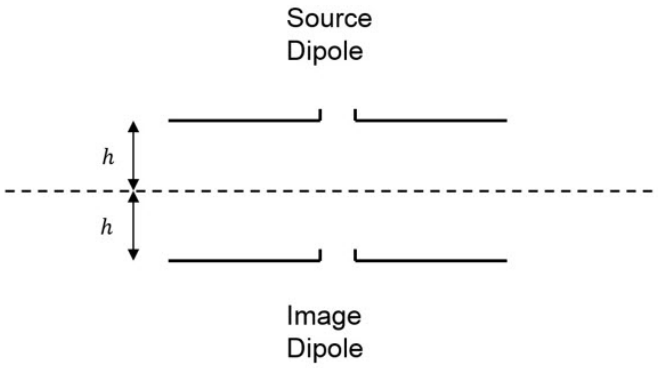

Fig. 4 A source dipole and its image in an infinite ground plane

The IT method can be used to calculate the mutual coupling between the dipole and its image, where the antenna input impedance is modified by the mutual impedance (McMichael 2013; Abedin and Ali 2005).

$$Z_d = Z_{11} + Z_{12}e^{j\Psi}\ , \tag{23}$$

where Ψ is the reflection-phase of the ground plane (for PEC it is 180°). The self and mutual impedance terms can be calculated using the induced EMF method for the dipole and its image (Abedin and Ali 2005). It is matched when the input impedance equals the source impedance. The phase of the mutual impedance can be determined to enforce this condition, but this matching condition is at a single frequency and may not result in the desired radiation pattern. Different EBG structures could give a desired frequency dependent reflection-phase but not all would enhance the antenna performance. For a given dipole height and EBG thickness, this model can provide insight into whether the EBG performs like a pseudo-artificial magnetic conductor (AMC) or pseudo-PEC according to whether the input resistance is increased or decreased, respectively. This report will not include EBG analysis using IT, but it can be useful to optimize the impedance matching for a give antenna.

2.4 The Periodic Boundary Condition (PBC) Approach

PBC is the numerical method by which the phase of an EBG's reflection coefficient can be determined. It is the most commonly used method to simulate an EBG without an antenna. This numerical solution requires creating a unit cell of the EBG and placing it within a periodic boundary that will replicate the structure to make it infinite in 2 directions. A plane wave is then launched either on the surface normal or off axis in order to calculate the transmission and reflection coefficients associated with the EBG structure's impedance mismatch to free space. For antenna applications, limiting the plane wave to normal incidence is often sufficient for simulating the EBG without an antenna present. This method (just as with the analytical approaches) uses phase of the reflection coefficient, with reference to the EBG surface, as the only means to characterize the EBG's operational bandwidth, which is defined over some range of frequencies that result in the reflected fields being close to or in phase with the source fields.

Traditionally, the bandwidth of the EBG is centered at the zero-phase crossing of the reflection coefficient (Sievenpiper et al. 1999) where the surface is said to act like a perfect magnetic conductor (PMC) but as mentioned, what bounds this center frequency is debatable. PBC does not offer any insight into this ambiguity to help distinguish what range of frequencies to use. It has other drawbacks as well. PBC is based on a plane wave approximation and does not include edge effects, so the reflection coefficient phase determined by PBC is not quite the same as for an EBG in the NF of an antenna. However, a major advantage to this method is reduced

simulation time and computational resources, which can be desirable or even critical to the antenna engineer.

2.5 The Phase of the Near Electric Field (NEF)

A particular issue with the analytical models and PBC is that each one characterizes an EBG's performance in terms of the phase of the reflection coefficient. It is of particular issue because the reflection coefficient assumes far-field phenomenon, which means that the phase of interest and the actual phase of the EBG structure in the NF of an antenna may not be the same. Another issue is that the analytical models and PBC study an infinite structure devoid of any antenna dependency. Studying an infinite structure may be misleading as it may not accurately describe the characteristics of the fabricated EBG structure, and not including an antenna in the simulations will neglect the impact that the antenna's physical geometry will have on the phase of the reflected fields.

This report includes an additional analysis technique that examines the phase of the scattered dominate near E-field component at the EBG surface (in the case of a dipole that means the component that lies parallel to the dipole). This method still requires the use of a plane wave excitation with the appropriate polarization just like PBC, but its advantage is that a finite structure is studied rather than an infinite structure. The antenna of interest (terminated with a 50-Ω load) can also be included with the EBG structure for the NF analysis, which makes the analysis dependent on both the antenna and the EBG, giving more insight into the EBG for a particular antenna. Studying the phase of the scattered NEF is also more analogous to the actual physical implementation of the EBG for antenna applications, as the EBG is in the antenna NF. This method is called the NEF method and will be used in comparison to the other methods for characterizing EBG surfaces. From this point onward, the phases determined by the PBC and NEF with dipole simulations will be differentiated and referred to as the reflection-phase and *scattered-phase*, respectively.

3. Analysis of an EBG from the Antenna Engineering Handbook

The fourth edition of the antenna engineering handbook (Volakis 2007), presents design parameters for 2 different EBGs. The first is what is most commonly seen in the literature where the patch widths are an order of magnitude smaller than the free space wavelength. The other EBG in the antenna engineering handbook, however, stood out in that the patch widths where larger than typical (a factor of 8 times smaller than the free space wavelength) and the operational bandwidth for best impedance matching for a given antenna was stated to be within the phase

regime of 90° ± 45° (Volakis 2007; Yang and Rahmat-Samii 2003). This bandwidth was determined by varying the length of a given dipole so as to determine where its return loss resulted in a impedance match to 50 Ω. The range of frequencies over which these dipoles were matched would correspond to the above mentioned phase regime. The literature also presented 3 E-plane and H-plane patterns corresponding to 3 dipoles selected from the test group that were matched over the desired frequency range.

3.1 Numerical Model in FEKO

Expecting that FEKO would reproduce the published results reasonably, the EBG from the antenna engineering handbook was reconstructed using the same design parameters and excited with the 3 dipoles whose patterns are shown in the text and source material. The referenced EBG is designed for the free space wavelength of λ_{12GHz}. The square patches have a width $0.12\lambda_{12GHz}$. The gap width separating the patches is $0.02\lambda_{12GHz}$, and the EBG thickness is $0.04\lambda_{12GHz}$. The EBG includes vias with a radius of $0.005\lambda_{12GHz}$ and has a dielectric substrate with a relative dielectric constant of 2.2. Note that in terms of the wavelength in the dielectric substrate, $\lambda_d = \frac{\lambda}{\sqrt{\varepsilon_r}}$, the patch widths are actually larger relative to the width determined from the free space wavelength, $0.18\lambda_d = \frac{\lambda_d}{5.6}$. The lengths of the 3 dipoles are $0.48\lambda_{12GHz}$, $0.36\lambda_{12GHz}$, and $0.32\lambda_{12GHz}$ and all have the same radius as the vias.

The dipoles are placed at a height of $0.02\lambda_{12GHz}$ above the surface of the EBG. The vias were simulated using cuboids to save computational time and resources. It was determined that the use of PEC cylinders did not have any appreciable effect upon the simulation results. It should also be noted that the EBG used in the following sections is the full 8 unit cell times 8 unit cell model (Fig. 5) rather than truncated to $\lambda_{12GHz} \times \lambda_{12GHz}$ because there was some confusion as to which model was actually used in the source material (Yang and Rahmat-Samii 2003), Also, truncating the outer patches may introduce unaccounted for effects due to the vias near the edge of the truncated EBG possibly radiating.

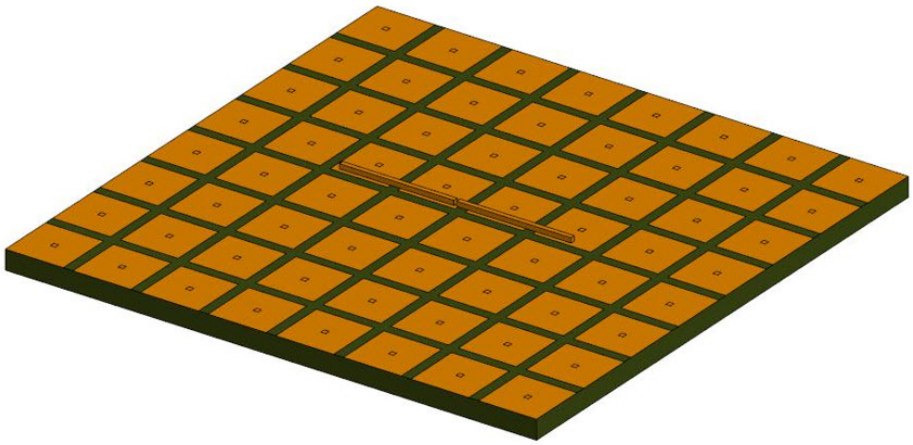

Fig. 5 The reconstructed FEKO model of the EBG shown in Volakis (2007) and Yang and Rahmat-Samii (2003)

3.2 Numerical and Analytical Results

The reflection coefficient for the dipoles above the 8 unit cell by 8 unit cell EBG as described in Volakis (2007) and in Yang and Rahmat-Samii (2003) is shown in Fig. 6. The calculated reflection coefficient using MoM shows that the dipole resonant frequencies are shifted compared to the time-domain finite-difference (TDFD) results from the referenced literature, a difference of about 800 MHz for the $0.48\lambda_{12GHz}$ dipole, 680 MHz for the $0.36\lambda_{12GHz}$, and 460 MHz for the $0.32\lambda_{12GHz}$ dipole. The trend in resonant frequency is as expected according to the dipole lengths (decreasing as the dipole length increases), but the dipoles are not as well matched and are shifted to higher frequencies compared to the published results. Figures 7a and 7b show the E-plane and H-plane directivity patterns for the 3 dipoles at 12 GHz, 13.6 GHz, and 15.3 GHz; these are the same resonant frequencies as plotted in the literature (Volakis 2007 and in Yang and Rahmat-Samii 2003). Both the E-plane and H-plane patterns for the $0.36\lambda_{12GHz}$ dipole and the $0.32\ \lambda_{12GHz}$ look reasonable when compared to the published results, but the $0.48\lambda_{12GHz}$ dipole, conversely, looks nothing like the directivity pattern in the published results. There are deep nulls about ±30° away from bore sight in the E-plane pattern, and the peak directivity is about zero dBi instead of the claimed 8 dBi in the literature.

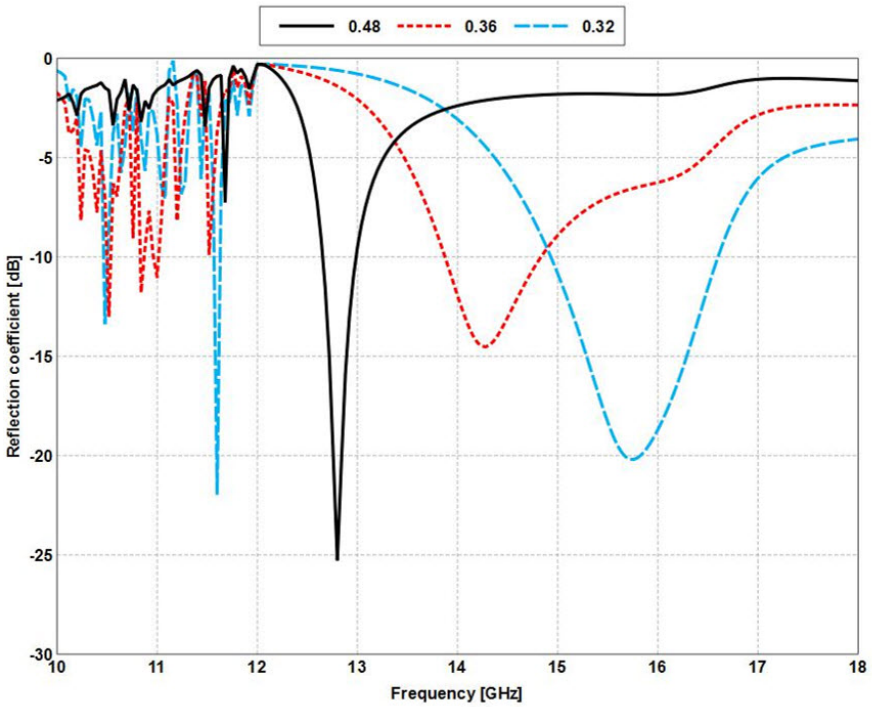

Fig. 6 The reflection coefficient for a dipole above the EBG from Volakis (2007) simulated in FEKO with the dipole length as a parameter

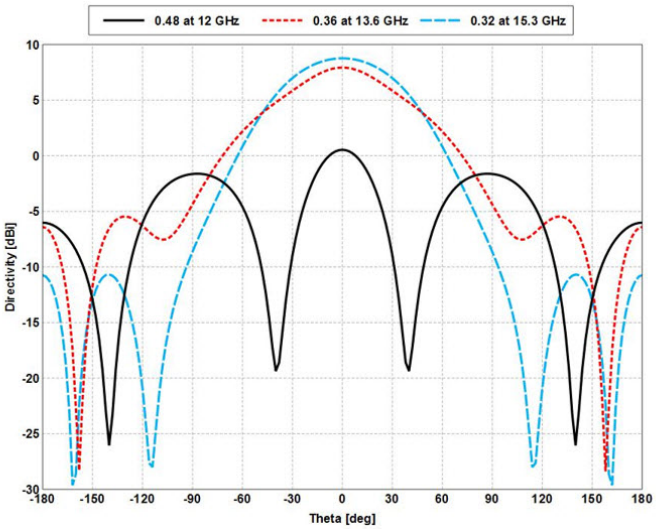

a)

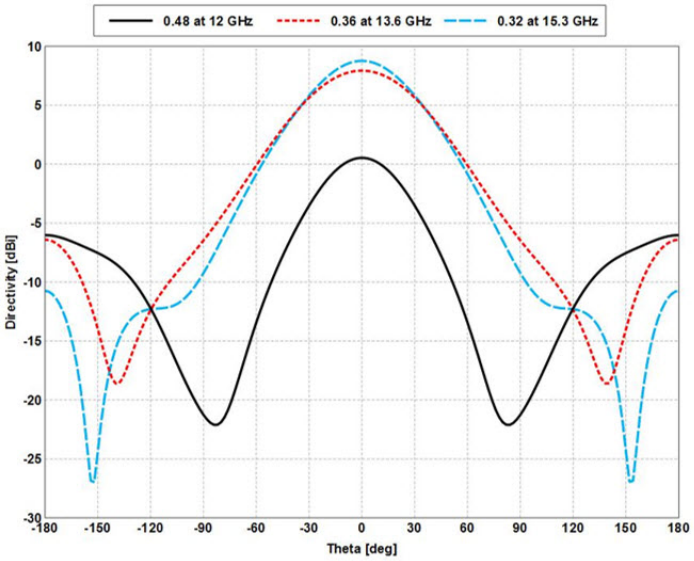

b)

Fig. 7 The dipole directivity patterns at the frequencies shown in Volakis (2007). a) E-plane and b) H-plane

When looking at the directivity patterns that correspond to the resonant frequencies calculated by FEKO, Fig. 8a and b, the $0.36\lambda_{12GHz}$ dipole still looks reasonable. The $0.48\lambda_{12GHz}$ and $0.32\lambda_{12GHz}$ dipoles, however, still do not agree with the published results shown in Volakis (2007) and in Yang and Rahmat-Samii (2003). Attempts were made with the TDFD code GEMS (www.2comu.com) to better reproduce the results from the published literature; however, GEMS agreed with the results from FEKO instead of the results from the published literature. For more confirmation,

the FEKO models were simulated with High-Frequency Structural Simulator (HFSS) (www.ansys.com) and Computer Simulation Technology (CST) Microwave Studio (www.cst.com). Ultimately, the results from the antenna engineering handbook (Volakis 2007) and the source material (Yang and Rahmat-Samii 2003) could not be reproduced with either FEKO, GEMS, HFSS, or CST.

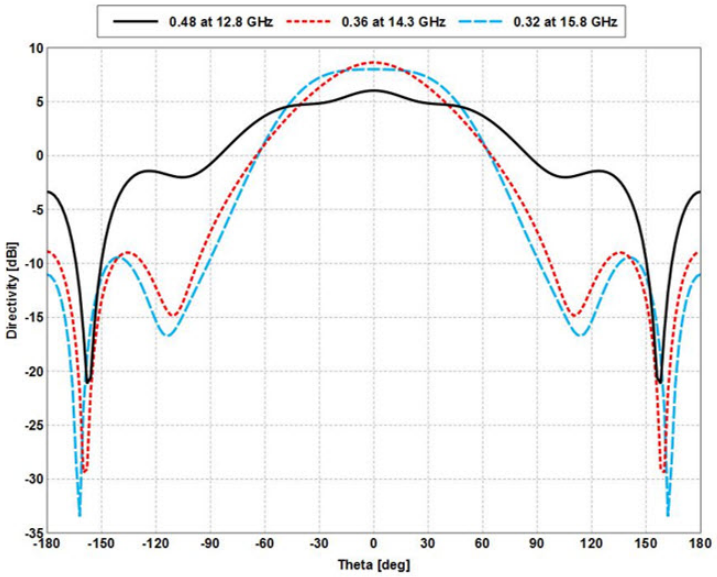

a)

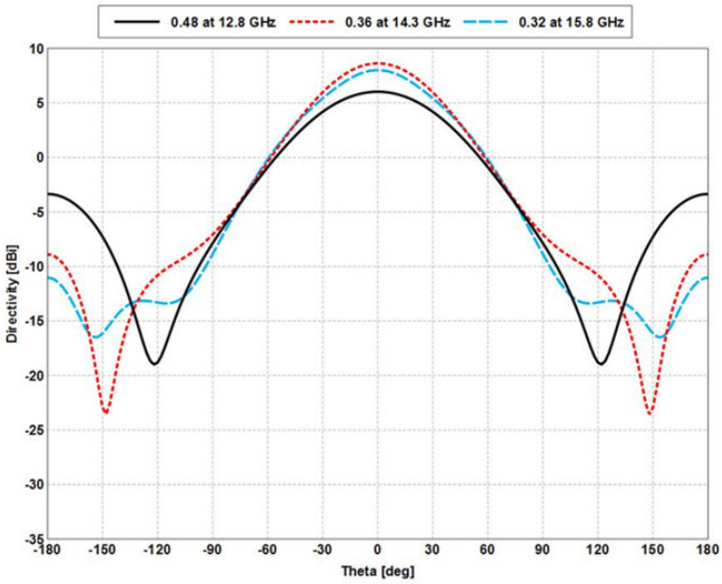

b)

Fig. 8 The dipole directivity patterns at the resonant frequencies calculated by FEKO. a) E-plane and b) H-plane b.

When computing the transmission and reflection coefficients from a PBC unit cell in FEKO, the phase reference can be defined at any point in space. It was determined from the literature that most PBC analysis of EBG's is done using TDFD that requires placing an observation plane in a region where there are only scattered fields. To determine the reflection coefficient from this method requires a normalization procedure to project the phase reference to the surface of the EBG. This procedure is found in Yang and Rahmat-Samii (2003).

The normalization process is fairly straight forward. An observational plane is placed at a distance of $0.5\lambda_{12GHz}$ away from the EBG surface; in a TDFD code, this observational plane lies in the scattered field region. The reflected field is computed from the scattered fields detected at the observational plane. This reflected field is then normalized to the reflected field of a PEC surface that is placed at the location of the EBG's surface and simulated using the same method. A phase correction of 180° is then added to the phase of the normalized reflected field, thereby projecting the phase reference of the reflected field in the scattered region to the surface of the EBG.

Two PBC simulations were done in order to see if the normalization method described in Yang and Rahmat-Samii (2003) and the phase reference of the EBG surface from FEKO would result in the same reflection coefficient phase. Figure 9 shows the reflection coefficient phase from the PBC results comparing the phase at the EBG surface to the normalized phase. The normalized phase was computed only to 18 GHz because, as can be seen from the figure, the difference between the 2 curves is negligible, so the phase reference in FEKO gives correct results.

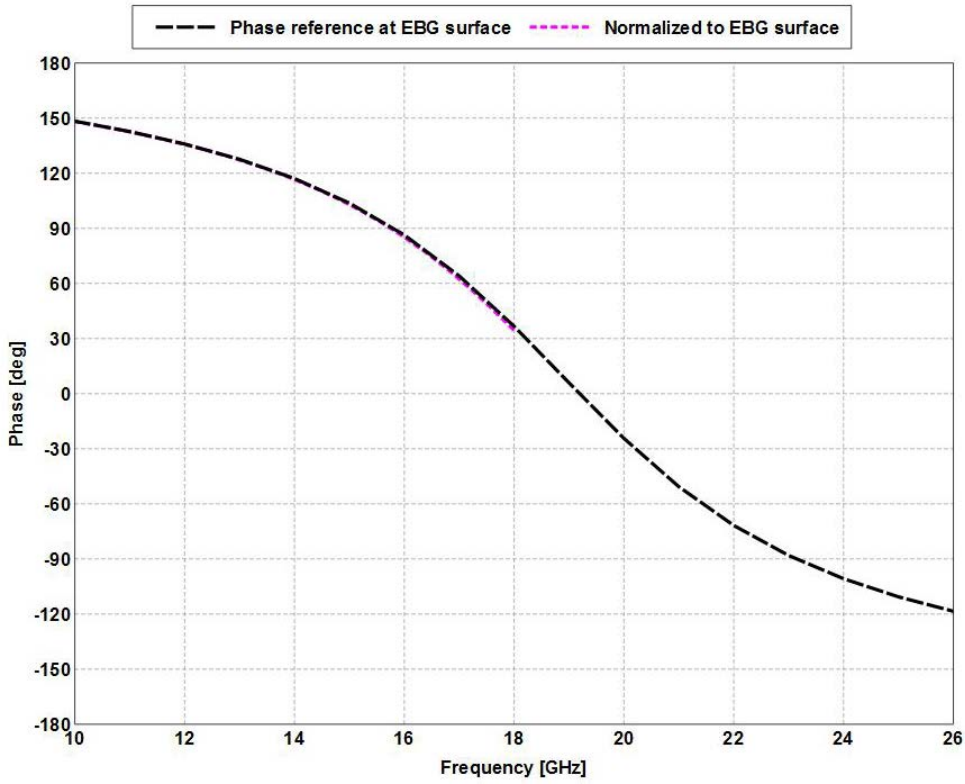

Fig. 9 The FEKO reflection coefficient phase at the EBG surface compared to the normalized phase

Comparing the results from FEKO's PBC analysis to the published results in the antenna engineering handbook (Volakis 2007) and the source material (Yang and Rahmat-Samii 2003), the zero-phase crossing is shifted from what looks to be about 17 GHz in the published literature to about 19 GHz in FEKO. After checking the unit cell parameters, fine meshing, and using square and then cylindrical vias, it was determined that the model results were correct. In GEMS, the position of the observation plane in the scattered field region is not known exactly so it was not used for comparison to FEKO's results (Volakis 2007; Yang and Rahmat-Samii 2003).

Applying the analytical models with MATLAB (www.mathworks.com) to the EBG shows varying results. The CM results (using both equations for the gap capacitance) (Fig. 10), agree better with the published results for the reflection-phase as the 2 approximations bound the results from (Volakis 2007 and from Yang and Rahmat-Smii 2003). The TLM in Fig. 11, however, shows a zero-phase crossing in the reflection-phase a few 100 MHz above 19 GHz which better agrees with the results from FEKO and not with what is found in the published literature. Figure 12 plots the analytical and numerical models showing the difference between the CM, TLM, and the PBC results from FEKO. The TLM and the PBC

results from FEKO were validated by reproducing the published results seen in Fig. 8 in Luukkonen et al. (2008) (Fig. 13). Because the published results from from the Luukkonen report were repeatable, it was deemed that the results from the TLM and the FEKO PBC simulation for the EBG from the antenna engineering handbook (Volakis 2007) and the reference material (Yang and Rahmat-Samii 2003) are correct. The source for the discrepancy in results is not clear, but the EBG parameters provided do not seem to correspond to the published results in Volakis (2007) and in Yang and Rahmat-Samii (2003).

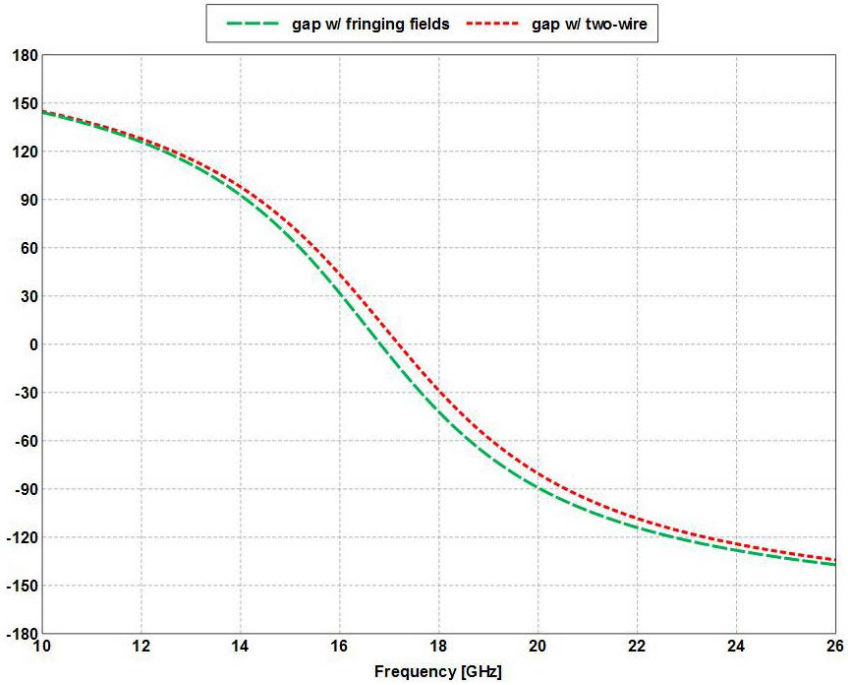

Fig. 10 The reflection coefficient phase using a CM for the EBG from Volakis (2007) and from Yang and Rahmat-Samii (2003)

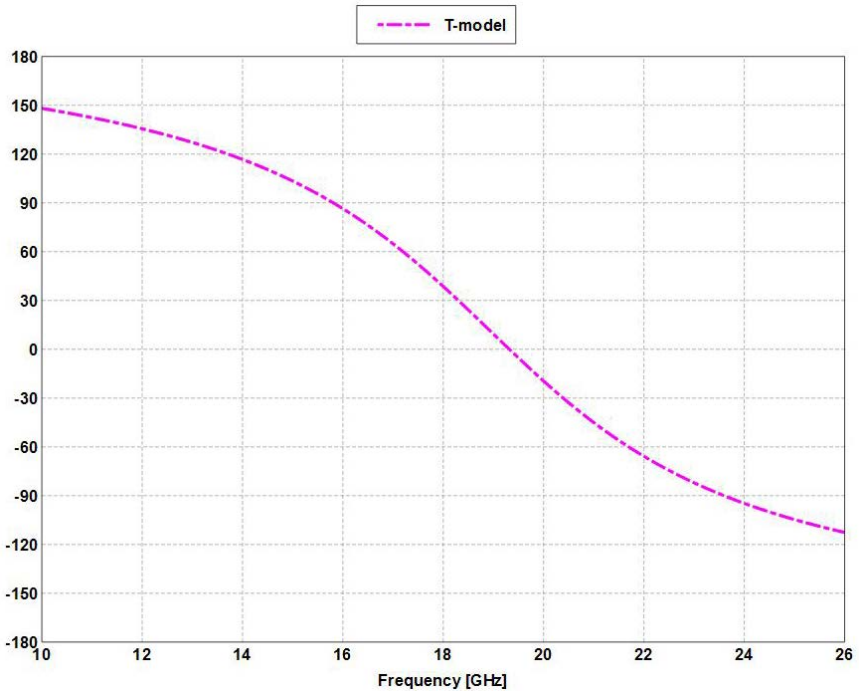

Fig. 11 The reflection coefficient phase results using a TLM for the EBG from Volakis (2007) and from Yang and Rahmat-Samii (2003)

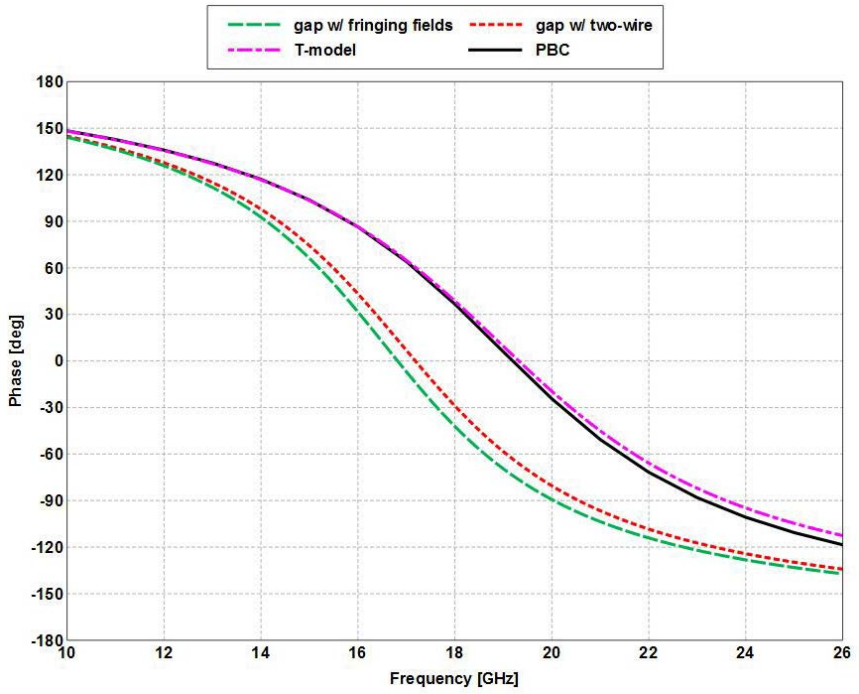

Fig. 12 The comparison of the analytical and numericals models for the EBG from Volakis (2007) and from Yang and Rahmat-Samii (2003)

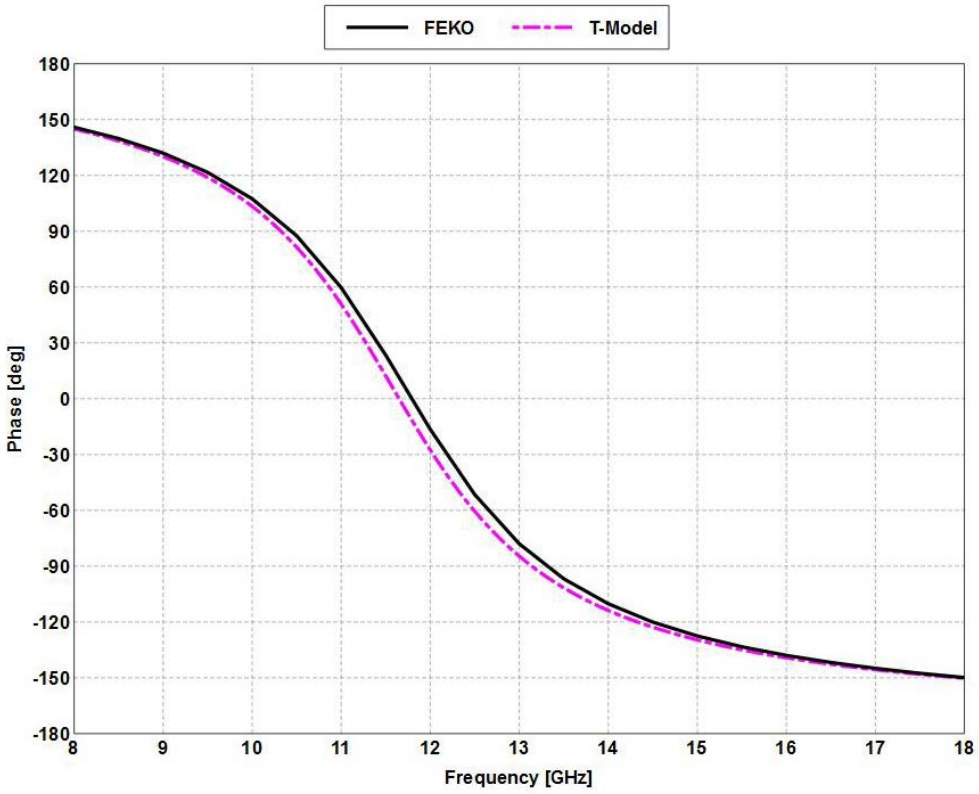

Fig. 13 The reflection coefficient results for the EBG from Luukkonen et al. (2008)

4. EBG Analysis without Vias and Substrate

The focus of this section will be on a modified EBG that has been published in Kamadin et al. (2011) and its simulated effect on a resonant strip dipole. This EBG does not have vias. The patch widths and EBG thickness of the original model were scaled to 450 MHz while the gap width was left the same as that found in the published literature. Table 1 lists the physical specifications of the EBG along with dimensions normalized to the free space wavelength, λ_{450MHz}. Figure 14 shows the FEKO model. For this section, a dielectric substrate is not included. The dipoles used in this section are planar and have a constant trace width (w = 4 mm) small enough so that the dipole can be considered thin. A comparison of the EBG with thin gaps to the same EBG with wide gaps and the impact the 2 EBGs have on the strip dipole is also made.

Table 1 Design specifications for the 4 × 4 EBG

Parameter	Specifications
Patch width	150.64 mm (λ_{450MHz}/4.4)
Gap width	2.67 mm* (λ_{450MHz}/250)
EBG thickness	66.62 mm (λ_{450MHz}/10)
Total EBG width	610.56 mm (~λ_{450MHz})

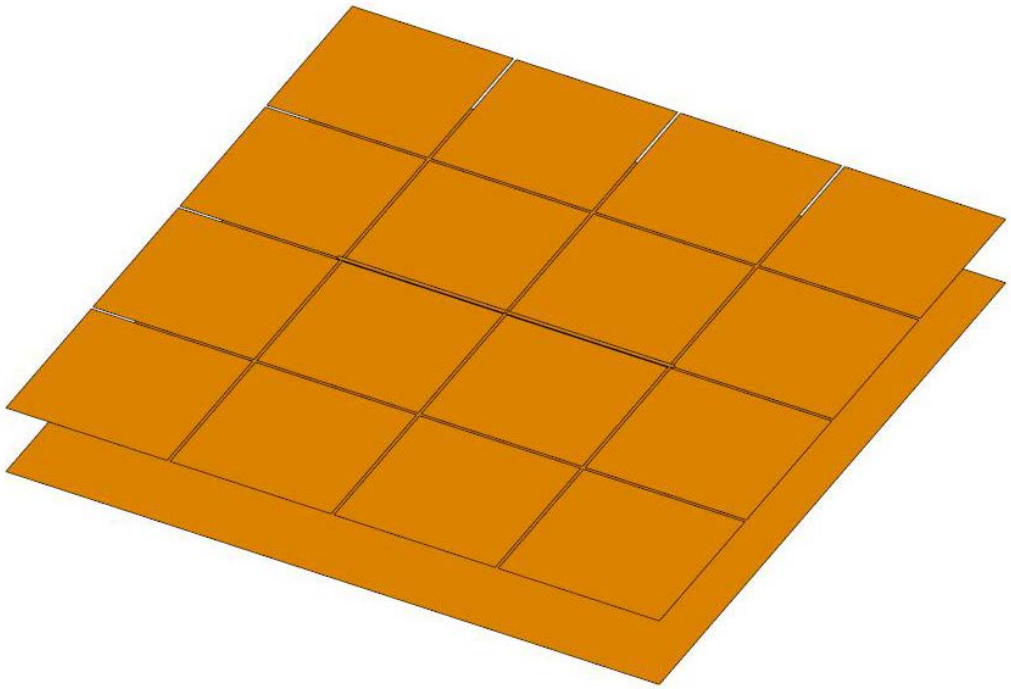

Fig. 14 The FEKO model for the 4 × 4 EBG with dimensions summarized in Table 1

4.1 Thin-Gap EBG

Since the patch widths were increased without changing the periodicity, the EBG of this subsection has a very thin-gap width, being $\frac{\lambda_d}{250}$ in width. The various analytical and numerical models are compared to investigate which method is best for the EBG basic design. In this case, the periodicity *D* is very close to the patch width, with $\frac{w}{D} = 0.98$.

4.1.1 EBG Analysis: Thin Gap

Figure 15 shows results from the CM for the thin-gap EBG. Because the patches are so large compared to the gap width, an additional CM is included where only the shunt capacitance is contributing by neglecting the gap capacitance, C_g. There is a significant difference between the 2 different approximations for the gap capacitance C_g, as the result of the 2-wire method for the zero-phase crossing is 259 MHz and the result of the field-gap method for the zero-phase crossing is 207 MHz with a steeper slope. So for such a thin gap, the CM approach has a larger uncertainty. For the case where the shunt capacitance dominates, the zero-phase crossing is estimated to occur at 317 MHz and shows a less steep slope compared to the other 2. Note that these zero-phase frequencies are much lower than the preferred scale frequency of 450 MHz. In typical EBG design, it is expected that the design frequency corresponds to the frequency point where the reflection coefficient phase crosses zero.

Figure 16 is the result for the TLM of the EBG. The zero-phase crossing calculated by the model is 302 MHz. Just like the CM results, this frequency does not correspond to the scale frequency of 450 MHz and produces a different reflection coefficient phase than the CM, being much higher than both gap CMs and about 15 MHz lower than the no-gap CM. The PBC results (Fig. 17) show the zero-phase crossing for the EBG is at 332.8 MHz and, just as with the 2 analytical models, is not at the scaled frequency of 450 MHz. PBC does show a less steep slope that suggests a wider operational bandwidth. Estimating the bandwidth with the 2 analytical models show very different results, with the no-gap CM showing the larger bandwidth: CM_{BW} = 140 MHz versus TLM_{BW} = 129 MHz. Both analytical model bandwidths assume a phase range of 0° ± 90°, so measuring the same phase range on the PBC results shows a bandwidth of about 153 MHz, larger than both analytical models.

Figure 18 shows the results for the NEF approach with and without a 450 MHz resonant strip dipole terminated in a 50 Ω load. Note that the results are dependent on the antenna termination, so the appropriate source impedance should be used. These results differ greatly from the reflection coefficient phase determined by PBC and the analytical models. The inclusion of the strip dipole geometry in the NEF simulation has a significant impact on the phase of the scattered NEF, especially at lower frequencies where the phase increased by an amount that ranges between 30° and 40° and now peaks at about 140° rather than 110°. There is less of an effect on the phase at higher frequencies, where the change is a 5° to 10° more negative phase

with the strip dipole included. The zero-phase crossing for the NEF results with and without the strip dipole is 408 and 387 MHz, a difference of 75 and 54 MHz from the PBC results, respectively.

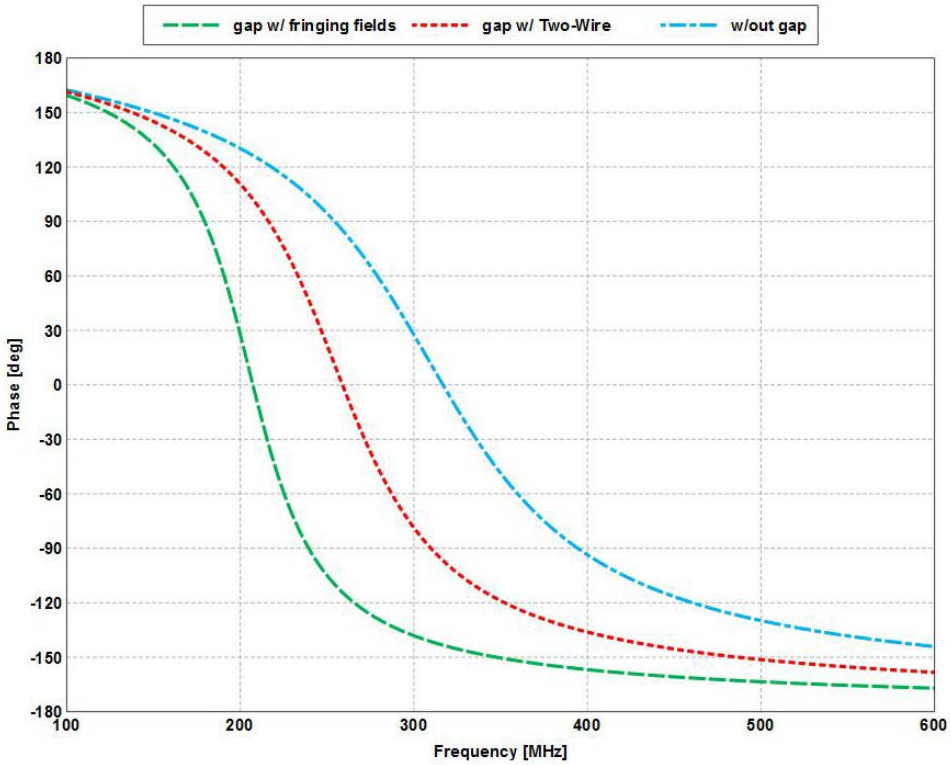

Fig. 15 The reflection coefficient phase calculated with the CM for the 4 × 4 thin-gap EBG

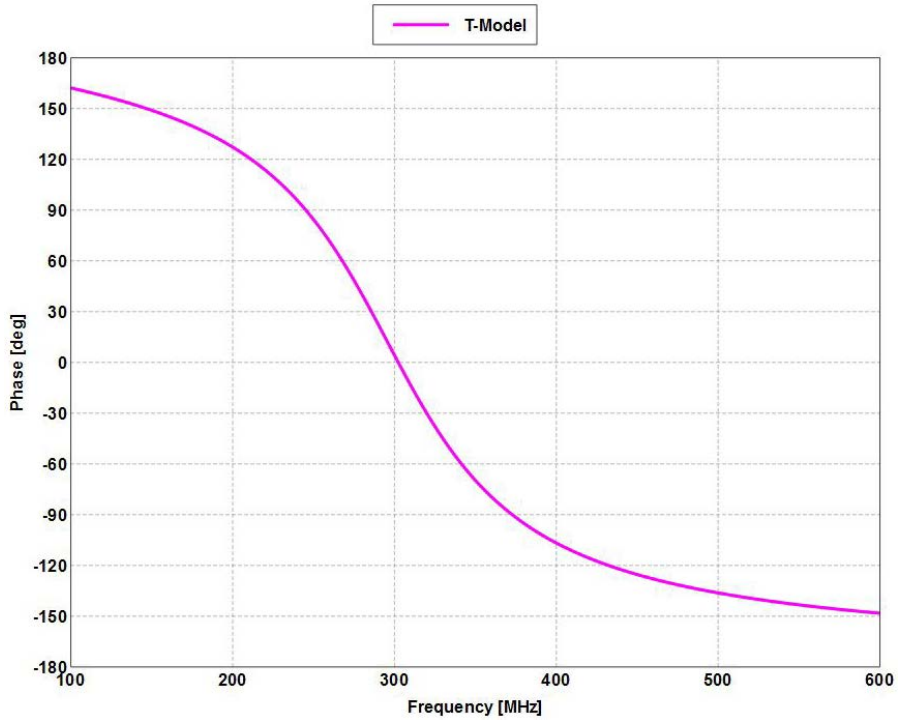

Fig. 16 The reflection coefficient phase calculated with the TLM for the 4 × 4 thin-gap EBG

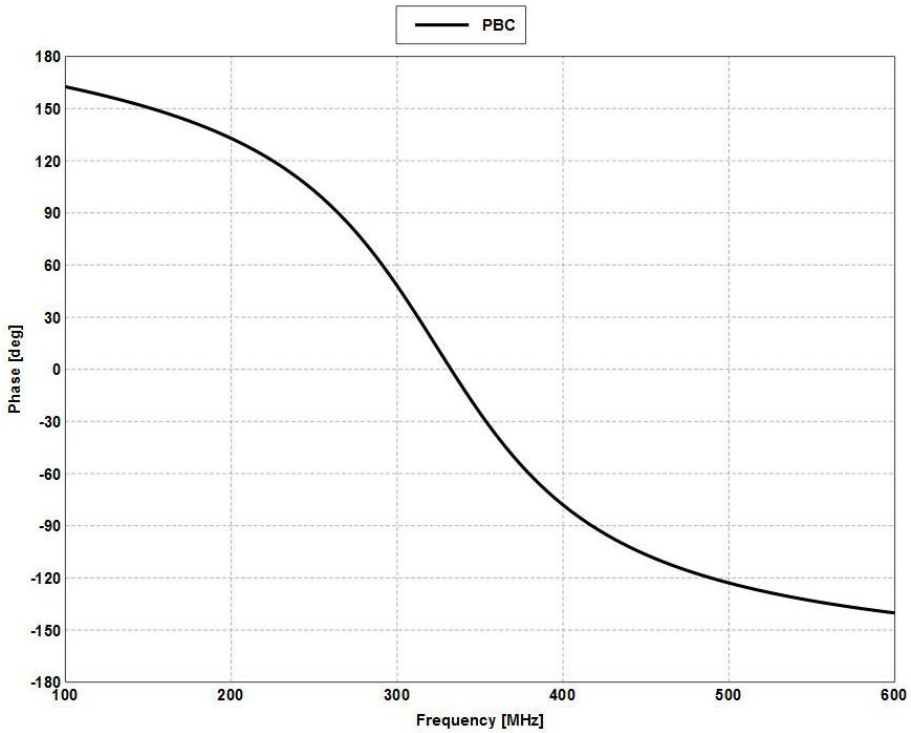

Fig. 17 The reflection coefficient phase calculated with PBC for the 4 × 4 thin-gap EBG

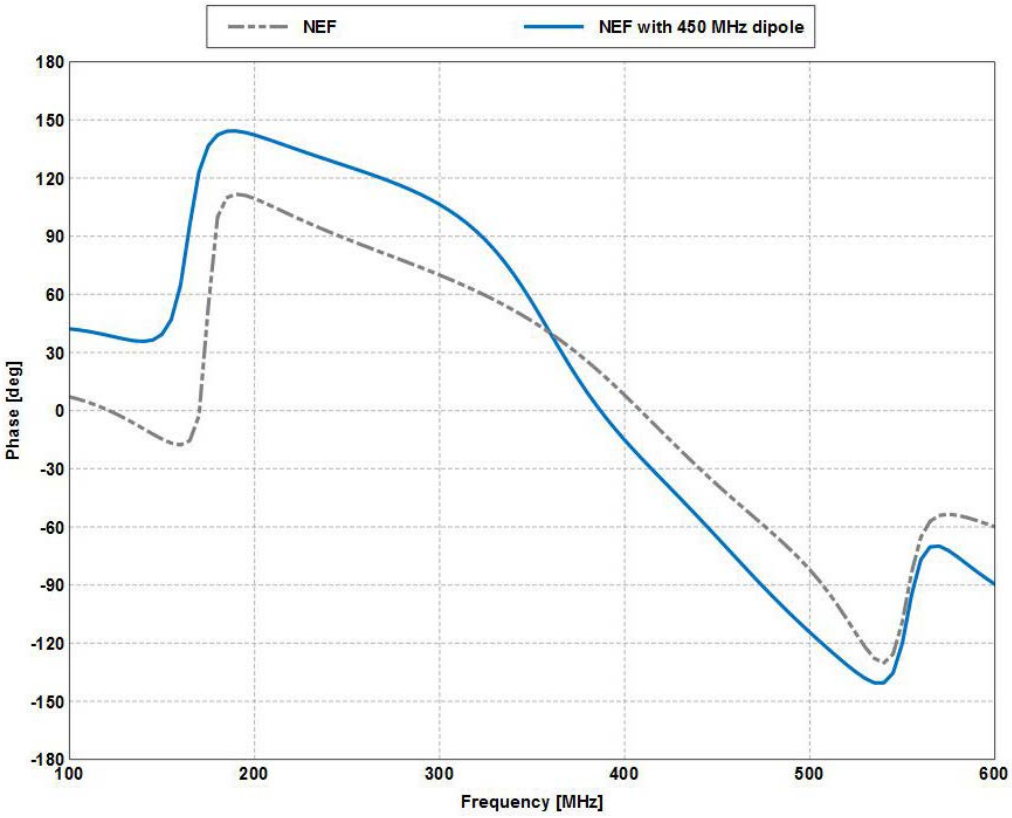

Fig. 18 The NF phase calculated by FEKO for the 4 × 4 thin-gap EBG with and without a 450 MHz load terminated resonant strip dipole

The NEF results also show more structure than the PBC simulation, with phase oscillations between 100 and 200 MHz and another less intense oscillation between 500 and 600 MHz. The bandwidths predicted by both NEF simulations are quite different than the other models (as can be seen by the slope of the curves), but the one of particular interest (and will be the focus for all NEF analysis in this report) includes the resonant strip dipole geometry. The antenna included NEF simulation calculates the EBG bandwidth to be about 151 MHz. The bandwidths calculated by the PBC and NEF with strip dipole are practically the same, and of the 2 analytical models, the no-gap CM is the closest in estimating the bandwidth when compared to the numerical models.

Figure 19 shows the results for the analytical and numerical models together, highlighting the differences between them. From this figure, it is suggested that the CM would be the preferred analytical model, but considering the uncertainty in how the capacitances should be approximated, the TLM would be preferred. It is also obvious that the CM neglecting C_g, TLM, and PBC agree within 10–15 MHz of each other. However, those 3 results have no agreement at all with the NEF results. It is important to note that while the PBC and NEF with dipole results show similar

bandwidths, the range of frequencies that correspond to those bandwidths are different. The NEF with dipole shows a higher frequency range than the PBC, a difference of about 60 MHz. With the phase differences between the PBC (infinite structure) and NEF (finite structure) simulations, it is questionable to assume the PBC method is sufficient for EBG design when antenna applications are considered. Table 2 shows the different bandwidth ranges taken from the PBC and NEF with dipole curves.

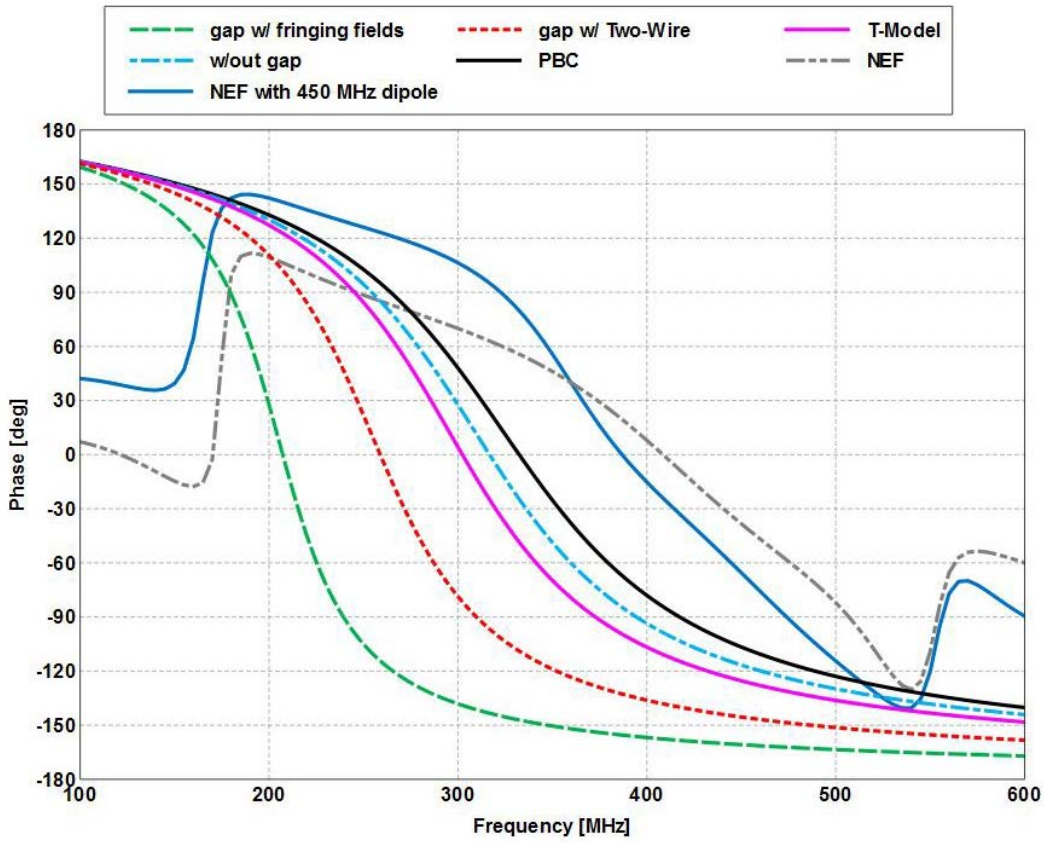

Fig. 19 The results from the analytical and numerical models for the 4 × 4 thin-gap EBG

Table 2 The phase ranges, frequency ranges and associated bandwidths for the 4 × 4 thin-gap EBG determined by the PBC and NEF with dipole simulations

Phase Range	Frequency Range (MHz)		Bandwidth (MHz)	
	PBC	NEF with Dipole	PBC	NEF with Dipole
0° ± 90°	264 – 417	323 – 474	153	151
0° ± 45°	302 – 366	357 – 430	64	73
90° ± 45°	195 – 302	222 – 356	107	134

4.1.2 Strip Dipole Analysis: Thin Gap

When using an EBG for antenna applications, it is important to understand the impact that it has on a given antenna. This means understanding how the EBG influences the input impedance of an antenna by reactive loading, how the EBG influences the gain and radiation pattern of the antenna, and how well an antenna can be scaled back to the design frequency when in the presence of the EBG. The goal of this subsection is to understand the EBG's influence on a strip dipole whose free space resonance corresponds to a phase angle (±90°, ±45°, and 0°) on either the PBC curve or the NEF with dipole curve (this is done to compare the 2 numerical methods). Table 3 lists the free space resonant frequencies of the dipoles and the corresponding phase angles comparing the reflection-phase and the scattered-phase. Performing this analysis with the analytical models is unnecessary, as they are approximations primarily used for starting the design process, and comparing the 2 numerical methods is to determine which one is preferred for analyzing an EBG for antenna applications.

Figure 20 shows the input reflection coefficient for the dipoles with resonant lengths scaled to different frequencies corresponding to the reflection-phase angles. The same scale factor is used for each dipole length to achieve an exact match in free space. The dipole half-length is $0.945\frac{\lambda}{4}$. All of the dipoles except for the –90° dipole are no longer matched at all and show a shift to lower frequencies that suggests an inductive loading effect by the EBG. There is also a higher order mode for each dipole, but it is matched only for the –90° dipole at about 550 MHz. It is important to understand how the EBG effects the antenna input impedance as a function of frequency. Figure 21a and b are the input resistance and reactance for

each dipole. There is a plateau in the resistance that spans nearly 100 MHz and improves from positive phase to negative phase angles. The magnitude of this plateau decreases at higher frequencies, which suggests that a higher frequency dipole would see impedance bandwidth improvements.

Table 3 The frequencies corresponding to particular reflection-phase angles and scattered-phase angles for the 4 × 4 thin-gap EBG

Phase	PBC (MHz)	NEF (MHz)
+90°	264	323
+45°	302	357
0°	332	387
–45°	366	430
–90°	417	474

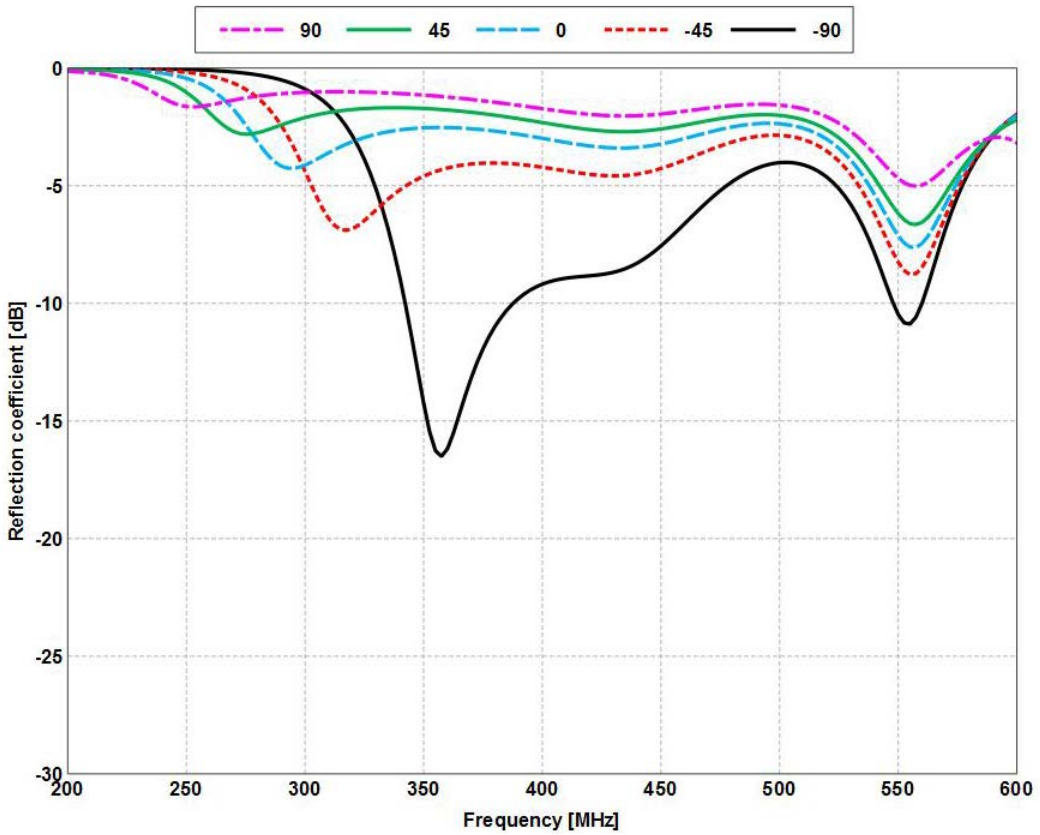

Fig. 20 The reflection coefficient for the resonant strip dipoles designed for the reflection-phase angles over the 4 × 4 thin-gap EBG

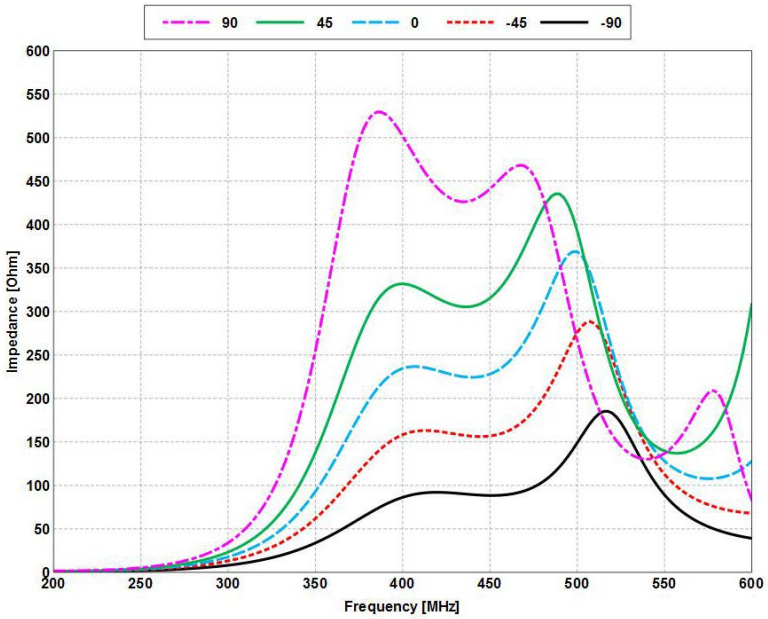

a)

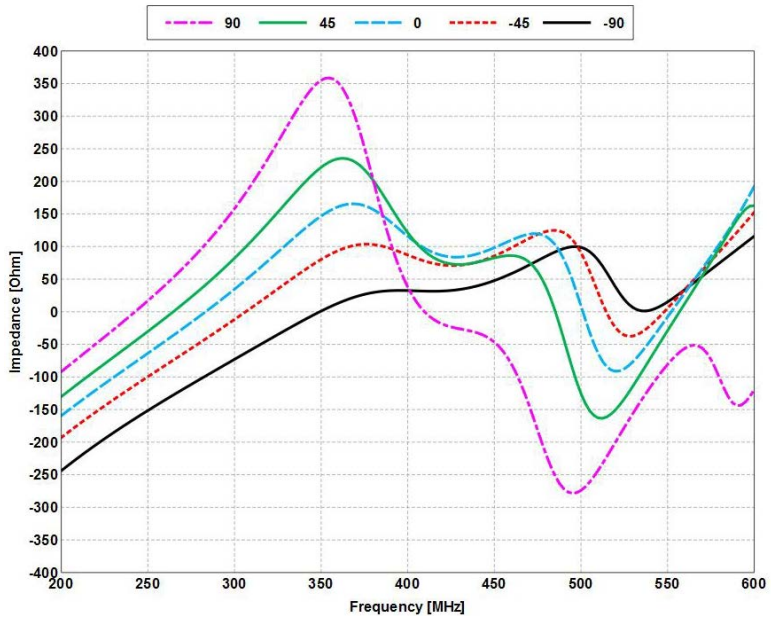

b)

Fig. 21 a) The input resistance for the resonant strip dipoles designed for the reflection-phase angles over the 4 × 4 thin-gap EBG. b) The input reactance for the resonant strip dipoles designed for the reflection-phase angles over the 4 × 4 thin-gap EBG.

A similar plateau, though less obvious, occurs in the reactance as well. The radiation patterns where the dipoles are best matched **(**Fig. 22a and b) show that although all phase angles but –90° are not matched to 50 Ω, all of the dipoles now have more directive patterns that radiate in a preferred direction instead of omnidirectional. Figure 23 shows the realized gain at bore sight ($\theta = 90°, \phi = 0°$)

versus frequency curve. The 1-dBi realized gain bandwidth is very broad for the matched dipole and is nearly 3 times larger than the impedance bandwidth (–10-dB reflection coefficient), 126 MHz versus 46 MHz. Based upon the results from the reflection coefficient and radiation patterns, the EBG bandwidth would be bounded only by the frequencies that correspond to reflection-phase angles that are less than –90° which is not what is seen in the published literature.

Figure 24 shows the input reflection coefficient for the dipoles with resonant lengths corresponding to the scattered-phase. From 0° to +90° the dipoles are not well matched to 50 Ω, with 0° showing a mediocre –10 dB match. The 2 dipoles in the negative phase regime, however, show very good matching and broad impedance bandwidths (for a dipole). Figure 25a and 25b show the resistance and reactance for each dipole. It is clear that there is an inductive loading effect on the input impedance characterized by a resonance occurring at a lower frequency. As expected, the plateau in the resistance has indeed decreased in magnitude for the higher-frequency dipoles. The wide plateau is what improves the dipole impedance bandwidth. The magnitude of the plateau ranges between 50 and 70 Ω for the –45° and –90° dipoles over the frequency range of 400 to 500 MHz. The reactance also has a flatter slope for –45° and –90°, showing the improvement in impedance bandwidth by nearly a factor of 2.

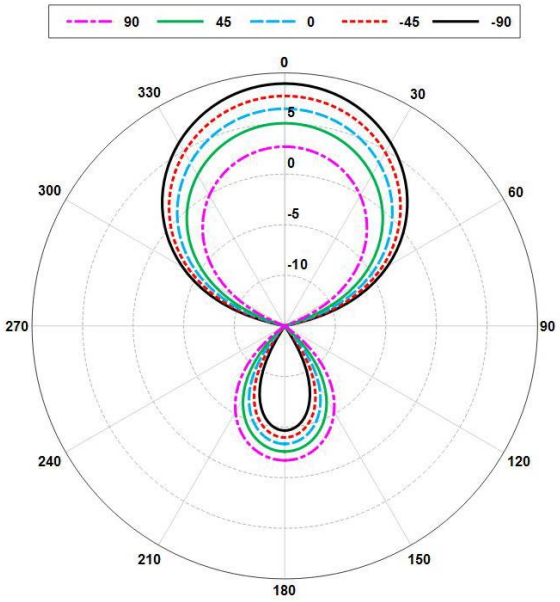

a)

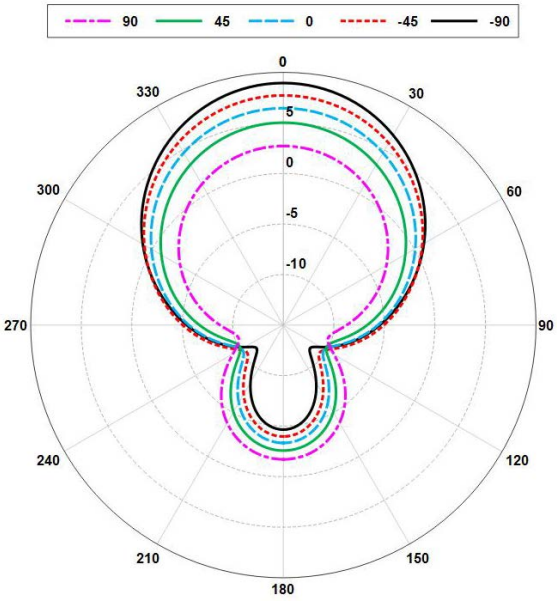

b)

Fig. 22 The realized gain pattern for the resonant strip dipoles designed for the reflection-phase angles over the 4 × 4 thin-gap EBG. a) E-plane and b) H-plane.

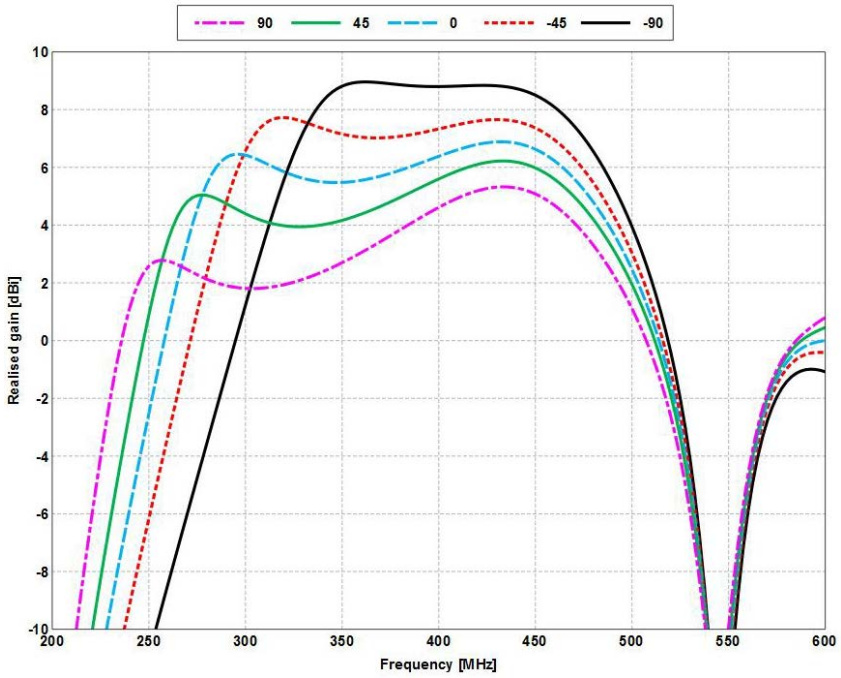

Fig. 23 The realized gain ($\theta = 90°$, $\phi = 0°$) vs. frequency for the resonant strip dipoles designed for the reflection-phase angles over the 4 × 4 thin-gap EBG

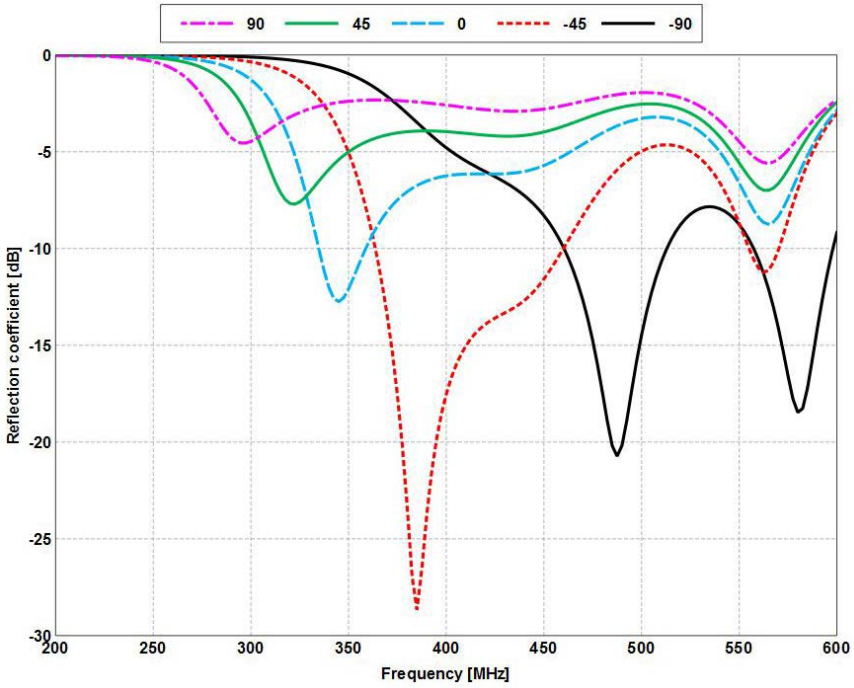

Fig. 24 The reflection coefficient for the resonant strip dipoles designed for the scattered-phase angles over the 4 × 4 thin-gap EBG

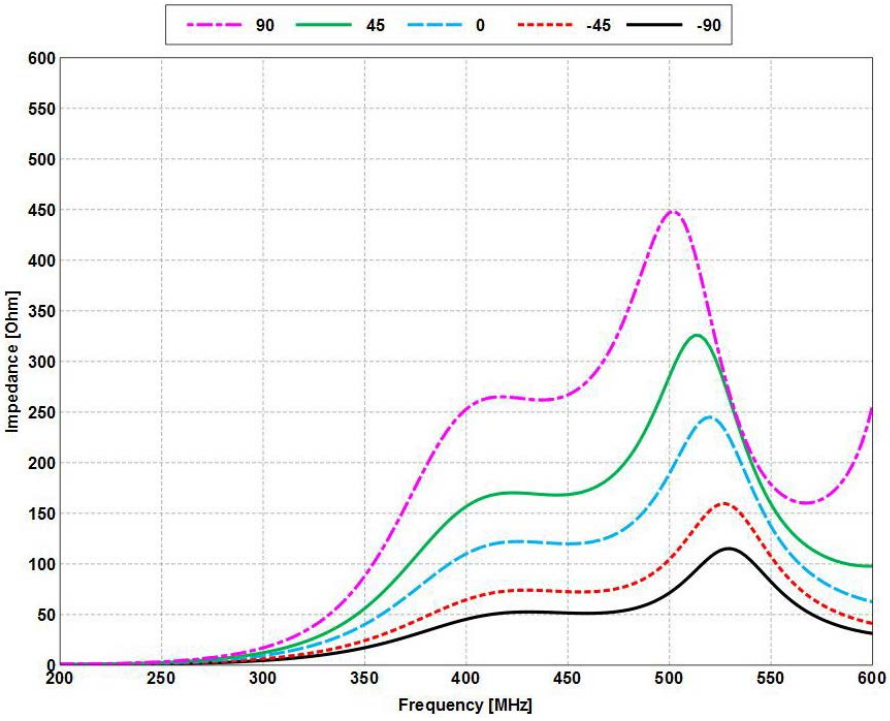

a)

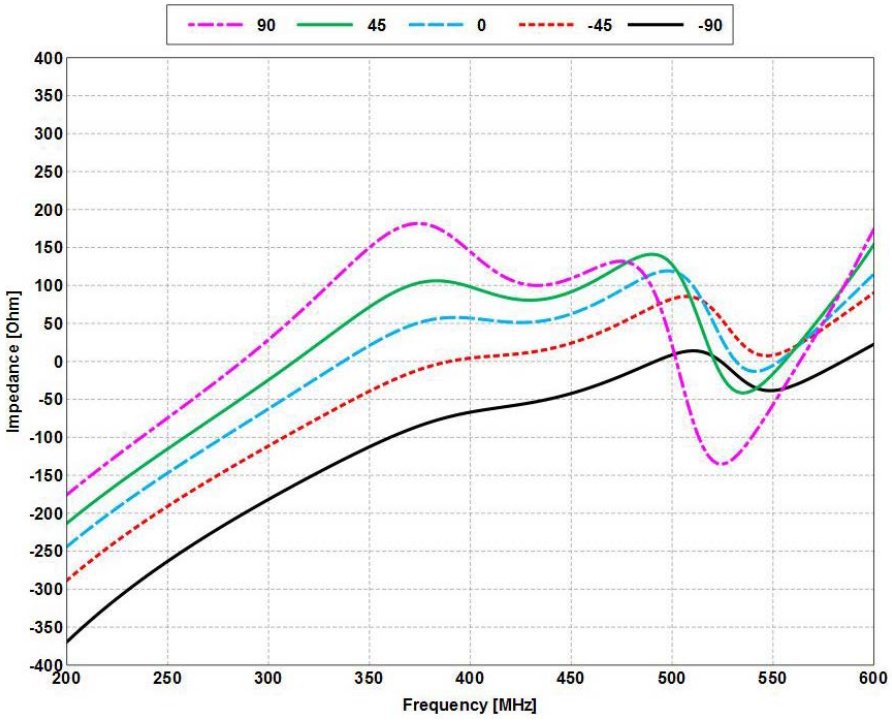

b)

Fig. 25 a) The input resistance for the resonant strip dipoles designed for the scattered-phase angles over the 4 × 4 thin-gap EBG. b) The input reactance for the resonant strip dipoles designed for the scattered-phase angles over the 4 × 4 thin-gap EBG.

Figure 26a and b show the radiation pattern for the dipoles where best matched. All five dipoles show very directive patterns, even the +90° dipole. A point to make is that these patterns do not vary nearly as much as the ones in Fig. 22a and b; however, at higher frequencies, the H-plane pattern becomes distorted, suggesting that any dipoles with resonances beyond the –90° dipole would have poor patterns in the H-plane. In any case, the EBG still improves the dipole realized gain by as much as 6.5 dBi when matched. Figure 27 shows the realized gain at bore sight ($\theta = 90°, \phi = 0°$) versus frequency curve. The 1-dBi bandwidth is still wider than the impedance bandwidth although the difference is now only 10 to 20 MHz instead of being 3 times larger.

From the simulation results of the reflection coefficient, impedance, and radiation pattern, the EBG can clearly improve the impedance bandwidth and pattern of a strip dipole over some frequency range, and from the results, the corresponding phase range would be bounded by 0° and –90° (more will be said about this in Section 5). The reflection-phase did not accurately determine what this frequency range is, whereas the scattered-phase did. This suggests that if an EBG's bandwidth is to be characterized by some phase curve for antenna applications, then that phase should be the scattered-phase and not the reflection-phase. Table 4 summarizes the frequency shift due to the loading effect and the new resonant frequencies of the strip dipoles in the presence of the EBG.

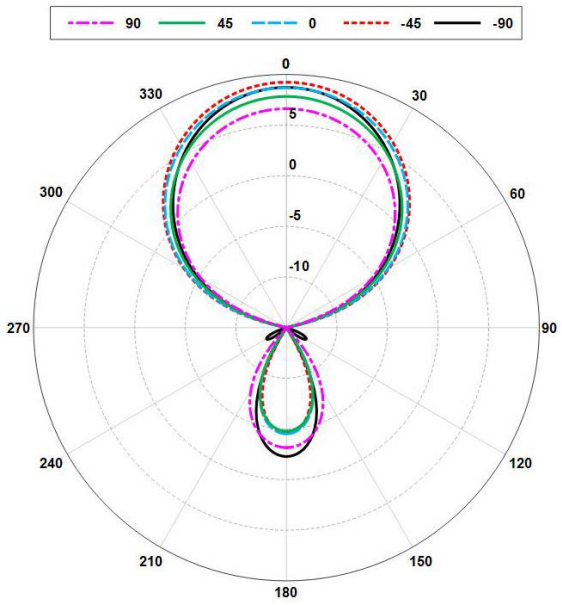

a)

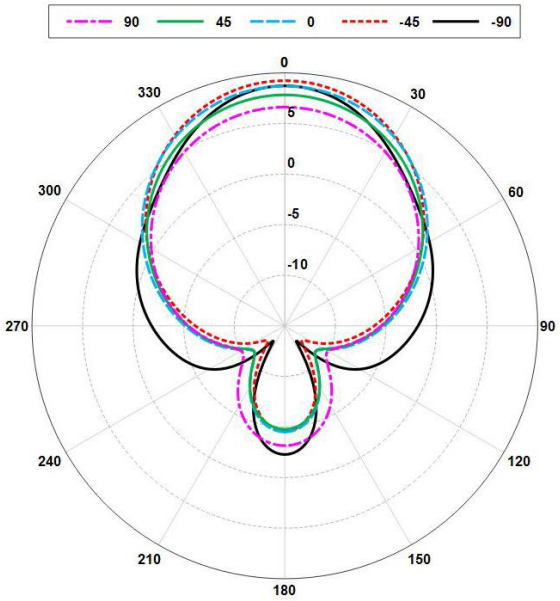

b)

Fig 26 The realized gain patterns for the resonant strip dipoles designed for the scattered-phase angles over the 4 × 4 thin-gap EBG. a) E-plane and b) H-plane.

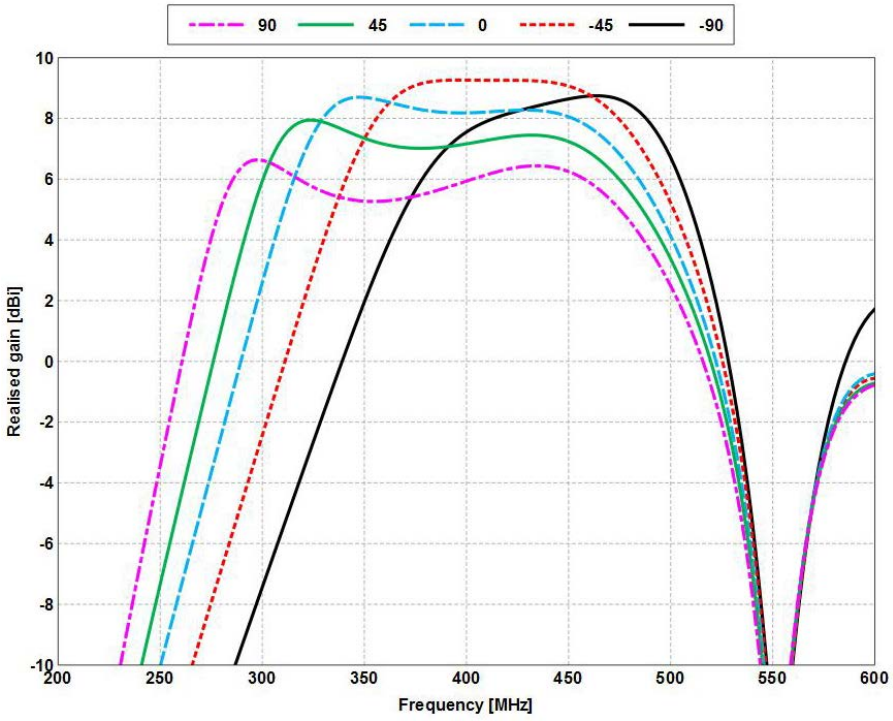

Fig. 27 The realized gain ($\theta = 90°$, $\phi = 0°$) vs. frequency for the resonant strip dipoles designed for the scattered-phase angles over the 4 × 4 thin-gap EBG

Table 4 The frequency shift amount due to the loading effect and the dipole resonant frequencies in the presence of the 4 × 4 thin-gap EBG

Phase (deg)	PBC (MHz)	Δf (MHz)	NEF (MHz)	Δf (MHz)
+90°	253	11	295	28
+45°	275	27	323	34
0°	295	37	345	42
–45°	318	48	385	45
–90°	358	59	458	16

4.1.3 Strip Dipole Scalability: Thin Gap

The scalability of an antenna in the presence of an EBG can determine how linear the loading effect is. The frequency shifts tabulated in Table 4 are different for each dipole, which means that the dipoles may not scale linearly when in the presence of the EBG. However, it may be possible that the dipoles will scale linearly within a particular frequency range. This subsection highlights the scalability of both the reflection-phase dipoles and the scattered-phase dipoles. Each dipole's length is

scaled according to an integer multiple of a common frequency. The frequency is determined by the difference between the dipole resonant frequency that shifted the most when in the presence of the EBG and the target frequency, which in this case is 450 MHz. For the reflection-phase dipoles the frequency scale factor is 92 MHz, and for the scattered-phase dipoles the frequency scale factor is 65 MHz.

From the reflection coefficient for the reflection-phase dipoles (Fig. 28) only the –45° and –90° dipoles are well matched, and only the –90° dipole is matched at 450 MHz. The other 3 dipoles show poor matching, which means that these dipoles did not scale well. The dipole resistance (Fig. 29a) has a plateau that spans about 100 MHz with a magnitude of about 50 Ω. Each of these dipoles would be well matched, but the reactance (Fig. 29b) for the reflection-phase dipoles that are not matched crosses zero at much higher frequencies (possibly at an anti-resonance). There are also large variations in the realized gain patterns (Fig. 30) at 450 MHz, but even the reflection-phase dipoles that are not matched show improved gain. The variation in the patterns is more easily seen in the realized gain versus frequency plot (Fig. 31) where the gain levels vary by several decibels. Note that the second mode near 550 MHz corresponds to a bifurcated beam.

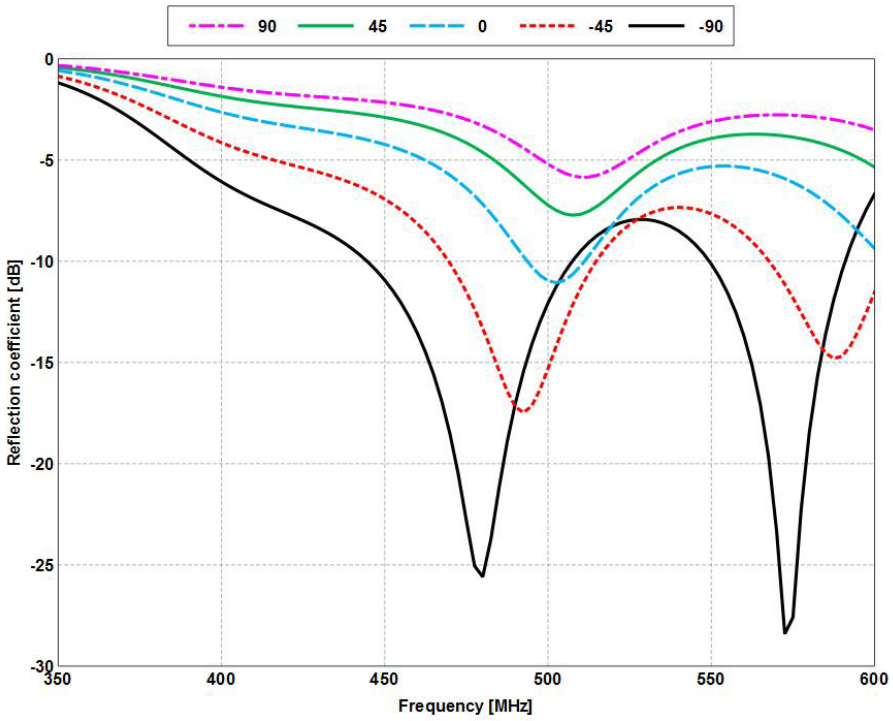

Fig. 28 The reflection coefficient for the reflection-phase dipoles with resonant lengths scaled to 450 MHz in the presence of the 4 × 4 thin-gap EBG

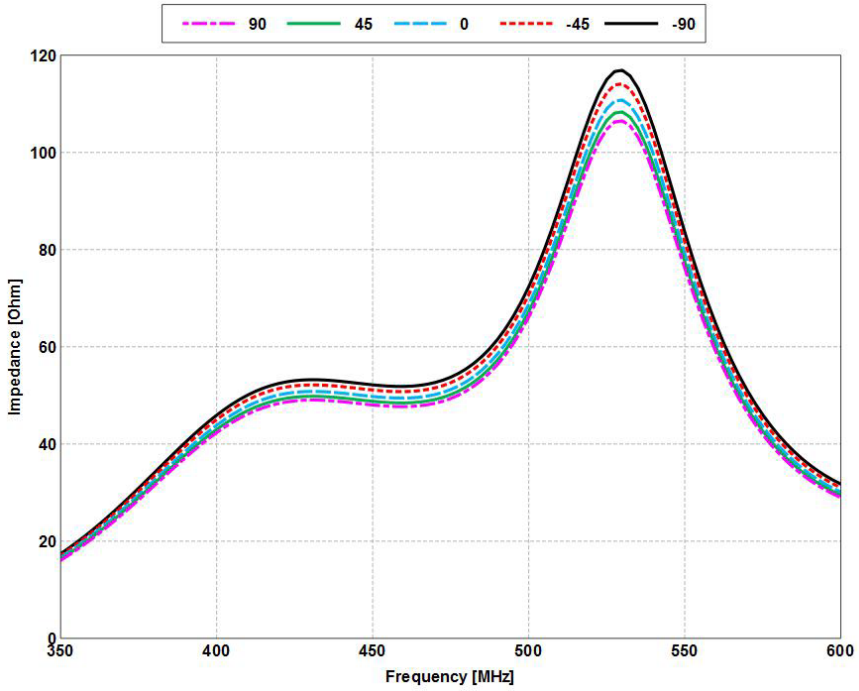

a)

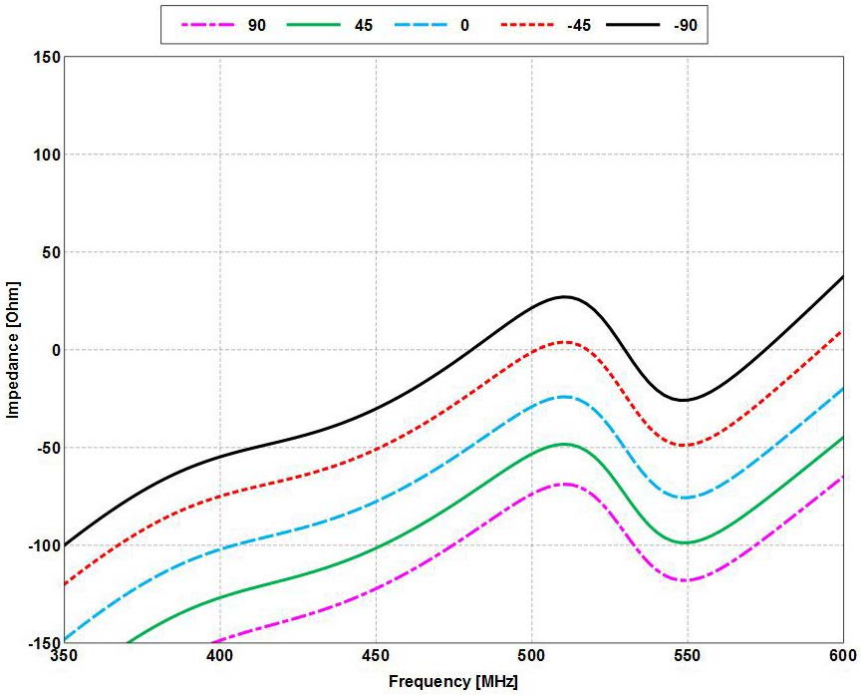

b)

Fig. 29 a) The input resistance for the reflection-phase dipoles with resonant lengths scaled to 450 MHz in the presence of the 4 × 4 thin-gap EBG. b) The input reactance for the reflection-phase dipoles with resonant lengths scaled to 450 MHz in the presence of the 4 × 4 thin-gap EBG.

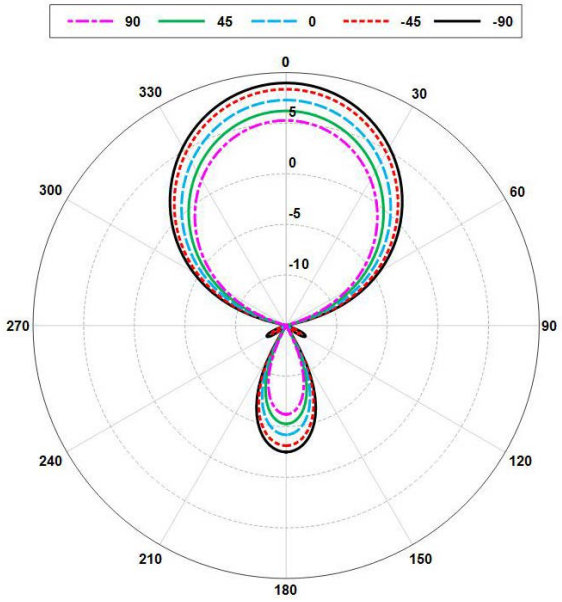

a)

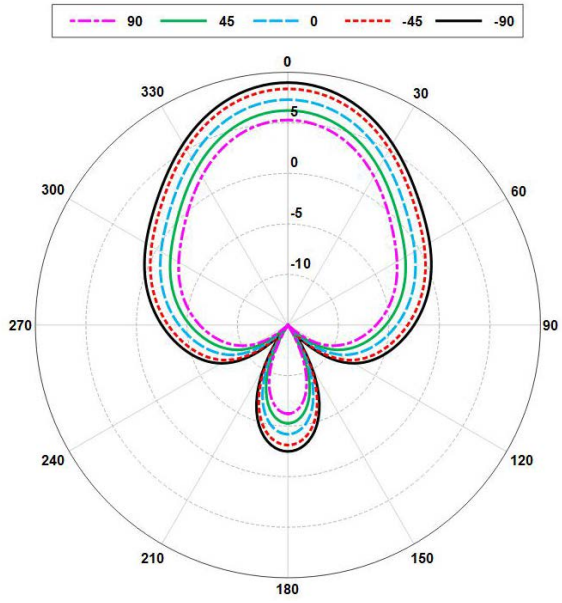

b)

Fig. 30 The realized gain pattern for the reflection-phase dipoles with resonant lengths scaled to 450 MHz in the presence of the 4 × 4 thin-gap EBG. a) E-plane and b) H-plane.

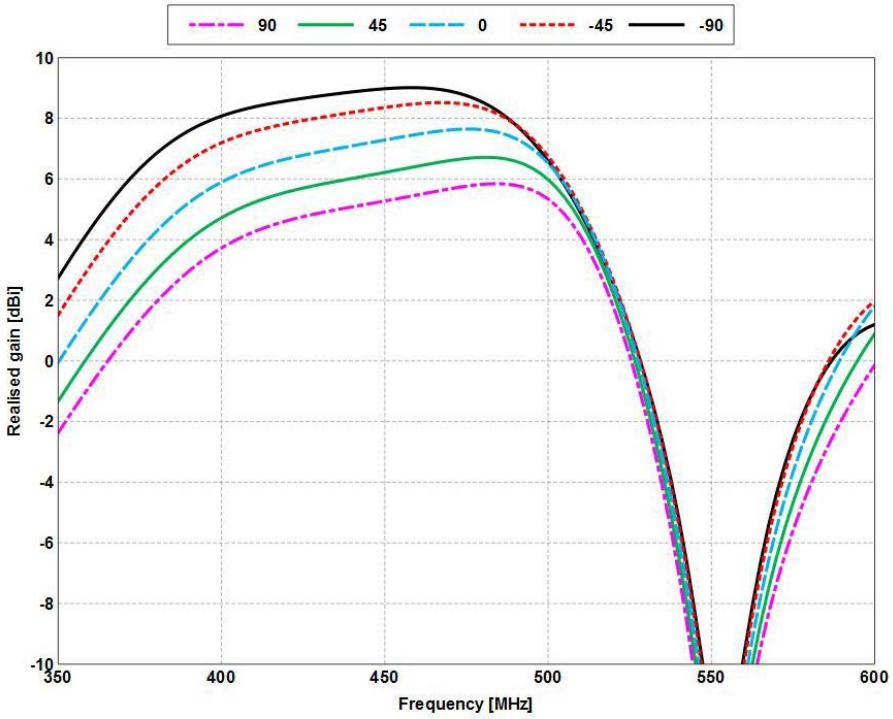

Fig. 31 The realized gain ($\theta = 90°$, $\phi = 0°$) vs. frequency for the reflection-phase dipoles with resonant lengths scaled to 450 MHz in the presence of the 4 × 4 thin-gap EBG

The same procedure was repeated for the scattered-phase dipoles with the exception of the –90° dipole as its reflection coefficient was already near 450 MHz. As said before, the dipole lengths are scaled according to an integer multiple of a common scale frequency of 65 MHz. Figure 32 shows the reflection coefficient for the scaled dipoles, where the 4 dipoles that were scaled are now matched but not at 450 MHz with the exception of the –45° dipole. The reflection coefficients are more tightly grouped for the scattered-phase dipoles compared to the reflection coefficients of the reflection-phase dipoles in Fig. 28. As with the reflection-phase dipoles, the plateau in the resistance (Fig. 33a) shows a broad match to 50 Ω, but only the –45° dipole is resonant in the band of that plateau (Fig. 33b). The other dipole resonant lengths have been reduced too much, so that a larger impedance bandwidth cannot be obtained. While the scattered-phase dipoles may not be well matched at the target frequency, there is much less variation in the radiation pattern compared to the reflection-phase dipoles (Fig. 34) and the gain levels (Fig. 35) vary less as well.

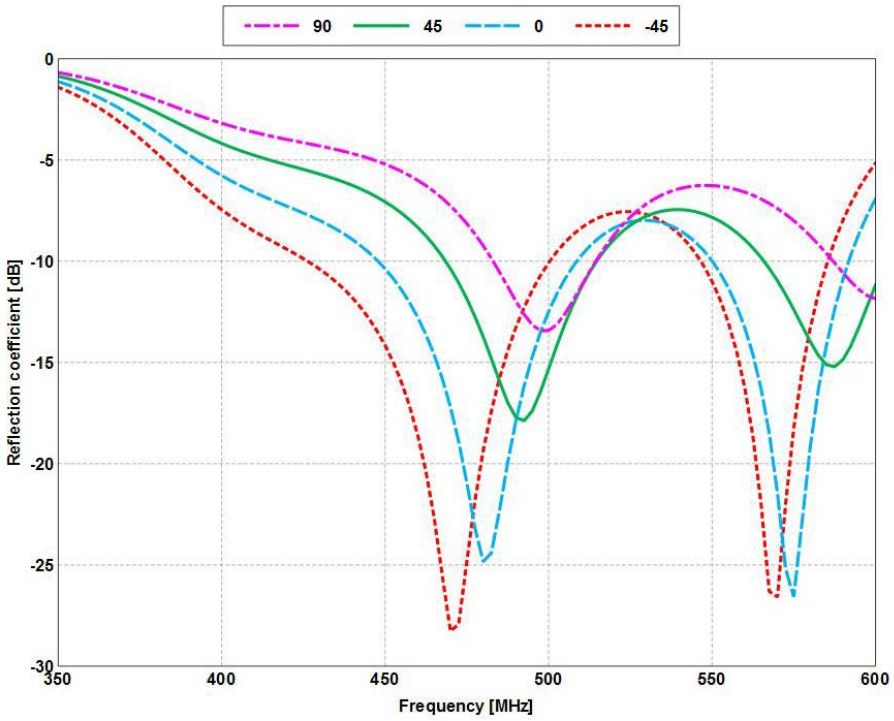

Fig. 32 The reflection coefficient for the scattered-phase dipoles with resonant lengths scaled to 450 MHz in the presence of the 4 × 4 thin-gap EBG

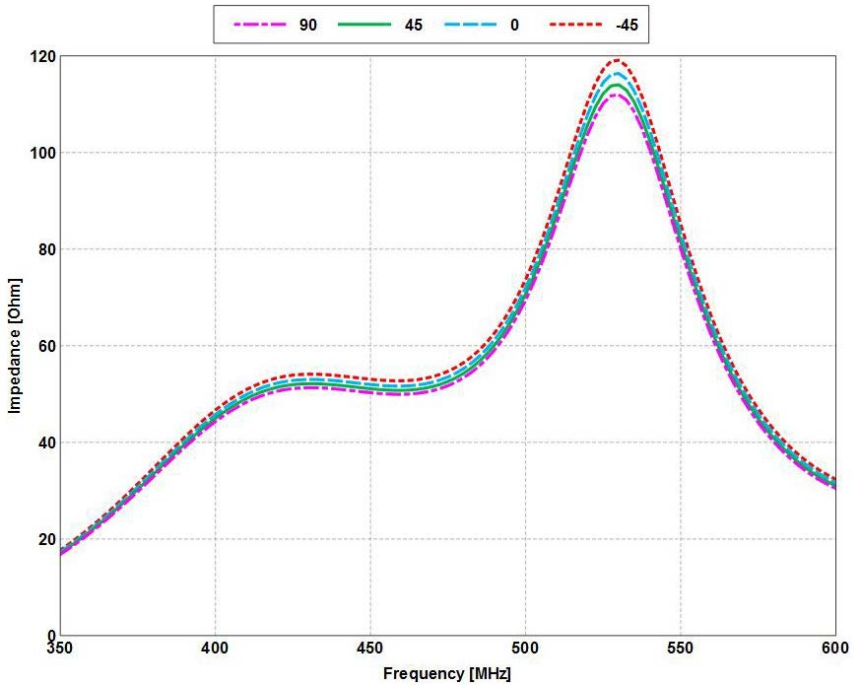

a)

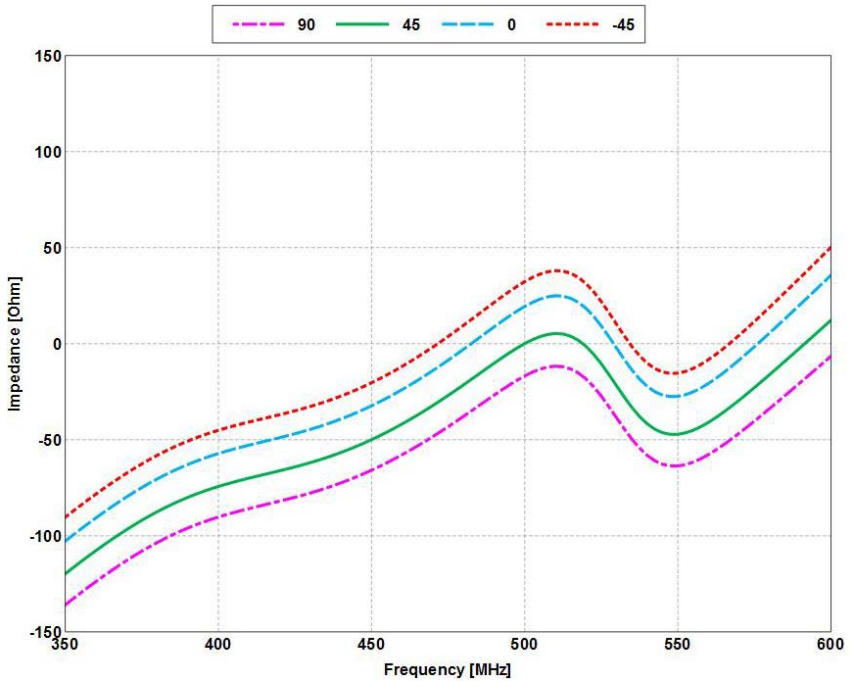

b)

Fig. 33 a) The input resistance for the scattered-phase dipoles with resonant lengths scaled to 450 MHz in the presence of the 4 × 4 thin-gap EBG. b) The input reactance for the scattered-phase dipoles with resonant lengths scaled to 450 MHz in the presence of the 4 × 4 thin-gap EBG.

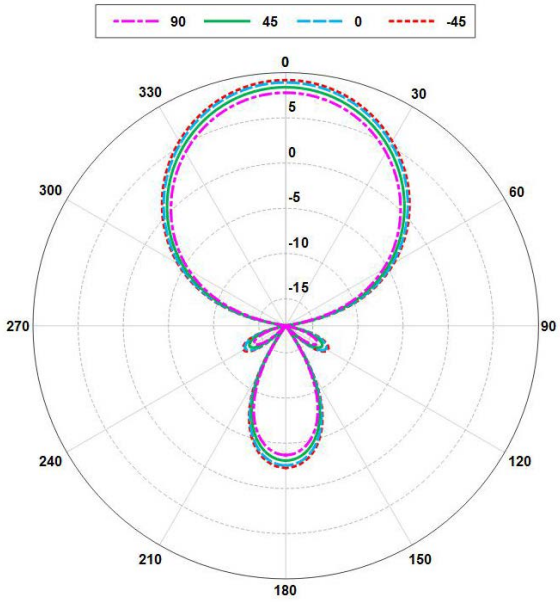

a)

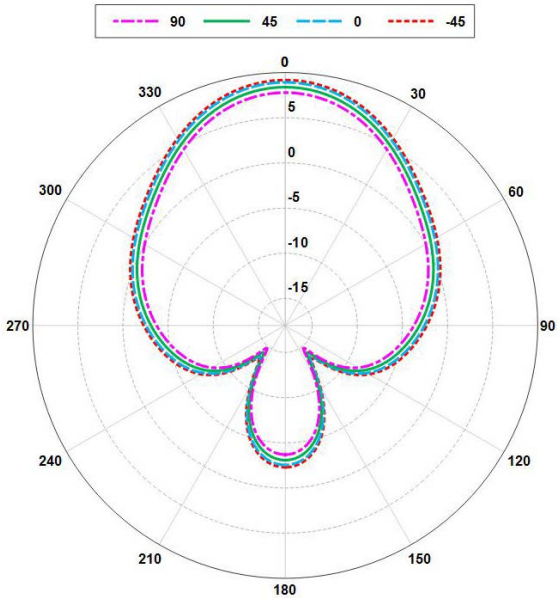

b)

Fig. 34 The realized gain pattern for the scattered-phase dipoles with resonant lengths scaled to 450 MHz in the presence of the 4 × 4 thin-gap EBG. a) E-plane and b) H-plane.

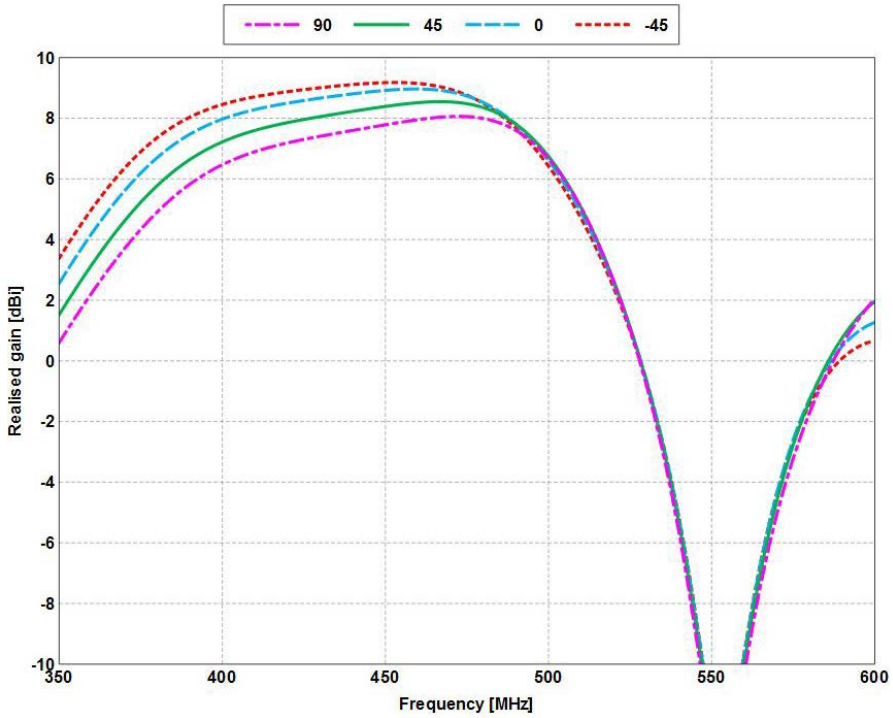

Fig. 35 The realized gain ($\theta = 90°$, $\phi = 0°$) vs. frequency for the scattered-phase dipoles with resonant lengths scaled to 450 MHz in the presence of the 4 × 4 thin-gap EBG

Comparing the reflection-phase results to the scattered-phase results, from a simulation standpoint, it is obvious that it is the phase of the NFs of the EBG that need to be considered for antenna applications. If the typical bandwidth range is used (0° ± 90°) then the reflection-phase would determine the bandwidth to be over the frequency range of 264–417 MHz, yet, when dipoles that are resonant at the frequencies corresponding to particular phase angles within this range are not matched where it would be expected (0° should give the best results), then it is questionable to suppose that the reflection-phase is indeed the best determination of the EBG's bandwidth for antenna applications. Instead, the scattered-phase gave a better estimation of what frequency range would be of benefit to the strip dipole as the frequency range determined by the antenna dependent finite model (0° ± 90°) is 323–474 MHz, and the dipoles that were designed for particular phase frequencies within the range showed better simulation results.

4.2 Wide-Gap EBG

In this section, the EBG from Section 4.1 is modified slightly by scaling the gap by the same factor as the patches so that the gap width is about an order of magnitude smaller than the patch width or $g = \frac{\lambda_{450}}{45}$. The same analysis that was done in Section 4.1 for the thin-gap EBG is repeated for the wide-gap EBG.

4.2-1 EBG Analysis: Wide Gap

Just as with the thin gap EBG, the analytical and numerical models show a wide range of differences, but the TLM, PBC, and NEF show better agreement (Fig. 36). Unlike with the thin-gap EBG, the TLM shows better agreement with PBC and NEF instead of the no-gap CM. Here, all 3 circuit models show poor agreement, and given the relative good agreement seen for the TLM in Fig. 19, the preferred analytical model for estimating the reflection phase would be the TLM. This implies that the analytical models are best for large-gap widths, given the equation's dependency on logarithmic and inverse hyperbolic functions that decrease rapidly with small arguments. The NEF analysis shows an even greater dissimilarity to the PBC when the dipole is not included, but when the dipole is included, the PBC and NEF with dipole more closely agree. However, the NEF with dipole now shows a much smaller bandwidth than the PBC in all phase range cases but most significant at 0° ± 90° (217 versus 150 MHz), see Table 5.

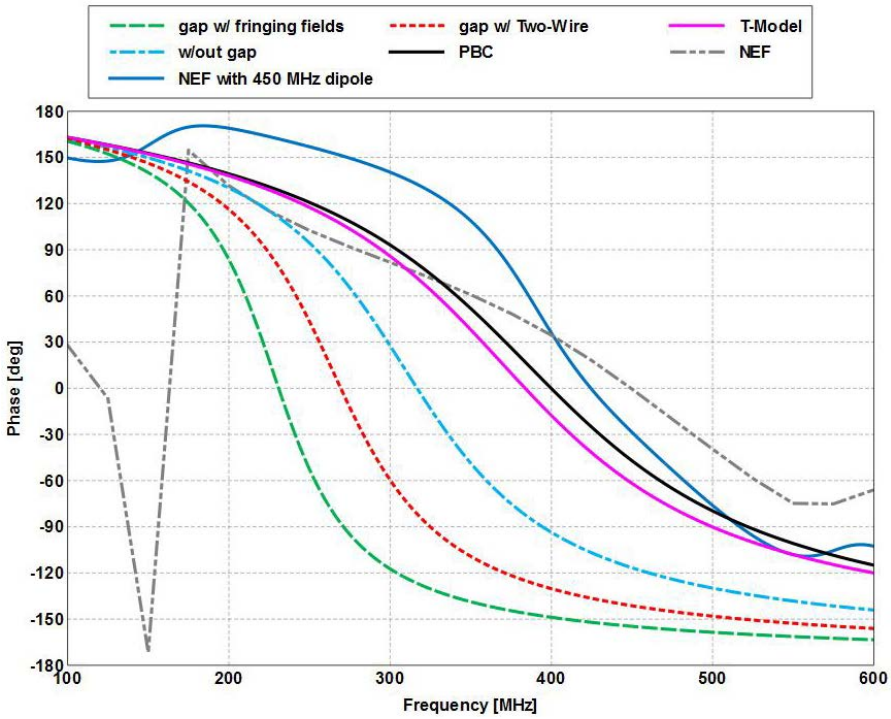

Fig. 36 The results from the analytical and numerical models for the 4 × 4 wide-gap EBG

Table 5 The phase ranges, frequency ranges and associated bandwidths for the 4 × 4 wide-gap EBG determined by the PBC and NEF with dipole simulations

Phase Range (deg)	Frequency Range (MHz)		Bandwidth (MHz)	
	PBC	NEF with Dipole	PBC	NEF with Dipole
0° ± 90°	304 – 521	367 – 517	217	150
0° ± 45°	357 – 447	395 – 467	90	72
90° ± 45°	213 – 357	312 – 395	144	83

4.2.2 Strip Dipole Analysis: Wide Gap

The same procedure used in Section 4.1.2 is repeated in this section for the wide-gap EBG. Table 6 lists the intended phase angles and the corresponding frequencies determined from the PBC phase (reflection-phase) and those determined using the NEF with dipole phase (scattered-phase). The reflection coefficients for the reflection-phase dipoles look to be near evenly spaced (Fig. 37). The separation between each reflection coefficient is about 50 MHz, with the exception of the –90° dipole, which is larger. Also, the dipoles that are resonant in the negative reflection-phase regime are now matched unlike with the reflection-phase dipoles in the presence of the thin-gap EBG where only the –90° dipole was matched. The higher resonance at 550 MHz has either disappeared or has been shifted to a higher frequency. The plateau seen in the resistance for the resonant dipoles in the presence of the thin gap EBG is no longer present for dipoles in the presence of the wide-gap EBG (Fig. 38a), which results in a narrower impedance bandwidth.

The magnitude of the resistance is largest for the positive reflection-phase dipoles and is smallest for the negative reflection-phase dipoles, suggesting that the higher frequency dipoles are either moving into or are within the frequency range of the EBG that is beneficial to the antenna performance. This behavior can also be seen in the input reactance of the reflection-phase dipoles (Fig. 38b), where the slopes are flatter for the negative reflection-phase dipoles. The radiation patterns vary less for the reflection-phase dipoles in the presence of the wide-gap EBG than the thin-gap EBG (Fig. 39). The dipole gains are still improved by as much as 6.5 dBi, but the pattern distortions in the H-plane are now more noticeable than in Fig. 22b. The 1-dBi realized gain bandwidth has now decreased with the widening of the gap (Fig. 40). This is to be expected given that the 50-Ω plateau in the

resistance is no longer present. The decrease in realized gain is due to the decreased impedance bandwidth. The realized gain bandwidth is still wider than the impedance bandwidth however, by about 10 MHz.

Table 6 The frequencies corresponding to particular reflection-phase angles and scattered-phase angles for the 4 × 4 wide-gap EBG

Phase (deg)	PBC (MHz)	NEF (MHz)
+90°	304	367
+45°	357	395
0°	400	424
–45°	447	467
–90°	521	517

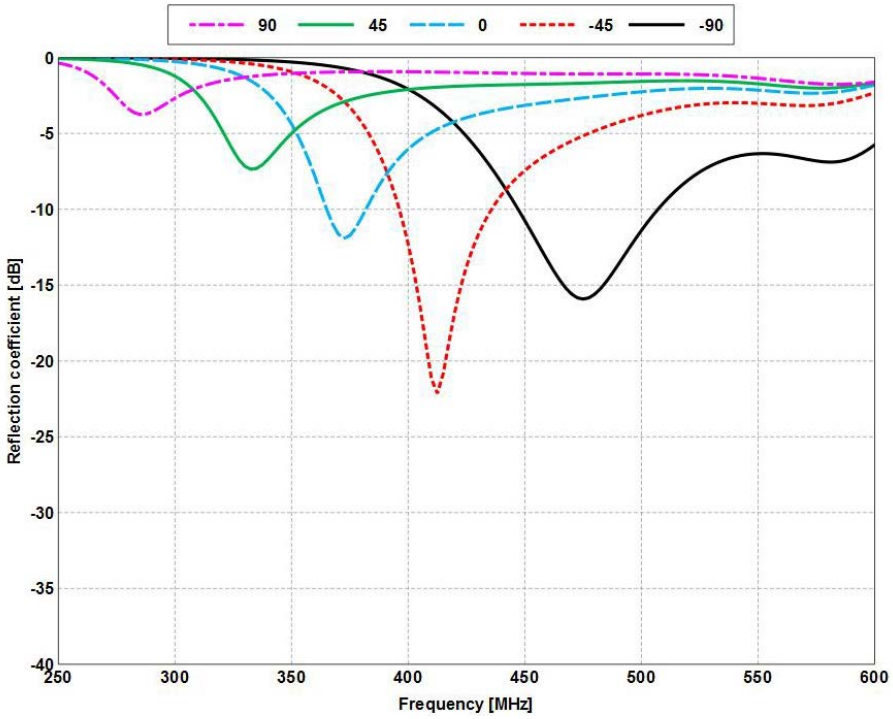

Fig. 37 The reflection coefficient for the resonant strip dipoles designed for the reflection-phase angles over the 4 × 4 wide-gap EBG

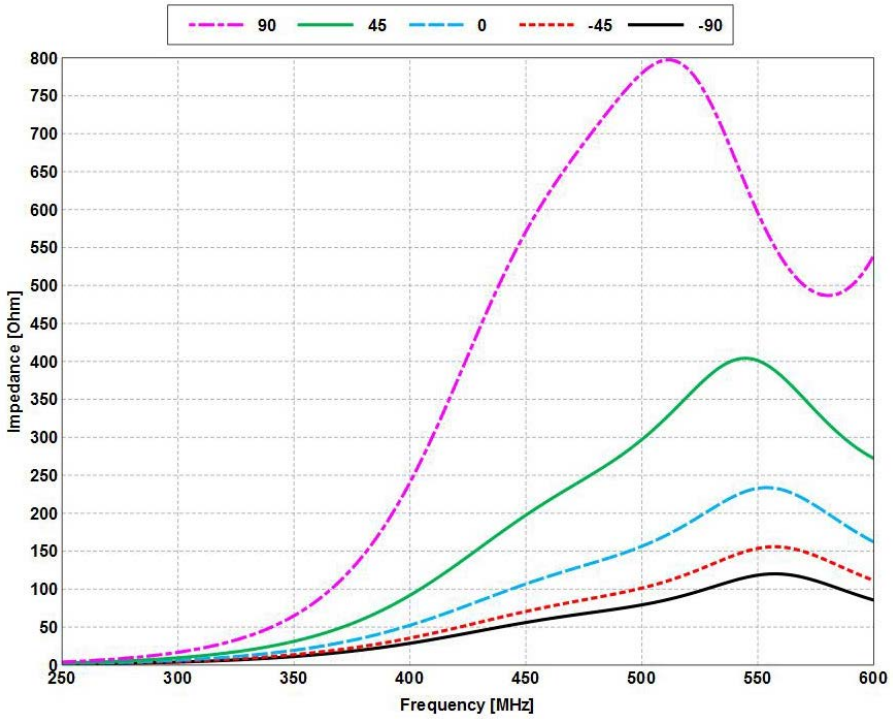

a)

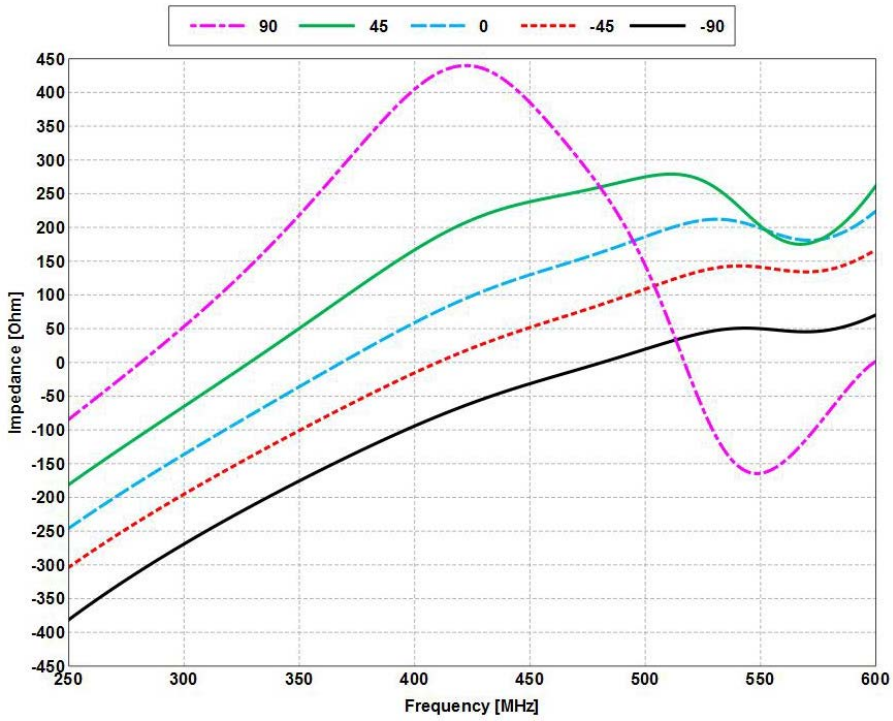

b)

Fig. 38 a) The input resistance for the resonant strip dipoles designed for the reflection-phase angles over the 4 × 4 wide-gap EBG. b) The input reactance for the resonant strip dipoles designed for the reflection-phase angles over the 4 × 4 wide-gap EBG.

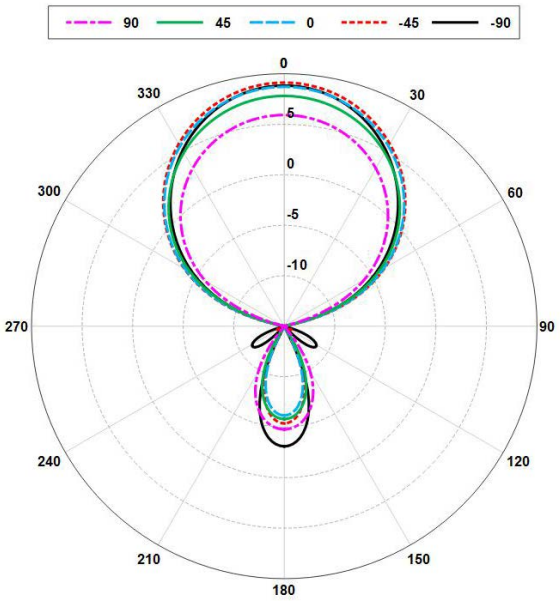

a)

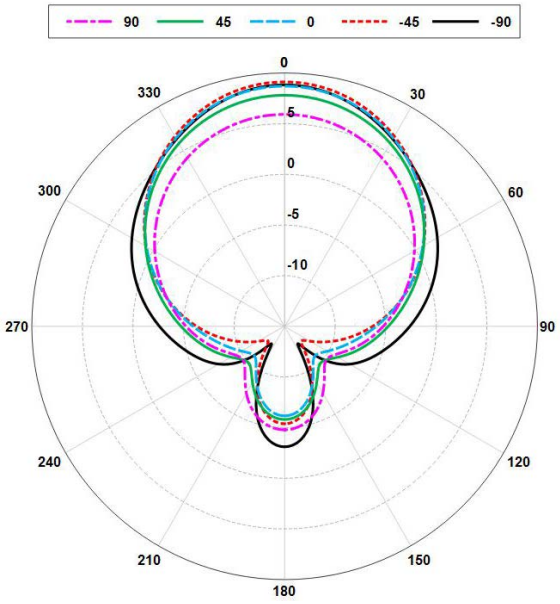

b)

Fig. 39 The realized gain patterns for the resonant strip dipoles designed for the reflection-phase angles over the 4 × 4 wide-gap EBG. a) E-plane and b) H-plane.

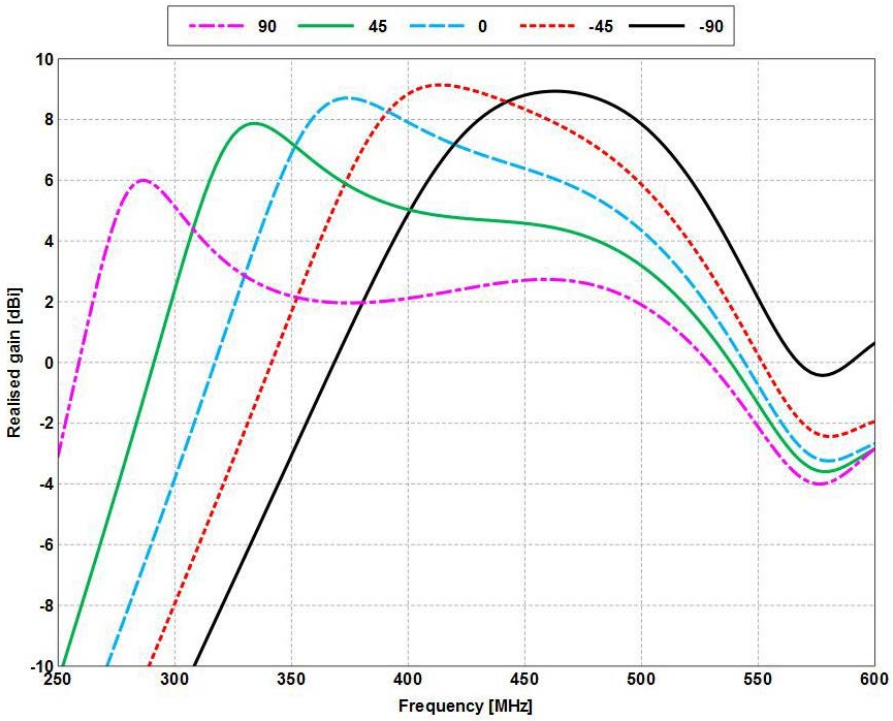

Fig. 40 The realized gain ($\theta = 90°$, $\phi = 0°$) vs. frequency for the resonant strip dipoles designed for the reflection-phase angles over the 4 × 4 wide-gap EBG

For the scattered-phase dipoles, only +90° is not matched per the reflection coefficient (Fig. 41) unlike the reflection-phase dipoles where only 3 of the dipoles were matched. The dipole resonant frequencies are well spaced by about 25–30 MHz and show decreased impedance bandwidth compared to the scattered-phase dipoles in the presence of the thin-gap EBG. Just as with the reflection-phase dipoles, the plateau in the resistance is no longer present (Fig. 42a), nor are the slopes for the reactance as flat (Fig. 42b) compared to the thin-gap case. The near constant separation between the dipole resonances is clearer in the reactance.

There is less variation in the radiation pattern compared to the reflection-phase dipoles in the presence of the wide-gap EBG and also compared to the scattered-phase dipoles in the presence of the thin-gap EBG (Fig. 43). Figure 44 shows the bore sight realized gain ($\theta = 90°$, $\phi = 0°$) versus frequency. The gain curves are more tightly grouped than the realized gain versus frequency curves for the reflection-phase dipoles, showing again that the scattered-phase better determines the frequency range for the EBG that is beneficial to the strip dipole performance. Table 7 summarizes the new frequencies for the best impedance match and the shift in frequency due to the loading effect.

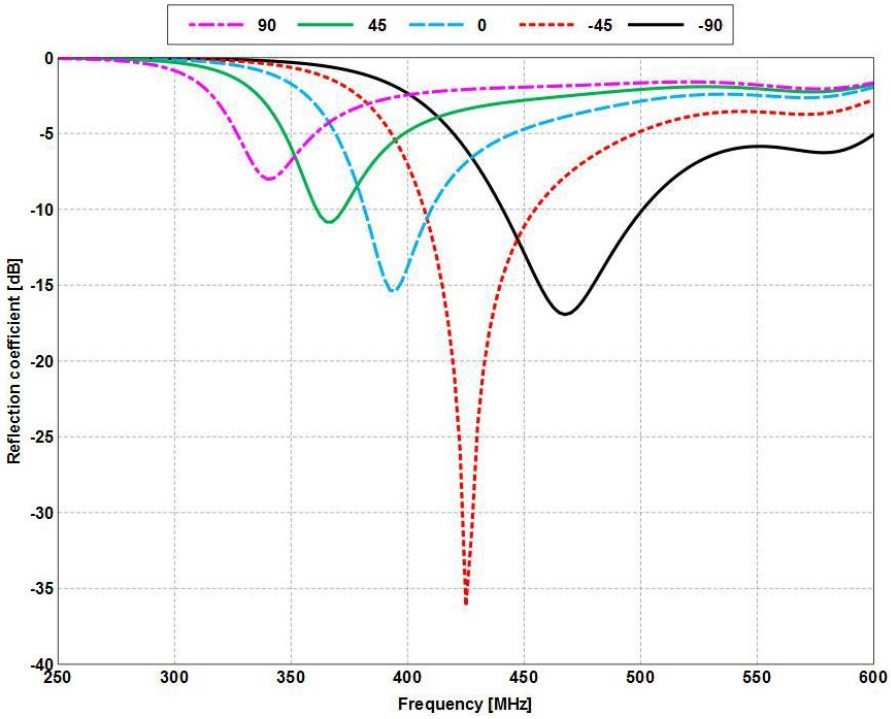

Fig. 41 The reflection coefficient for the resonant strip dipoles designed for the scattered-phase angles over the 4 × 4 wide-gap EBG

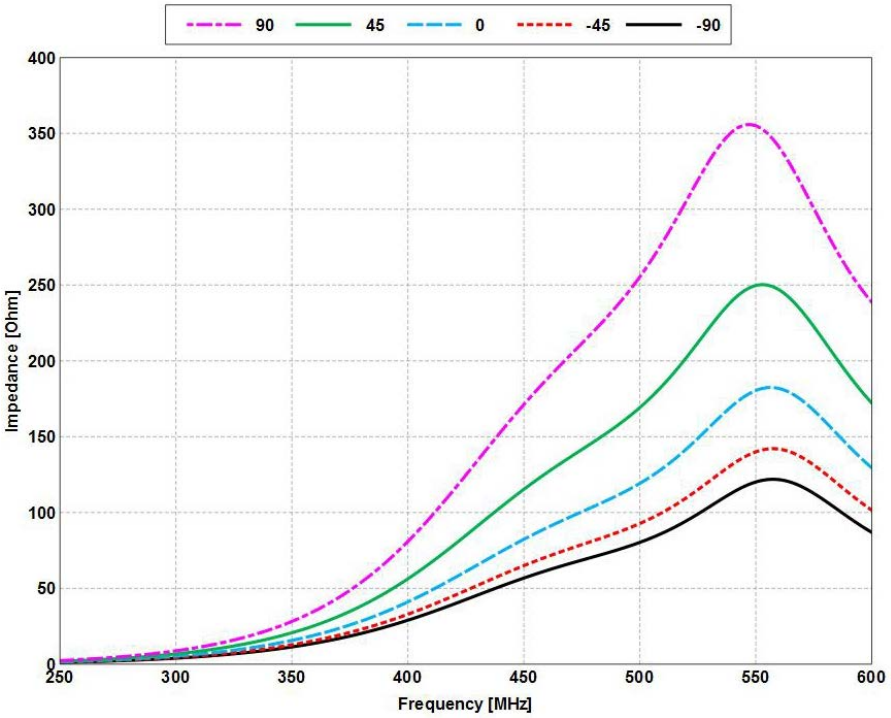

a)

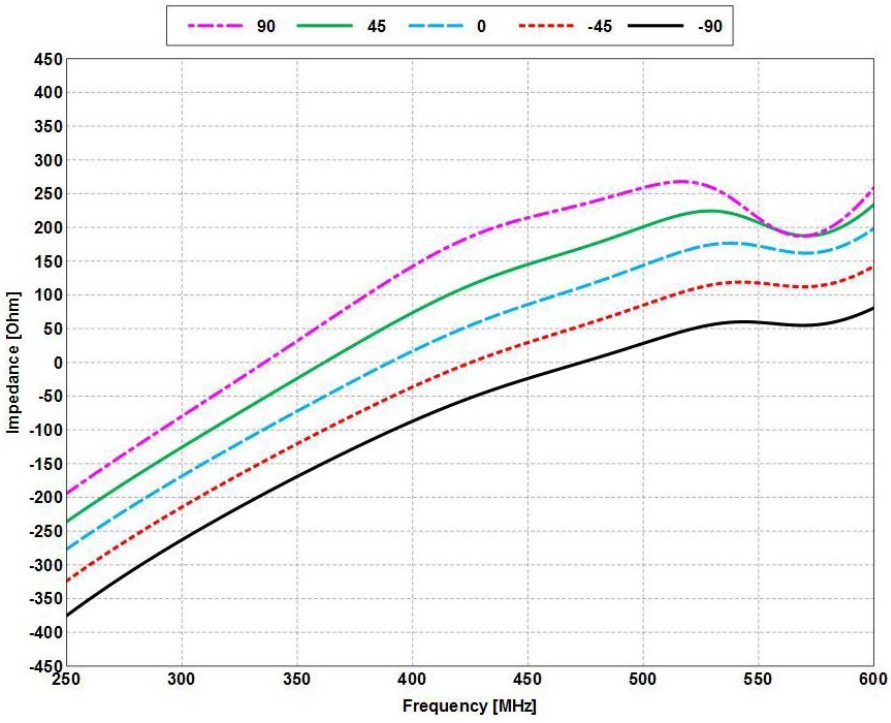

b)

Fig. 42 a) The input resistance for the resonant strip dipoles designed for the reflection-phase angles over the 4 × 4 wide-gap EBG. b) The input reactance for the resonant strip dipoles designed for the reflection-phase angles over the 4 × 4 wide-gap EBG.

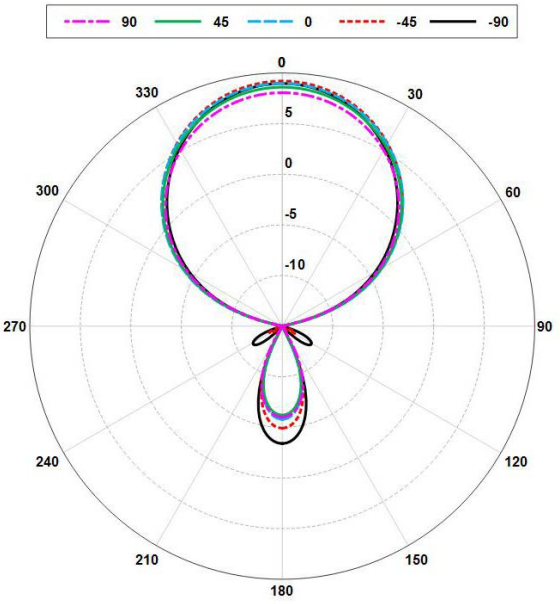

a)

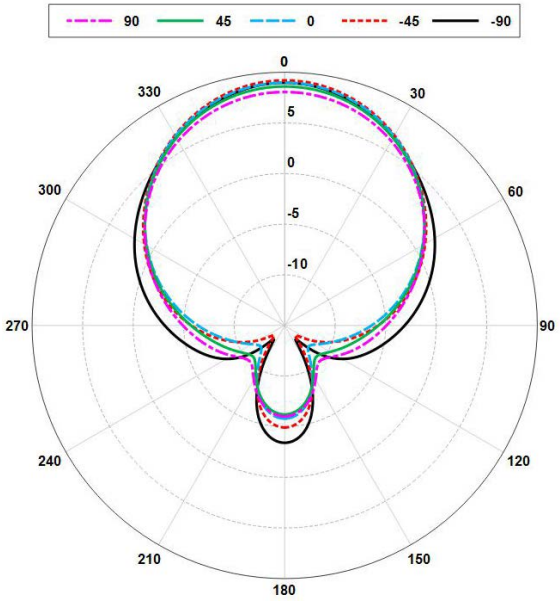

b)

Fig. 43 The realized gain patterns for the resonant strip dipoles designed for the reflection-phase angles over the 4 × 4 wide-gap EBG. a) E-plane and b) H-plane.

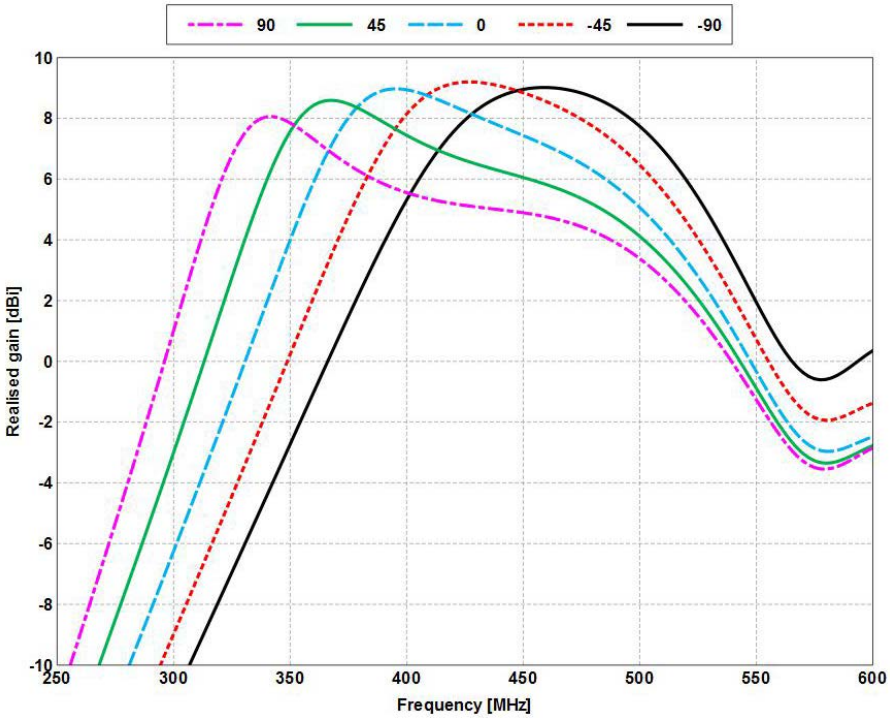

Fig. 44 The realized gain ($\theta = 90°$, $\phi = 0°$) vs. frequency for the resonant strip dipoles designed for the reflection-phase angles over the 4 × 4 wide-gap EBG

Table 7 The frequency shift amount due to the loading effect and the dipole resonant frequencies in the presence of the 4 × 4 wide-gap EBG

Phase (deg)	PBC (MHz)	Δf (MHz)	NEF (MHz)	Δf (MHz)
+90°	285	19	340	27
+45°	333	24	368	27
0°	373	27	424	29
–45°	413	34	425	42
–90°	475	46	468	49

The wide-gap EBG appears to have the same effects as the thin-gap EBG on the strip dipoles with the exception that the thin-gap EBG offered a wider impedance bandwidth, which led to a wider 1 dBi realized gain bandwidth. The pattern distortions in the H-plane were also not as prevalent in the wide-gap EBG as they were in the thin-gap EBG. It is possible that the smaller predicted EBG bandwidth by the NEF with dipole simulations for the wide-gap EBG is somehow correlated to the smaller impedance bandwidths for the strip dipoles, but to be certain would require more study. However, the simulations do suggest that to maximize the

benefit of an EBG for a strip dipole, a thin gap on the order of $\frac{\lambda}{150}$ would be recommended for maximum impedance bandwidth as there is no particular downside to using a thinner-gap EBG, only an upside.

4.2-3 Strip Dipole Scalability: Wide Gap

Because the wide gap EBG led to a more uniform spacing for both the reflection-phase and scattered-phase dipole reflection coefficients, it is expected that all of the dipoles will scale much more linearly in the presence of the wide-gap EBG. The method used for scaling the dipole lengths is the same as in Section 4.1.3 except that the common frequency scale factor is now 40 MHz for the reflection-phase dipoles and 42 MHz for the scattered-phase dipoles. The reflection-phase dipoles scale very well, and look to have done so linearly, as can be seen in the reflection coefficient (Fig. 45). Each of the dipoles are well matched at 450 MHz with the farthest outlier (90°) lying about 20 MHz away from the target frequency. The resistance (Fig. 46a) and reactance (Fig. 46b) support how well the dipoles scaled as all of the curves lie over one another. To further show how linearly the dipoles scaled, the radiation patterns (Fig. 47) show near zero variation that can be seen in the realized gain ($\theta = 90°,\ \phi = 0°$) versus frequency plot in Fig. 48.

The scattered-phase dipoles also scaled better than their thin-gap EBG counterparts, but they did not scale as well as the reflection-phase dipoles did in the presence of the wide-gap EBG. Note that the –90° dipole was not scaled because it was already matched at the desired frequency. The 4 dipoles that were scaled are matched, with 3 of the 4 (+45°, 0°, and –45°) matched at the desired frequency (Fig. 49). The +45° and +90° scattered-phase dipoles were shortened too much in the scaling process, although from the resistance and reactance, the overcompensation was not large (Fig. 50a and b). A small adjustment of the +45° and +90° dipole lengths would render them in line with the other dipoles. The radiation patterns show even less variation between the 4 dipoles, even for the farthest outlier at +90°. All 4 dipoles show the expected directive patterns in both the E-plane and H-plane, though the beginnings of pattern distortion show in the H-plane at $\theta = 60°, 300°$ (Fig. 51). The realized gain versus frequency plot (Fig. 52) shows that the overcompensation for the +45° dipole was not too far off the mark, where some adjustment would be required for the +90° dipole.

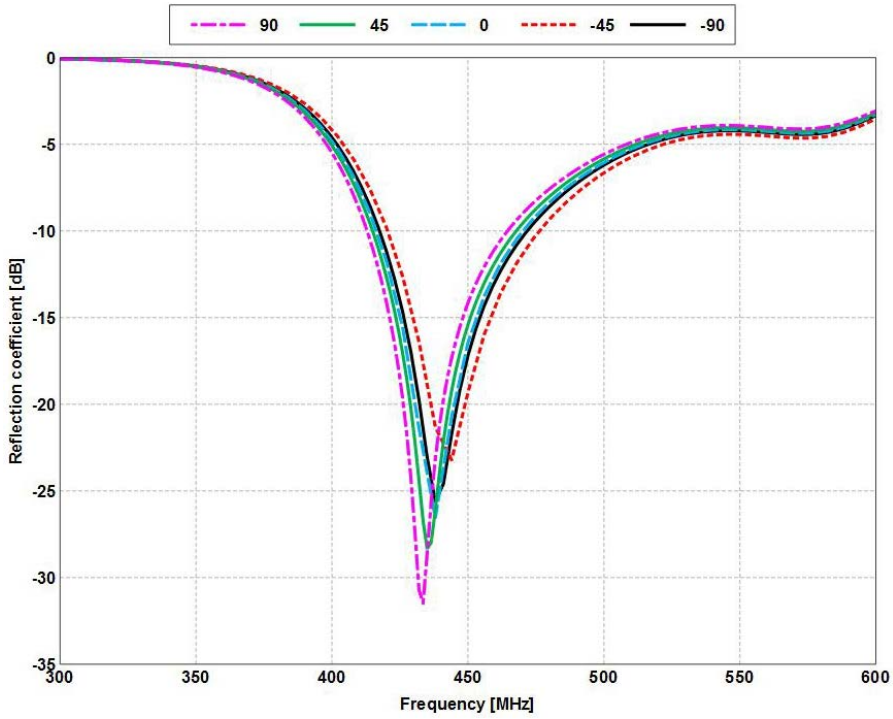

Fig. 45 The reflection coefficient for the reflection-phase dipoles with resonant lengths scaled to 450 MHz in the presence of the 4 × 4 wide-gap EBG

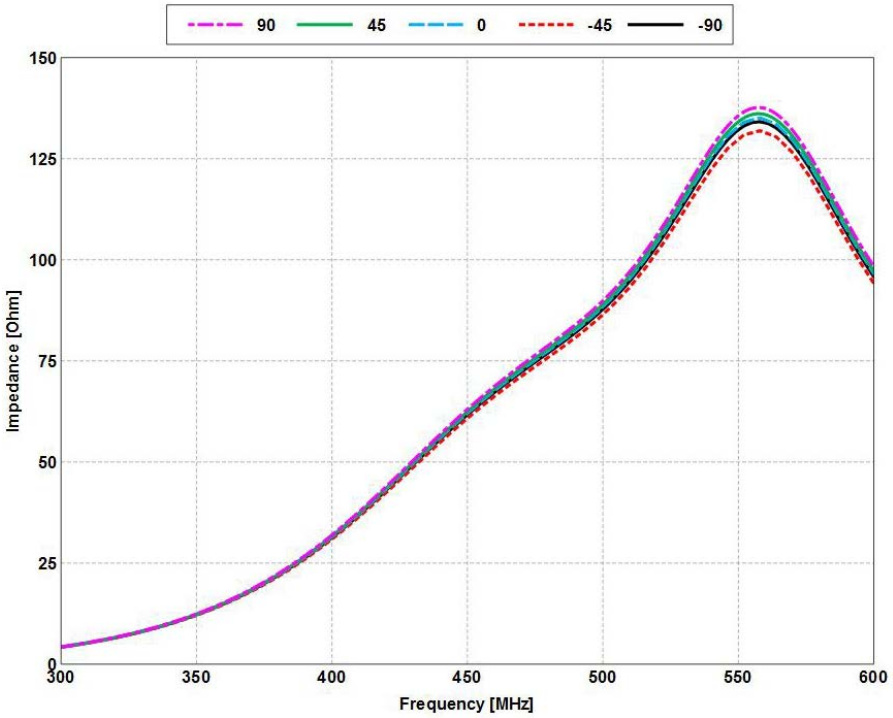

a)

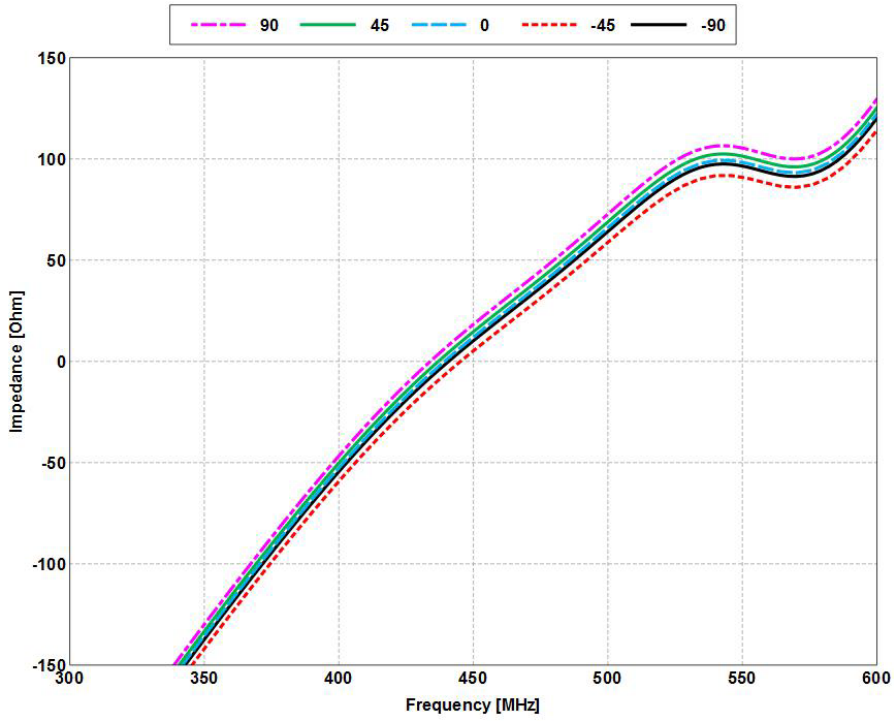

b)

Fig. 46 a) The input resistance for the reflection-phase dipoles with resonant lengths scaled to 450 MHz in the presence of the 4 × 4 wide-gap EBG. b) The input reactance for the reflection-phase dipoles with resonant lengths scaled to 450 MHz in the presence of the 4 × 4 wide-gap EBG.

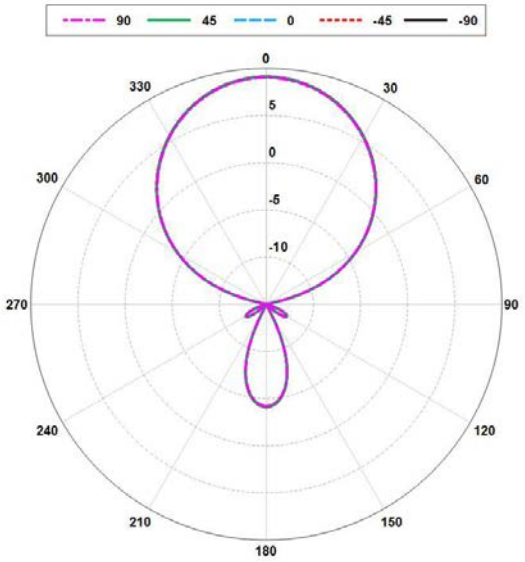

a)

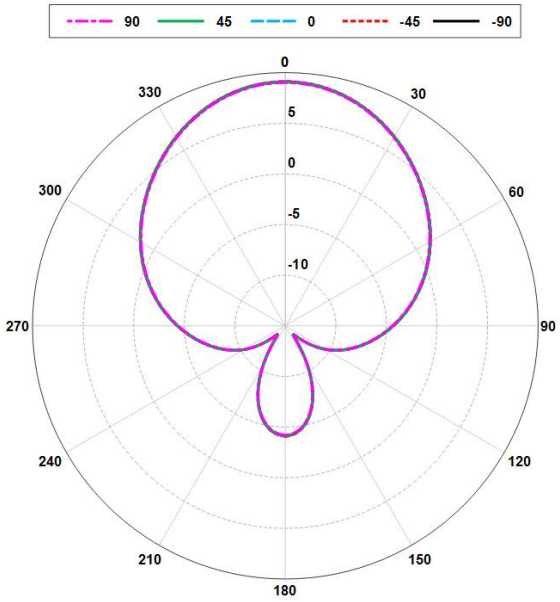

b)

Fig. 47 The realized gain patterns for the reflection-phase dipoles with resonant lengths scaled to 450 MHz in the presence of the 4 × 4 wide-gap EBG. a) E-plane and b) H-plane.

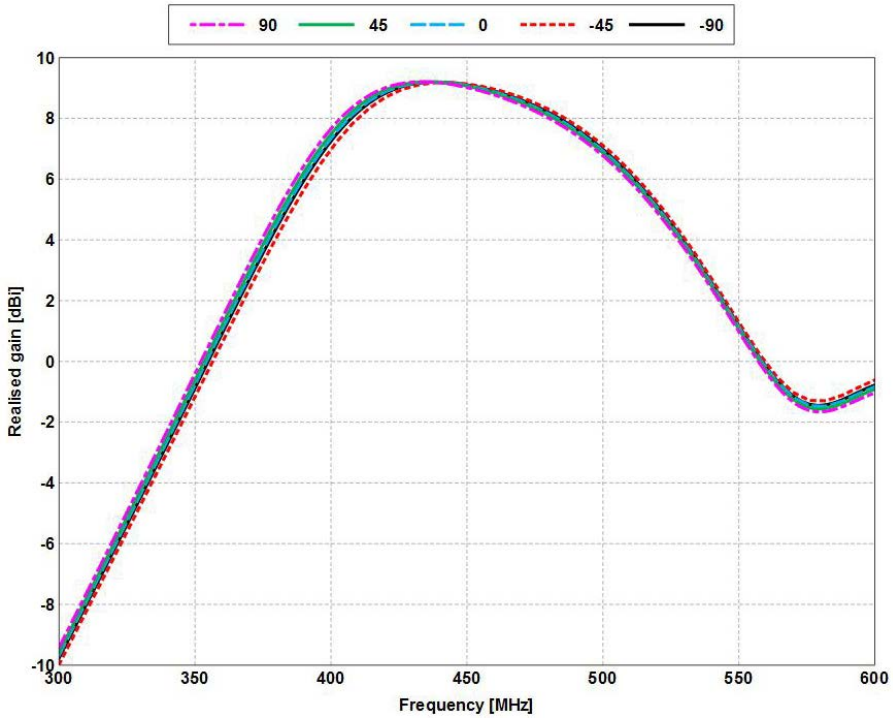

Fig. 48 The realized gain ($\theta = 90°$, $\phi = 0°$) vs. frequency for the reflection-phase dipoles with resonant lengths scaled to 450 MHz in the presence of the 4 × 4 wide-gap EBG

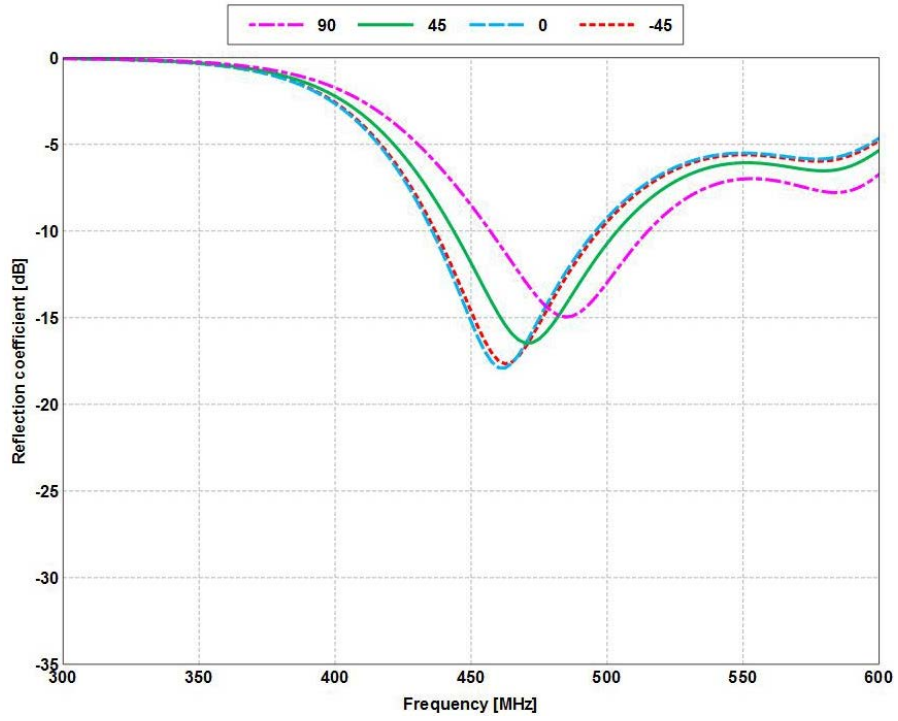

Fig. 49 The reflection coefficient for the scattered-phase dipoles with resonant lengths scaled to 450 MHz in the presence of the 4 × 4 wide-gap EBG

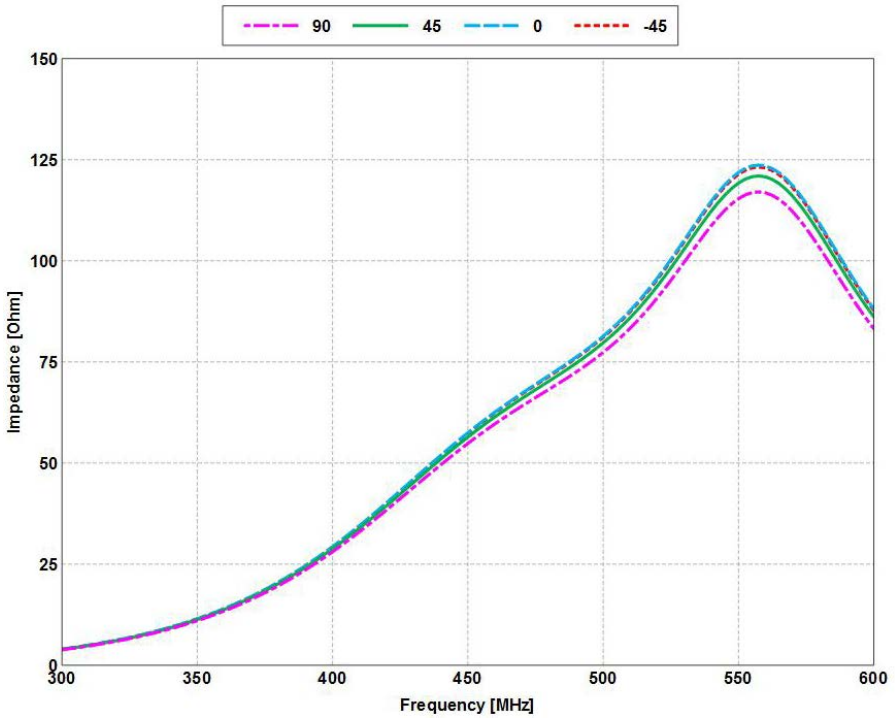

a)

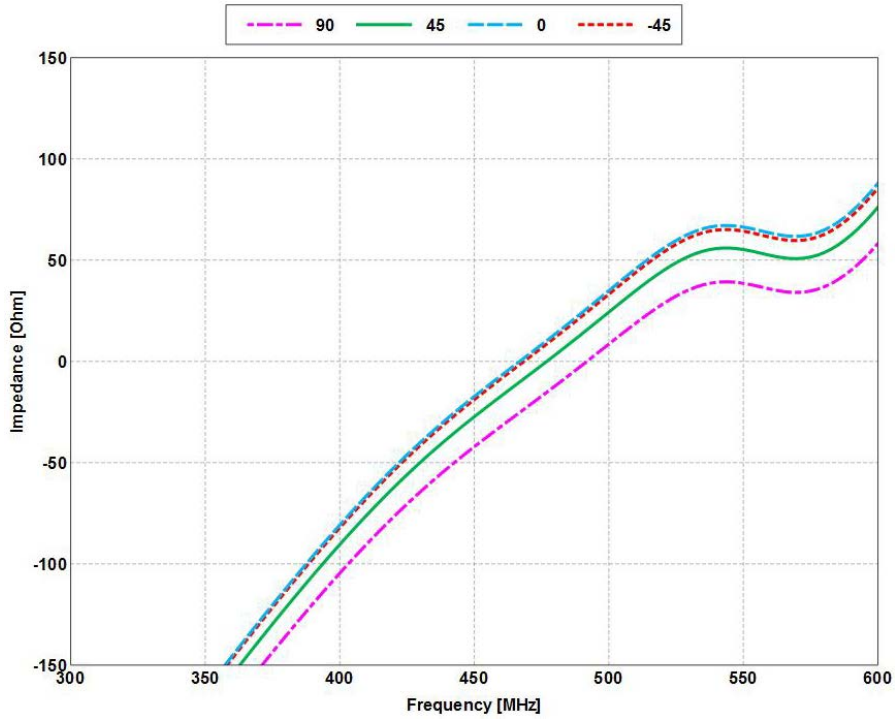

b)

Fig 50 a) The input resistance for the scattered-phase dipoles with resonant lengths scaled to 450 MHz in the presence of the 4 × 4 wide-gap EBG. b) The input reactance for the scattered-phase dipoles with resonant lengths scaled to 450 MHz in the presence of the 4 × 4 wide-gap EBG.

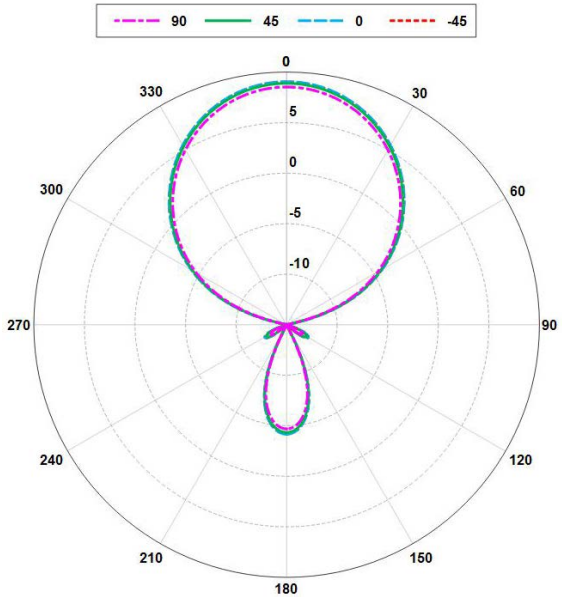

a)

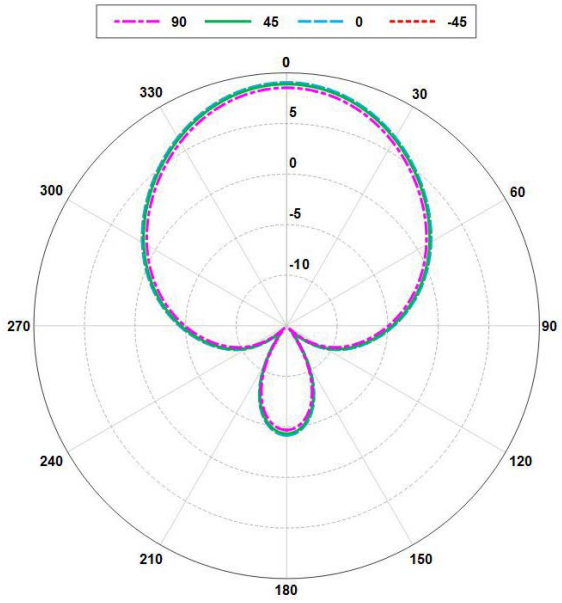

b)

Fig. 51 The realized gain patterns for the scattered-phase dipoles with resonant lengths scaled to 450 MHz in the presence of the 4 × 4 wide-gap EBG. a) E-plane and b) H-plane.

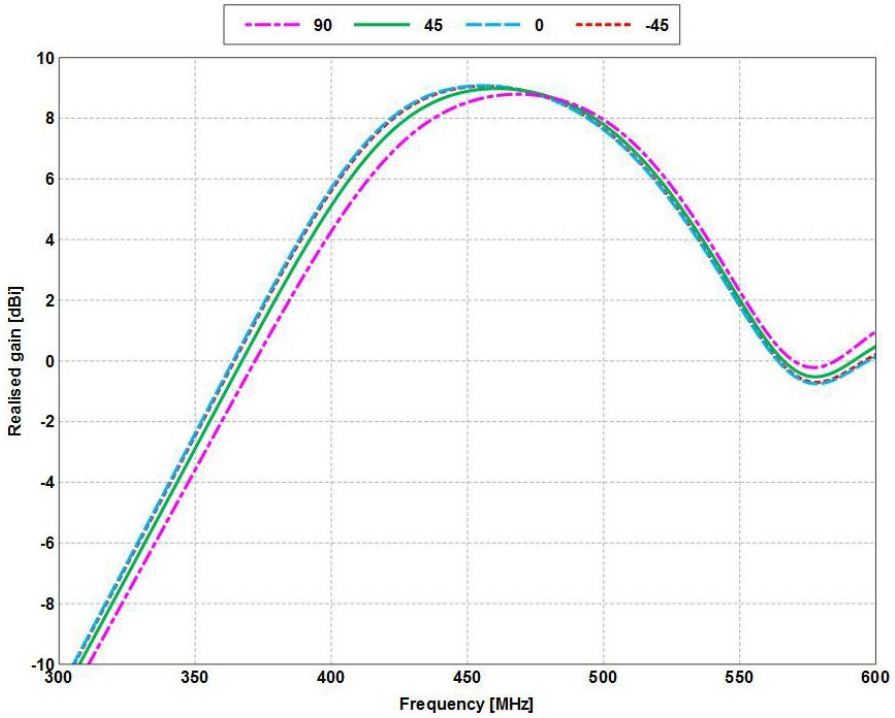

Fig. 52 The realized gain ($\theta = 90°$, $\phi = 0°$) vs. frequency for the scattered-phase dipoles with resonant lengths scaled to 450 MHz in the presence of the 4 × 4 wide-gap EBG

4.3 Thin-Gap EBG versus Wide-Gap EBG

Both the thin- and wide-gap EBGs functioned as desired for improving the performance of a strip dipole. The analysis of the 2 EBG's was straightforward, with the TLM being the more consistent of the 2 analytical models. The change in gap width had little effect on the results of the TLM unlike the CM, but the CM does allow for a rough analytical estimation for the operational EBG bandwidth (CM_{BW} = 140 MHz vs. TLM_{BW} = 129 MHz vs. PBC_{BW} = NEF_{BW} = 153 MHz for the thin-gap EBG). For the 2 numerical models, the reflection-phase did not accurately determine the frequency range for the operational bandwidth of the thin-gap EBG, but was more accurate for the wide-gap EBG, although it seemed to overestimate the size of the operational bandwidth. In both EBG cases, simulating the finite structure with the strip dipole resulted in a scattered-phase curve that better determined over what frequency range the strip dipole should be designed. However, neither numerical approach can give insight to the effect that the 2 EBGs would have on the strip dipole, but can provide a good starting point for numerical simulations.

Both EBGs improved the strip dipole performance by increasing the impedance bandwidth, realized gain bandwidth, pattern shape, and peak realized gain. Using a very thin-gap width significantly improved the dipole impedance bandwidth (and

realized gain bandwidth), because of the 50-Ω plateau in the resistance, without any significant drawbacks, which means that it would be beneficial to use thin gaps instead of wide gaps. The wide-gap EBG did allow the dipoles to scale more linearly, but given that additional adjustment to the dipole lengths would require a trial and error method or optimization, there still is not much of a reason to use a wider gap for the EBG.

At higher frequencies, the H-plane radiation pattern showed distortion (see Section 6). The distortion is due to a higher order mode of the EBG being excited by the dipole, resulting in a quadrupole pattern. The most important impact of the EBG on the dipole impedance is the inductive loading. The inductive nature of the EBG is explained from the CM equations for the inductance and capacitance, Eqs. 1 and 2. The inductance for this EBG would be calculated to be much larger than the capacitance, resulting in a structure that behaves like an inductive load. Adding a dielectric substrate or vias can change this behavior, but more will be said on this in Section 6.

The last point to make is that the strip dipoles that reference the positive phase angles (for both the reflection-phase and scattered-phase) were not well matched (if at all) when in the presence of either EBG, yet the dipoles that reference the negative phase angles were well matched but showed pattern distortion at higher frequencies (corresponding to more negative phase angles). The different behavior between the positive and negative phase angles suggest 2 regimes of behavior for the strip dipole excited EBG: pseudo-PEC in the positive phase regime and pseudo-AMC in the negative phase regime. These effects were also seen in Best and Hanna (2008) and mentioned in Kern et al. (2005).

5. Discussion of EBG Models and Design Guidelines

Given how ambiguous EBG design can be, this section will present a guideline for how to design a functional EBG for a dipole antenna. This section will give suggestions for what modeling method to use and justifications for particular design parameters based on the results from Section 4. It will also discuss EBG bandwidth based on the phase characteristic and actual impact on the performance of a strip dipole. The EBG's operational bandwidth will be determined specifically for a strip dipole, highlighting the dependency of the EBG's bandwidth for antenna applications on the antenna to be used.

5.1 Analytical and Numerical Models

For every engineering design problem, it is necessary to have a good analytical model to begin with even if the results from the analytical model may not agree with simulation results as well as desired. For EBG design, the 2 analytical models presented in this report, CM and TLM, are popular for their simplicity and rudimentary accuracy. While using both models at the same time can possibly give greater insight into the design of an EBG, such as predicting a particular loading behavior for certain physical aspects, this report clearly shows that the TLM is the better analytical model to choose as it had the most consistent results for variations of the EBG parameters (in this case, the dependence on the gap width). The TLM is limited in estimating the EBG bandwidth size since an iterative solver is required to solve the transcendental equation. Whereas the CM can easily and relatively accurately estimate the bandwidth impedance with only a few equations.

Comparing the simulation results for the 2 numerical models, PBC and NEF, the results for the NEF standout in that for both the thin- and wide-gap EBGs, the frequency range for the EBG bandwidth and the size of the EBG bandwidth were more accurately determined compared to PBC. Comparing the 2 numerical models is analogous to comparing green apples to red apples. Both the PBC and the NEF characterize the EBG structure by the phase of some reflected field, but for the PBC, that phase is the phase of the reflection coefficient whereas for the NEF the phase is for the scattered NFs. For antenna applications, the EBG will be located in the NF of the antenna of choice, so it is not sensible to characterize the EBG using the phase of the reflection coefficient, but rather using the phase of the scattered NFs. Even though the NEF has the added advantage of studying a finite structure, from Figs. 19 and 36, including the geometry of the strip dipole has an appreciable impact on the phase of the NFs, so it is best to include the antenna geometry (terminated with a 50-Ω load). This gives another advantage to the NEF, because it can have an antenna dependency (this will have to be explored further with other antenna geometries). So the NEF with antenna is the preferred numerical modeling approach for a strip dipole excited EBG, unless computational time and resources are a concern, in which case the PBC can suffice but may require more fine tuning of the antenna geometry.

It is possible that there is a correlation between the bandwidth estimated by the NEF with dipole simulations and the impedance bandwidth of the dipole. The size of the $0° \pm 90°$ and $0° \pm 45°$ bandwidths did not change much with the widening of the EBG gap. However, the dipoles did show a smaller impedance for the wide-gap EBG, but in both cases, the bandwidth estimated by the NEF with dipole simulations bounded the dipole impedance bandwidth. It may be that the estimated

bandwidth by the NEF could represent a minimum and maximum bandwidth associated with the dipole. Further investigation would be required to determine validity for the dipole and for other antenna geometries. What is certain, however, is that the PBC did not predict a narrower impedance bandwidth for the dipole in the presence of the wide-gap EBG. In fact, the PBC simulations for the wide-gap EBG suggested a much wider bandwidth than the thin-gap EBG (see Tables 2 and 5), yet the simulated dipole impedance bandwidth was wider when in the presence of the thin-gap EBG.

Of course, the phase characteristic of an EBG for either the reflection coefficient or the scattered NFs does not provide anything substantial about how the EBG will improve the performance of a nearby antenna. It indicates how an EBG will effect an incident plane wave in both cases, which is a situation that does not happen when an antenna is in close proximity to the EBG. Simulations with an antenna in close proximity to the EBG (in this case a strip dipole) are required in order to determine the impact of the EBG on the radiation pattern, realized gain, and impedance bandwidth. Then the antenna can be adjusted to obtain the desired center frequency.

5.2 EBG Design Parameters

In the literature, typical design parameters for EBGs require the patch widths to be about an order of magnitude smaller than the design wavelength, the gap width to be at least an order of magnitude smaller than the patches, the EBG thickness to be less than a quarter of the design wavelength, and in many cases, vias are included along with a dielectric substrate (typically referred to as a mushroom EBG). Quite often, these combinations do not result in the design frequency correlating to the zero-phase crossing in the reflection-phase. This is troublesome, as EBG's are supposed to work best at the zero-phase crossing, yet this may not correspond to the design frequency when using typical design parameters.

Studying the TLM shows that there can be many different combinations of patch size, gap size, and EBG thickness that result in a zero-phase crossing at or near to the design frequency. The simulation result from Section 4 and the patch width for the EBG in Section 3, when estimated for the wavelength in the dielectric, both show that the patch width would be about 4 to 6 times smaller than the design wavelength (in the dielectric). This is not consistent with what is typically seen in the literature on EBGs for antenna applications since most authors normalize to the free space wavelength.

The main justification for using an EBG for antenna applications is to improve antenna performance while maintaining a low-profile structure, so to justify a particular patch size, gap size, and EBG thickness the desired physical impact of

the EBG must be considered. By definition, low profile refers to a structure with a height that is smaller than 0.25λ (a quarter of the design wavelength in the dielectric), but an EBG's thickness can be smaller than 0.1λ. When considering the gap width, the results from Section 4 showed that the best impedance bandwidth and realized gain bandwidth occurred with a very small gap relative to the patch width, so the criterion for the gap width is that it should be at least an order of magnitude smaller than the patch width, which is consistent with the literature.

The physical parameters *w* (patch width), *g* (gap width), and *h* (EBG thickness) are inversely proportional to the product of the design frequency, f_0, and some constant:

$$w = \frac{c_0}{Mf_0}, \qquad g = \frac{c_0}{Pf_0}, \qquad h = \frac{c_0}{Nf_0} \tag{24}$$

With the physical guidelines from the previous paragraph and a simple script in MATLAB using Eq. 20 from Section 2.2, solutions for the constants in Eq. 24 that produce a zero-phase crossing at or near to the design frequency can be approximated. For this procedure, an EBG at a design frequency of 2.4 GHz without a dielectric substrate is considered. It is also necessary to assume something about the ratio of the patch width to gap width, in this case, it is assumed that the patch width is an order of magnitude larger than the gap width. The search criterion includes frequencies within ±5% of f_0 and returns the constants in integer combinations that correspond to each of those frequencies, which is sufficient.

Table 8 shows the results from the MATLAB script for the EBG without a dielectric substrate. It is clear that when the EBG thickness is an order of magnitude smaller than the design wavelength, the patch width is about 6 times smaller than the design wavelength and not an order of magnitude smaller. Repeating the search process with a substrate that has a small relative dielectric constant of 2.2, shows that the patches must decrease in size in order to produce a zero-phase crossing near the design frequency, see Table 9. Another consequence from the results is that the patches and gaps grow larger as the EBG height grows smaller; however, reducing the EBG thickness to smaller and smaller sizes can only be pushed so far because an antenna in close proximity to the EBG will be shorted by the patches that are now almost the size of the ground plane. The reverse is also true, where the patches and gaps grow smaller as the EBG thickness increases, but the increase in thickness defeats the purpose for using an EBG because it would no longer be low-profile compared to a standard reflector.

Table 8 The integer combinations for the EBG (without dielectric) design parameters that result in a zero-phase crossing in the reflection-phase near to the design frequency of 2.4 GHz

M	P	N	f0 (GHz)
21	210	5	2.29
22	220	5	2.31
23	230	5	2.33
24	240	5	2.36
25	250	5	2.37
13	130	6	2.31
14	140	6	2.36
15	150	6	2.41
16	160	6	2.45
17	170	6	2.49
10	100	7	2.34
11	110	7	2.42
12	120	7	2.49
8	80	8	2.34
9	90	8	2.44
7	70	9	2.37
8	80	9	2.51
6	**60**	**10**	**2.36**
5	50	11	2.3
6	60	11	2.49
5	50	12	2.41

Table 8 The integer combinations for the EBG (without dielectric) design parameters that result in a zero-phase crossing in the reflection-phase near to the design frequency of 2.4 GHz (continued)

M	P	N	f0 (GHz)
5	50	13	2.52
4	40	14	2.37
4	40	15	2.45
3	30	17	2.29
3	30	18	2.36
3	30	19	2.42
3	30	20	2.49
2	20	25	2.29

Table 9 The integer combinations for the EBG (with a dielectric of 2.2) design parameters that result in a zero-phase crossing in the reflection-phase at or near to the design frequency of 2.4 GHz

M	P	N	f0 (GHz)
18	180	8	2.30
19	190	8	2.33
20	200	8	2.36
21	210	8	2.39
22	220	8	2.41
23	230	8	2.44
24	240	8	2.46
25	250	8	2.48
14	140	9	2.32

Table 9 The integer combinations for the EBG (with a dielectric of 2.2) design parameters that result in a zero-phase crossing in the reflection-phase at or near to the design frequency of 2.4 GHz (continued)

M	P	N	f0 (GHz)
15	150	9	2.37
16	160	9	2.42
17	170	9	2.46
18	180	9	2.50
11	**110**	**10**	**2.30**
12	**120**	**10**	**2.37**
13	**130**	**10**	**2.43**
14	**140**	**10**	**2.49**
10	100	11	2.36
11	110	11	2.44
8	80	12	2.28
9	90	12	2.39
10	100	12	2.49
8	80	13	2.39
9	90	13	2.51
7	70	14	2.36
8	80	14	2.50
6	60	15	2.30
7	70	15	2.46
6	60	16	2.38
6	60	17	2.47

The EBG from Section 4 has patches that are roughly 4.5 times smaller than the design wavelength, and the EBG from Section 3 has patches that are about 5.6 times smaller than the design wavelength when the wavelength in the dielectric is considered. This suggests that when first designing an EBG without a substrate, the patches must be smaller than the design wavelength by a factor of about 5, which is more consistent with the results from the TLM (see Tables 8 and 9). Combining the results from the TLM with the patch widths from the EBGs in Sections 3 and 4 and considering the desired physical size of the EBG, a rudimentary set of design parameters can be determined for an EBG without a dielectric substrate:

$$w = \frac{\lambda_0}{5}, \qquad g \leq \frac{w}{10}, \qquad h = \frac{\lambda_0}{10}. \tag{25}$$

Of course, designing an EBG with a dielectric substrate would only require the above parameters to be scaled accordingly (see Section 6). These parameters will allow an antenna engineer to design a basic square EBG without having to use any analytical or numerical model outside of simulating the antenna with the EBG. Simulations using either the PBC or NEF method will not be necessary. For the NEF analysis of the EBG in Section 4, the ratio of the patch width to the wavelength at the frequency where the NF phase crosses zero is about 5, which is consistent with Eq. 25, so it would be unnecessary to perform the analysis unless some modifications were made to the EBG or an antenna other than the strip dipole was used.

Note that these design parameters were determined in part from using a strip dipole, a specific antenna. Whether or not these parameters are general for all antenna types remains to be seen. Further investigation into different antennas may yield different parameters such as asymmetric patches, variation in the periodicity, multiple layers, or an entirely different textured surface. Some antennas may require an EBG to be designed strictly from optimization, especially for multiband antennas. Such antennas could require the EBG to have a complicated textured surface or multiple surfaces to achieve multiple resonances and may not be straightforward in designing from an analytical approach (Kern et al. 2005).

5.3 EBG Bandwidth Specific to a Strip Dipole Antenna

Once an EBG is designed, it is typical to define its bandwidth from the reflection-phase, but it has been shown that for antenna applications, it is the scattered-phase that better determines the bandwidth. Regardless, the analytical models all assume the same infinite structure and EBG surface impedance mismatch to free space as the PBC, so it is important to define a particular bandwidth for the reflection-phase as a first principle even if it may not characterize the EBG bandwidth exactly as

desired for antennas. As stated in the introduction, the literature states 3 different phase ranges for the bandwidth: $\varphi = 0° \pm 90°$ (Sievenpiper et al. 1999), $0° \pm 45°$ (Hansen 2002), and $90° \pm 45°$ (Volakis 2007; Yang and Rahmat-Samii 2003). What was seen in Section 4, however, is that for the reflection-phase dipoles and the scattered-phase dipoles, those that were in the negative phase regime were better matched than those in the positive phase regime. This means that the bandwidth could possibly be defined between 0° and –90°, but the fact that there is some ambiguity to the phase range and that the reflection-phase does not give insight into how the EBG effects an antenna, it would be better to define the bandwidth based upon how the EBG effects the impedance and radiation pattern of an antenna.

Further, the antenna over an EBG can have different impedance and realized gain bandwidths that can be optimized by adjusting the EBG parameters which would not be captured with the reflection-phase. A good example is the small-gap EBG in Section 4 that produced a greater improvement in the strip dipole's impedance bandwidth when compared to the wide-gap EBG, although the reflection-phase results for the small-gap EBG showed a steeper slope (smaller EBG bandwidth at 153 MHz) when compared to the reflection-phase results for the wide-gap EBG (larger EBG bandwidth at 217 MHz). This is a contradiction that cannot be captured nor explained by either numerical approach.

As mentioned previously, the EBG effect on the strip dipole corresponds either to a pseudo-PEC ground plane or to a pseudo-AMC ground plane (Best and Hanna 2008). From the impedance of the various strip dipoles in Section 4, it is clear that the positive phase regime of the EBG appears to the dipole as a pseudo-PEC ground plane, reducing the dipole resistance, and when in the negative phase regime, the EBG appears as a pseudo-AMC ground plane, increasing the dipole resistance and distorting the H-plane pattern. These properties become more prevalent as the dipole lengths are tuned to the outer bounds of either the reflection-phase or scattered-phase (>+90° for PEC and <–90° for AMC). The EBG also appeared to the strip dipoles as an inductive load, which if the loading effect specific to each strip dipole is taken into consideration (requiring the dipole lengths to be adjusted) then all dipoles that are resonant at $\varphi \leq +45°$ would be matched to 50 Ω.

For the dipoles that are adjusted at higher frequencies, the patterns will distort significantly reducing the gain at $\theta = 90°$, $\phi = 0°$ and producing a split beam pattern. If the loading effects, pattern effects, and ground plane behavior in the 2 phase regimes are all taken into consideration, then the phase range of the EBG bandwidth for a strip dipole excitation, defined by the reflection-phase, would be $0° \pm 45°$ (often up to –90° in the negative phase regime). Note that this phase range can also be applied to the scattered-phase, but the phase range is more restrictive compared to the reflection-phase.

6. EBG Design Example for a Strip Dipole

This section presents a simulation example for how to design an EBG to improve the performance of a resonant strip dipole antenna centered at 2.437 GHz for Wi-Fi band 802.11g/n. From Section 4, it is clear that there are some tradeoffs between using a wide gap width versus using a thin gap width. The simulations suggest that using a thin gap width allows for a wider –10-dB reflection coefficient bandwidth and subsequently a wider realized gain bandwidth (±1 dBi) with little tradeoff. Both wide- and thin-gap examples are shown in the following sections along with simulations for including a dielectric substrate. The last section will highlight the impact of using vias and of adding and removing unit cells.

6.1 Wide-Gap versus Thin-Gap EBG

For both the wide- and thin-gap examples, the design frequency is in the middle of the Wi-Fi band 802.11g/n centered at 2.437 GHz with a bandwidth of 83.5 MHz. The goal is to cover the entire band with a strip dipole-EBG structure. Tables 10 and 11 give the EBG and strip dipole design parameters, respectively. The strip dipole's trace width is such that the dipole can be considered as a thin wire.

The PBC analysis is shown to demonstrate that these design parameters produce a zero-phase crossing in the reflection-phase at or near the design frequency (the zero-phase crossing in the NEF analysis will be different than the PBC but not enough to make an appreciable difference, see Section 5.2) (Fig. 53) for the wide- and thin-gap EBG. The thin gap has a lower zero-phase crossing than the wide gap, but the wide-gap zero-phase crossing is at 2.37 GHz, which is close to the design frequency of 2.437 GHz. The zero-phase crossing for the thin gap occurs at 2.09 GHz, which is farther from the design wavelength by 14%. The difference in zero-phase crossings is an excellent example of how the EBG reflection-phase is sensitive to small changes in the physical parameters. Figure 54a and b show the reflection coefficient for the strip dipole over the wide- and thin-gap EBGs, respectively. The figures also include the reflection coefficient for the dipoles having lengths that are adjusted back to the design frequency.

Table 10 The physical parameters for the section 6 EBG design example. λ is the free space wavelength.

EBG Parameters	Wide Gap	Small Gap
Patch width, *w*	λ/5	λ/5
Gap width, *g*	*w*/10	*w*/30
Thickness, *h*	λ/10	λ/10

Table 11 The dipole parameters for the section 6 EBG design example. λ is the free space wavelength.

Dipole Parameters	Design values normalized to wavelength
Length	$0.463\lambda_{2.437GHz}$
Gap for feed	$0.02\ \lambda_{2.437GHz}$
Height (above EBG)	1.575 mm ($0.013\ \lambda_{2.437GHz}$)
Trace width	$0.006\ \lambda_{2.437GHz}$

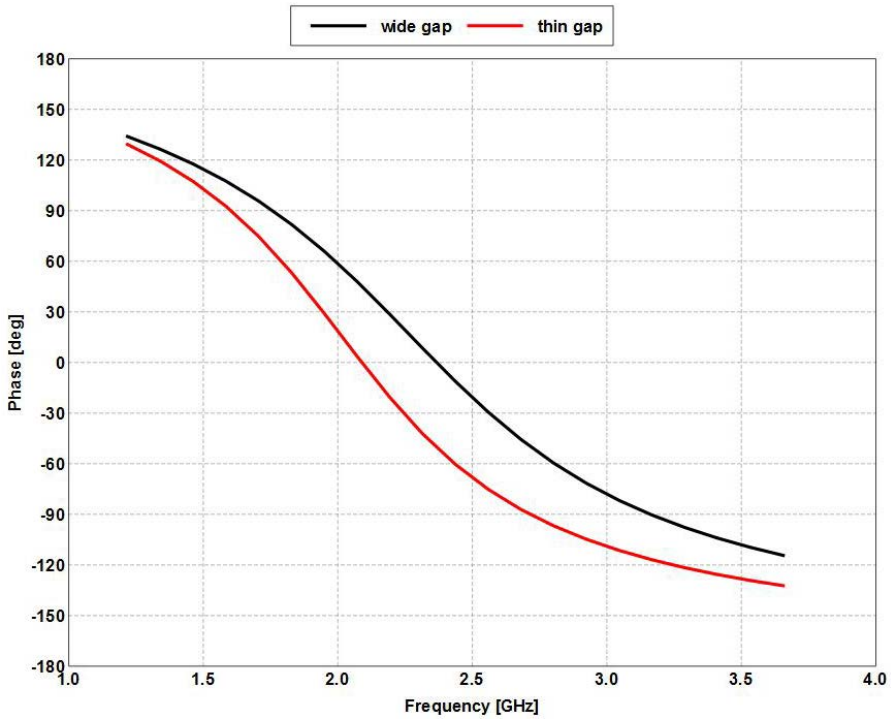

Fig. 53 The results for the wide- and thin-gap EBG reflection-phase at the design frequency of 2.437 GHz

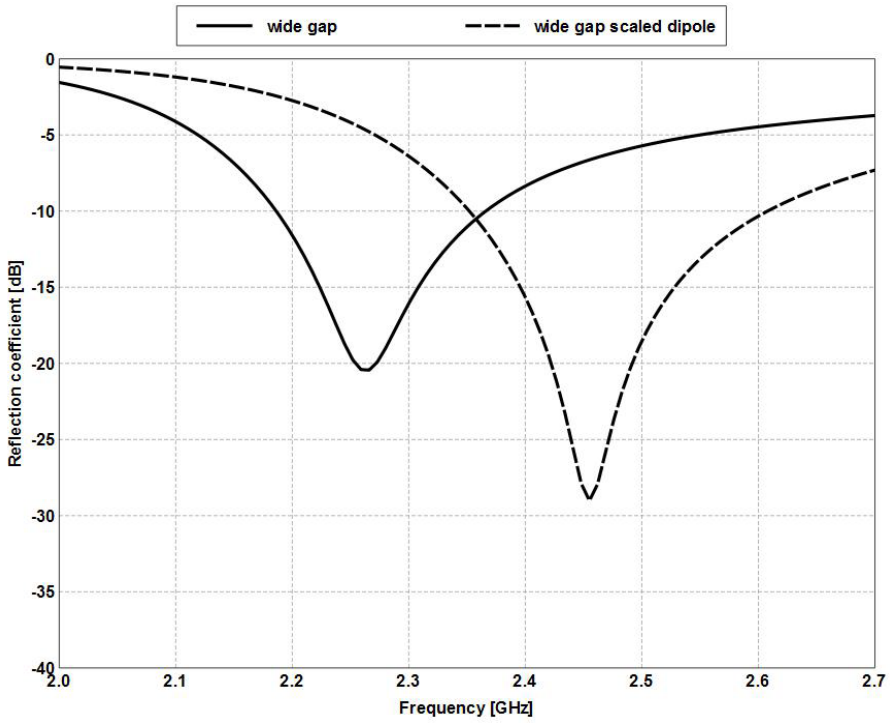

a)

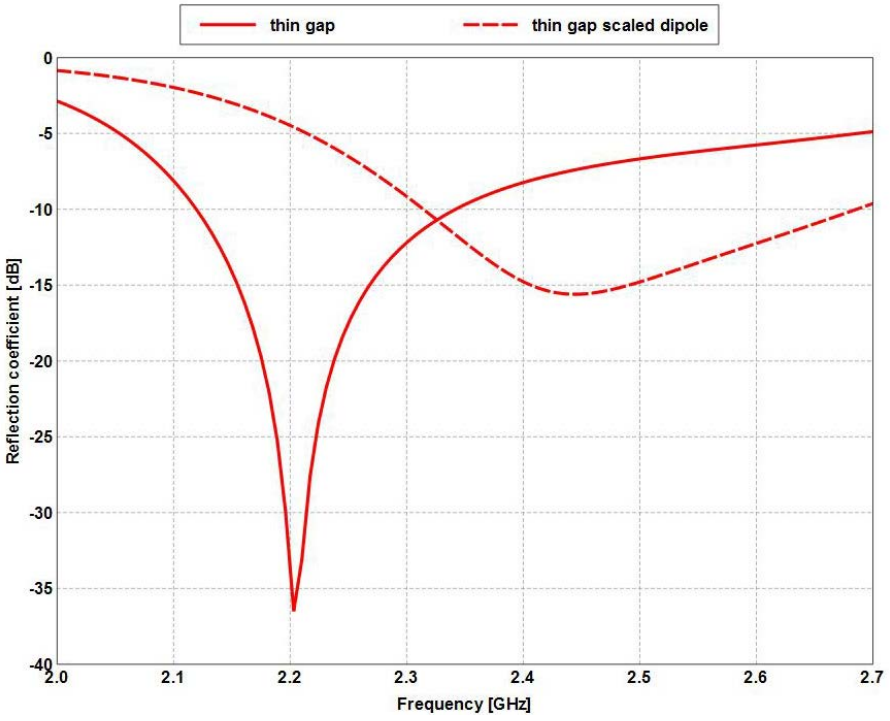

b)

Fig 54 a) The reflection coefficient for the resonant (2.437 GHz) strip dipole in the presence of the wide-gap EBG before and after adjusting the dipole length. b) The reflection coefficient for the resonant (2.437 GHz) strip dipole in the presence of the thin-gap EBG before and after adjusting the dipole length.

The dipole over the thin-gap EBG required a greater length adjustment to scale it back to the design frequency when compared to the dipole over the wide-gap EBG, but the thin-gap EBG resulted in a greater impedance bandwidth before and after length adjustments when compared to the wide-gap EBG, 222 MHz versus 180 MHz (23% larger before scaling) and 372 MHz versus 256 MHz (45% larger after scaling). Both EBGs improved the dipole impedance bandwidth with the biggest improvement after scaling. The impedance bandwidth for the dipole over the wide-gap EBG improved by 42% after scaling, and the impedance bandwidth of the dipole over the thin-gap EBG improved by 68% after scaling.

The 2 dipole-EBG structures have the same peak realized gain of around 9 dBi, but the ±1-dBi realized gain bandwidth is larger for the strip dipole that is in the presence of the thin-gap EBG before and after length adjustments, 471 MHz versus 318 MHz (48% larger before scaling) and 480 MHz versus 386 MHz (24% larger after scaling), (Fig. 55a and b). Figure 56a, b, c, and d are the input resistance and reactance for the 2 dipole-EBG structures. Both the resistance and reactance have flatter slopes for the thin-gap EBG compared to the wide-gap EBG, which explains the wider bandwidth and is consistent with the simulation results from Section 4. The plateau in the resistance that was seen in Section 4 has started to appear in the resistance for the thin-gap EBG at higher frequencies (Fig. 56b), which suggests that to improve the impedance bandwidth further would require gap widths that are even smaller than $\frac{w}{30}$. Again, this is consistent with the simulation results from Section 4.

The realized gain radiation patterns (Fig. 57a and b) are directive although there is some difference between the E-plane and H-plane shapes due to the fields lying either in the gaps (E-plane) or across the gaps (H-plane). The fields that lie across the gap produce an H-plane pattern that is more bulbous than the E-plane pattern, and just like in Section 4, if the dipole is scaled to a much higher frequency there will be distortion in the H-plane. The dipole scaling produces very little change in the pattern shapes, with only a minor increase in realized gain. The bandwidths, resonant frequencies, frequency shifts, and peak realized gain are summarized in Tables 12 and 13. The simulation example in this section has shown that the antenna specific EBG design parameters result in an EBG than improves the performance of a strip dipole.

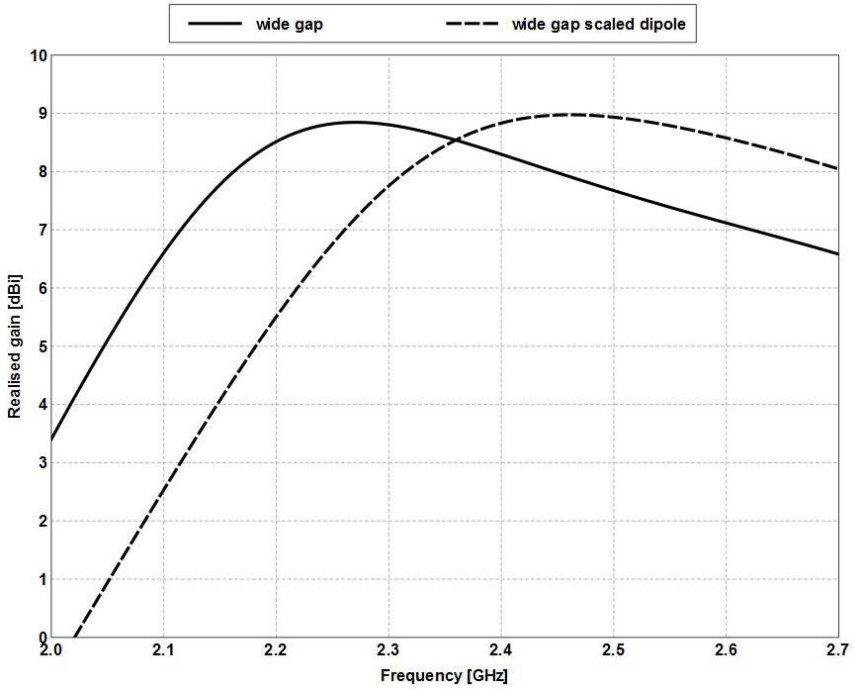

a)

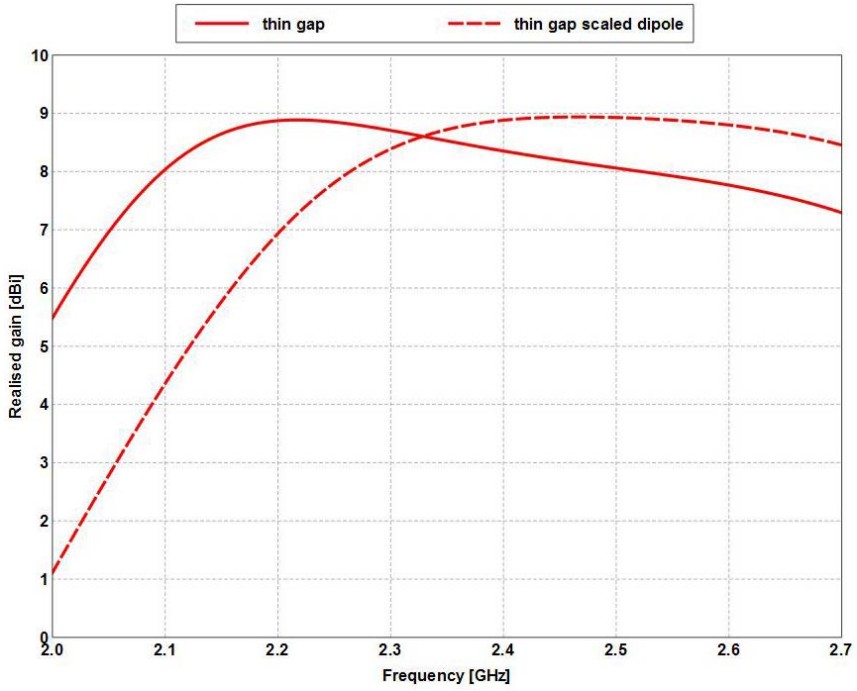

b)

Fig. 55 a) The realized gain vs. frequency ($\theta = 90°$, $\phi = 0°$) for the resonant (2.437 GHz) strip dipole in the presence of the wide-gap EBG before and after adjusting the dipole length. b) The realized gain vs. frequency ($\theta = 90°$, $\phi = 0°$) for the resonant (2.437 GHz) strip dipole in the presence of the thin-gap EBG before and after adjusting the dipole length.

Note: Figure 56a, b, c, and d spans the next 2 pages.

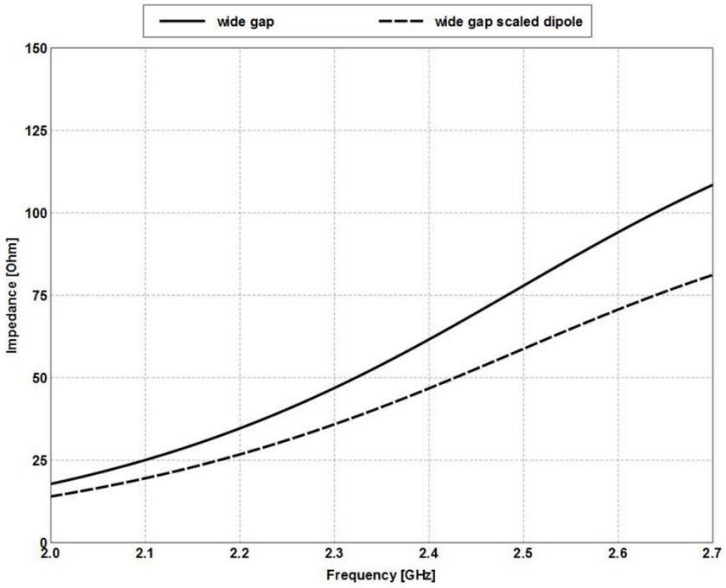

a)

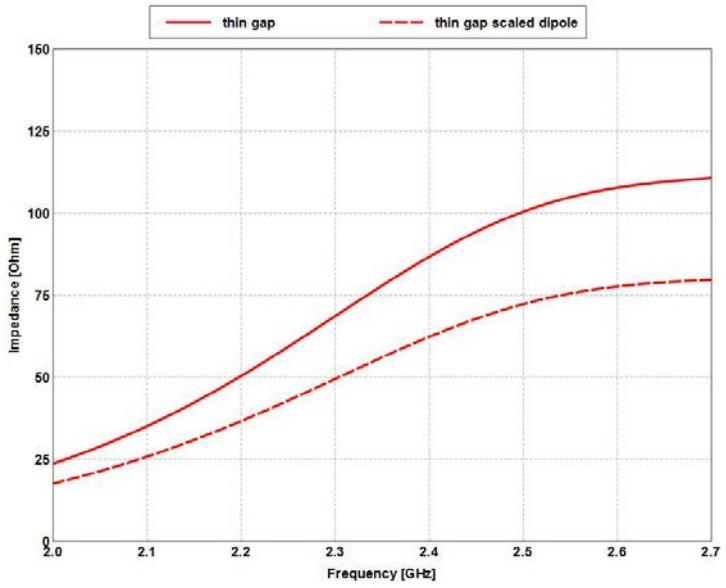

b)

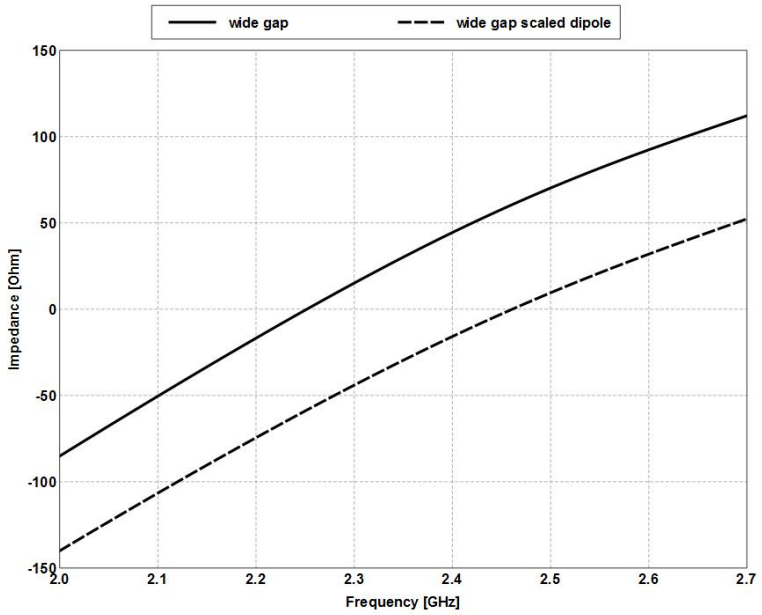

c)

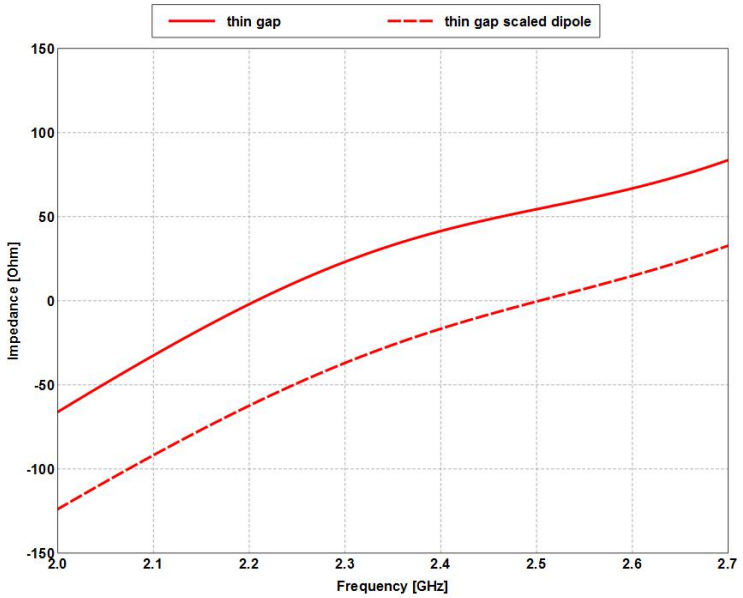

d)

Fig. 56 a) The input resistance for the resonant (2.437 GHz) strip dipole in the presence of the wide-gap EBG before and after adjusting the dipole length. b) The input resistance for the resonant (2.437 GHz) strip dipole in the presence of the thin-gap EBG before and after adjusting the dipole length. c) The input reactance for the resonant (2.437 GHz) strip dipole in the presence of the wide-gap EBG before and after adjusting the dipole length. d) The input reactance for the resonant (2.437 GHz) strip dipole in the presence of the thin-gap EBG before and after adjusting the dipole length.

Note: Figure 57a and b spans the next 2 pages.

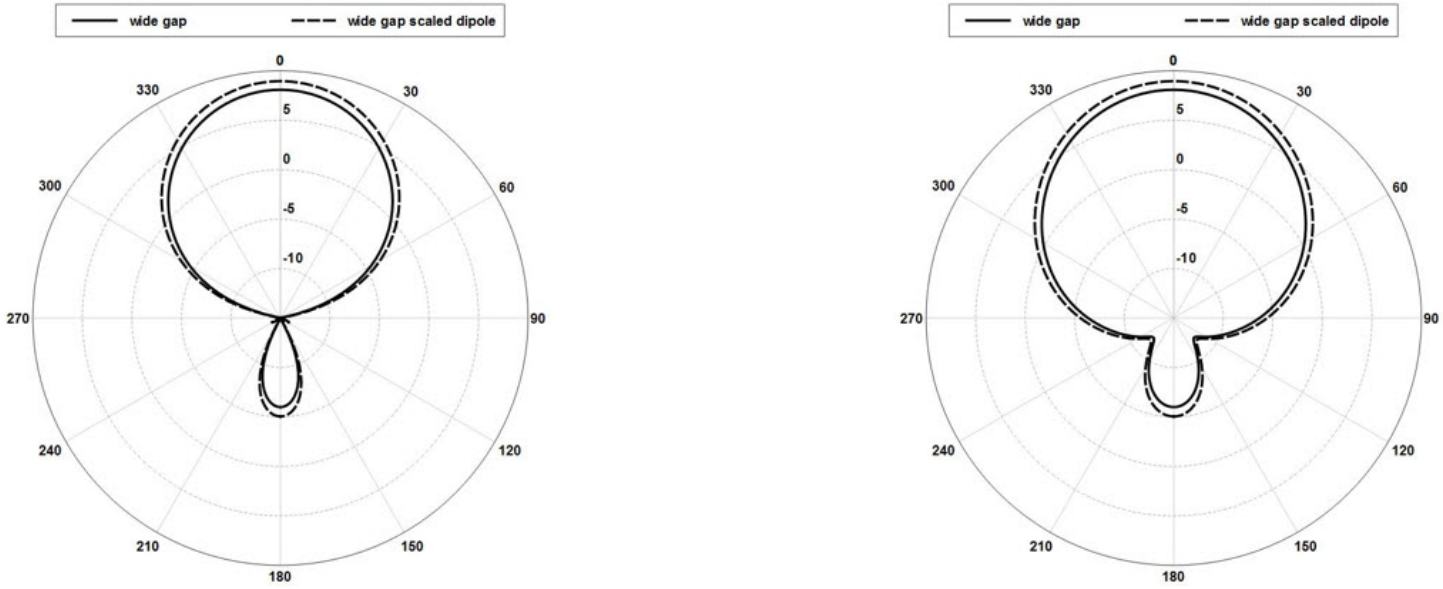

a)

b)

Fig. 57 a) The realized gain patterns for the resonant (2.437 GHz) strip dipole in the presence of the wide-gap EBG before and after adjusting the dipole length. E-plane (left) and H-plane (right). b) Realized gain patterns for the resonant (2.437 GHz) strip dipole in the presence of the thin-gap EBG before and after adjusting the dipole length. E-plane (left) and H-plane (right).

Table 12. The summarized results from the resonant strip dipoles above the wide gap and small gap before adjusting the dipole length

Gap Size	Frequency shift to scale (GHz)	Dipole Reflection Coefficient (GHz)	Reflection Coefficient BW_{-10dBi} (GHz)	Peak Realized Gain (dBi)	Realized Gain BW_{1dBi} (GHz)
Wide gap	2.370	2.266	0.180	8.8	0.318
Small gap	2.090	2.203	0.222	8.9	0.471

Table 13. The summarized results from the resonant strip dipoles above the wide gap and small gap after adjusting the dipole length

Gap Size	Frequency shift to scale (GHz)	Dipole Reflection Coefficient (GHz)	Reflection Coefficient BW_{-10dBi} (GHz)	Peak Realized Gain (dBi)	Realized Gain BW_{1dBi} (GHz)
Wide gap	0.194	2.455	0.256	9	0.386
Small gap	0.206	2.441	0.372	9	0.480

6.2 Inclusion of a Dielectric Substrate

Introducing a dielectric substrate with a low-relative permittivity of 2.2 causes a shift to lower frequencies in the reflection-phase for both the wide- and thin-gap EBGs. It is expected that scaling the EBG can compensate for the frequency shift in the reflection-phase caused by the dielectric substrate. Scaling the patch width, gap width, and EBG thickness by the square root of the relative permittivity results in a reflection-phase curve that is shifted to higher frequencies compared to the no substrate case. Scaling by the effective permittivity undershoots the nondielectric case but it is in closer agreement (Fig. 58a and b). This suggests that a scale factor that lies between the effective permittivity (which is a poor approximation to begin with) and the relative permittivity would have better results.

The process for the rest of the EBG design example involves including the dielectric substrate in both the wide- and thin-gap EBGs, scaling the EBG physical parameters by the square root of the effective permittivity to compensate for dielectric loading (patch width, gap width, and EBG thickness) and adjusting the effective permittivity by a scale factor to compensate for the approximation that the effective permittivity is an average value for an infinite dielectric half-space.

Because scaling the EBG reduces the thickness, the dipole will be placed closer to the ground plane resulting in an increase in the resistance due to the inherent AMC behavior of the EBG (Hansen 2002; Best and Hanna 2008). The increase in resistance requires the dipole's height above the EBG surface to be adjusted to compensate for the substrate by the following equation.

$$h' = h + \left(\sqrt{\varepsilon_{eff}} - 1\right)\frac{\lambda_0}{10\sqrt{\varepsilon_{eff}}} \tag{26}$$

Where *h'* is the adjusted dipole height above the EBG, *h* is the initial dipole height above the EBG, λ_0 is the free space wavelength at the design frequency, and ε_{eff} is the effective permittivity.

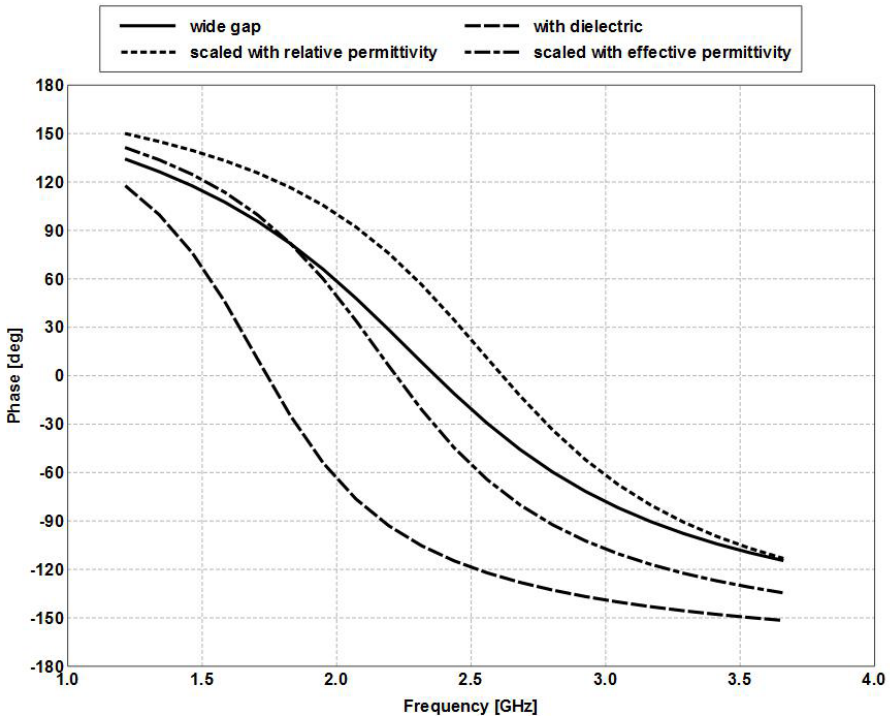

a)

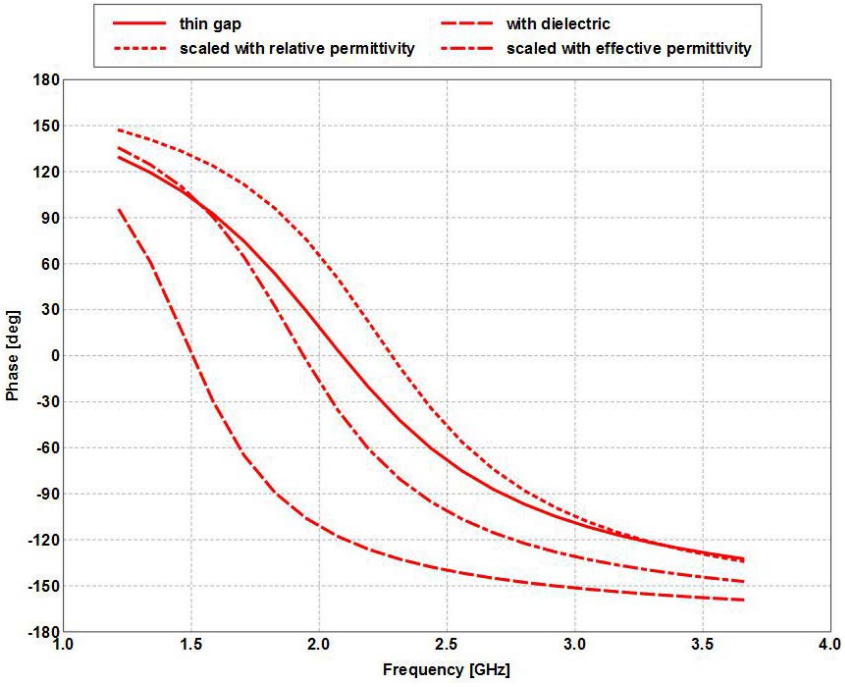

b)

Fig. 58 a) The reflection-phase of the wide-gap EBG with a dielectric substrate (relative permittivity 2.2); plot includes scaling adjustments using relative permittivity and effective permittivity. b) The reflection-phase of the thin-gap EBG with a dielectric substrate (relative permittivity 2.2); plot includes scaling adjustments using relative permittivity and effective permittivity.

When including the dielectric substrate in the wide-gap EBG, the dipole reflection coefficient (Fig. 59) does not shift to as low a frequency as when the dielectric substrate is not included. This is to be expected, as the CM predicts that adding a dielectric will increase the capacitance, making the EBG appear less inductive (or more capacitive). Scaling the EBG parameters to compensate for the frequency shift in the reflection-phase by the dielectric, shifts the reflection coefficient by 200 MHz to a frequency of 2.1 GHz where the loading effect is now mostly dominated by the EBG inductance and results in a well matched strip dipole. Adjusting the effective permittivity by a factor of 0.7 (which was determined through repeat simulations) to achieve a better approximation for the effective permittivity results in a reflection coefficient that shifts to about 2.3 GHz. Finally, by adjusting the height of the dipole by Eq. 26, the reflection coefficient results in a resonance close to 2.4 GHz and includes the entire 802.11g/n band. However, the dipole is not as well matched as hoped.

The input resistance shows that the inclusion of the dielectric substrate (Fig. 60a) produces a similar plateau that was seen in Section 4 for the thin-gap EBG. The plateau is best matched at around 80 Ω for each dielectric case with the exception of when the EBG is scaled and the effective permittivity and dipole height are not adjusted. The resistance for this case is increased, again, due to the AMC behavior and close proximity of the dipole. The input reactance (Fig. 60b) shows how the inductance decreases when a dielectric substrate is included and then increases when the EBG is appropriately scaled. Note that the dipole length was not adjusted at all during these comparisons, and if it was, a near 50-Ω match could have been achieved over a wide band. If the dipole length is not adjusted, however, an impedance transformer can be used to match the dipole and achieve a large impedance bandwidth.

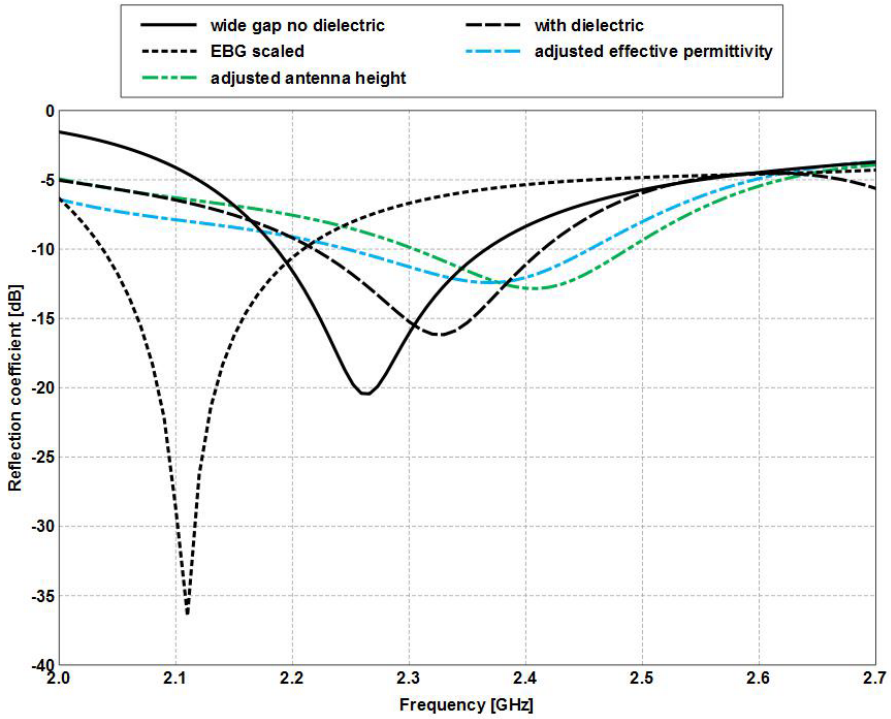

Fig. 59 The reflection coefficient for the resonant (2.437 GHz) strip dipole in the presence of the wide-gap EBG with a dielectric substrate (relative permittivity 2.2). The EBG geometry and antenna height were adjusted to compensate for dielectric effects.

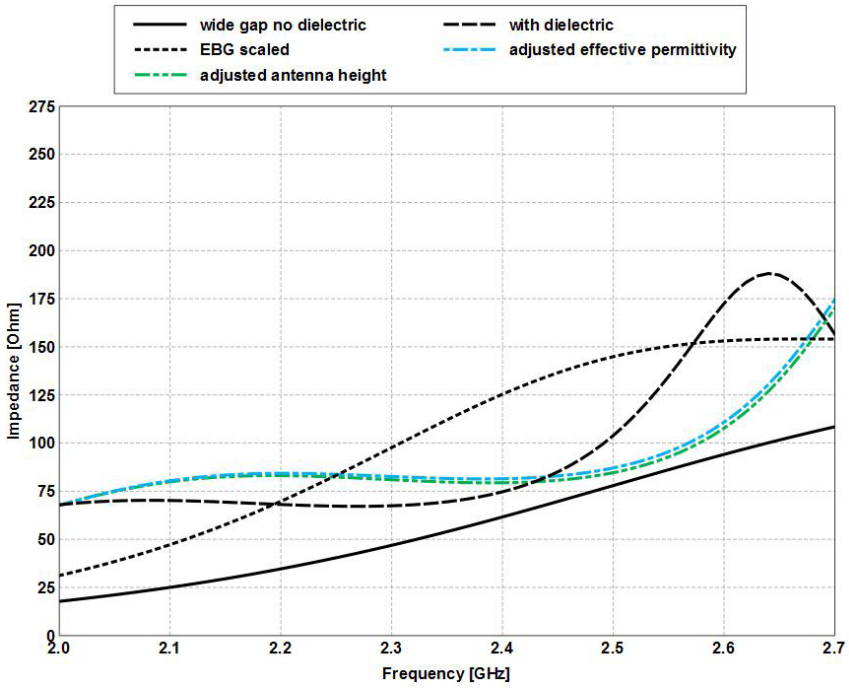

a)

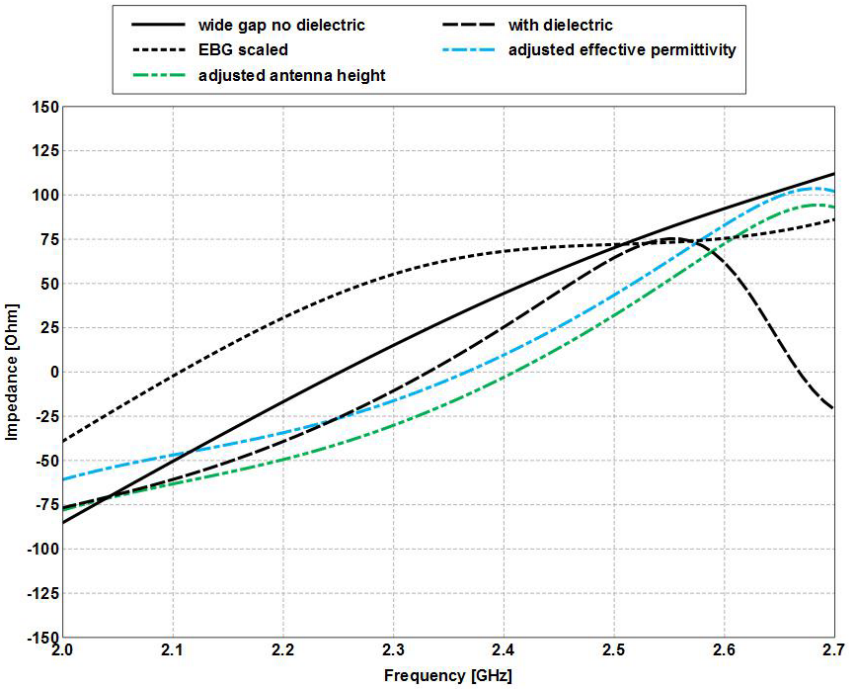

b)

Fig. 60 a) The input resistance for the resonant (2.437 GHz) strip dipole in the presence of the wide-gap EBG with a dielectric substrate (relative permittivity 2.2). The EBG geometry and antenna height were adjusted to compensate for dielectric effects. b) The input reactance for the resonant (2.437 GHz) strip dipole in the presence of the wide-gap EBG with a dielectric substrate (relative permittivity 2.2). The EBG geometry and antenna height were adjusted to compensate for dielectric effects.

The E-plane and H-plane patterns (Fig. 61) show a reduction in the realized gain by as much as 2 dBi even after all of the adjustments made to the EBG structure and dipole height. The H-plane shows the negative impact of the dielectric on pattern shape because there are severe bulges in the $\theta = 90°$ and $270°$ ($\varphi = 0°$) directions. These bulges can be associated with surface waves due to the dielectric, but these bulges were also seen in Section 4 when the dipoles were near the upper bound of the EBG's bandwidth and there was no dielectric substrate. From the current distribution comparisons (Fig. 62) between the wide-gap EBG without substrate and the wide-gap EBG with substrate, it is clear that the dielectric supports surface waves launched in the H-plane that radiate at the edges. Without the dielectric substrate, the EBG edges in the H-plane conduct a larger amount of current than the edges in the E-plane. This current begins to radiate at higher frequencies causing the distortion in the H-plane. When the dielectric substrate is introduced, the current on the edges is magnified (caused by surface waves or increased mutual coupling between the patches) resulting in greater pattern distortion. Figure 63 shows the realized gain versus frequency plot. Here, it is clear that using a dielectric (even after adjustments according to the wavelength in the dielectric) will have a severe negative impact on the realized gain.

The same process detailed for the wide-gap EBG with a dielectric substrate was also used for the thin-gap EBG. The reflection coefficient (Fig. 64) shows the same trend as before, where the input inductance decreases with the inclusion of a dielectric substrate, but increases when the EBG is scaled. The thinner gap for the EBG again improves the dipole impedance bandwidth. The resistance and reactance (Fig. 65a and b) show an improved impedance bandwidth when in the presence of the thin-gap EBG (due to the smaller gap) because the magnitude of the plateau in the resistance is now between 50 and 75 Ω. Again, the reactance shows the EBG becoming less inductive when a dielectric substrate is included and more inductive when the EBG is scaled. The radiation patterns, current distributions, and realized gain versus frequency curves (Figs. 66, 67, and 68) all show the same issues as with the wide-gap EBG.

The dielectric causes a decrease in the realized gain by at least 2 dBi with severe distortion in the H-plane patterns. The pattern distortion is actually more severe for the thin-gap EBG. The thinner gaps increase the coupling between the patches, which can be see when comparing the current distributions for the wide- and thin-gap EBGs without dielectric (Figs. 62 and 67). The current on the H-plane edges for the thin-gap EBG is greater than for the wide gap EBG, so when the dielectric substrate is included, the H-plane patterns are more greatly distorted. For large EBGs, thin dielectrics can be used to help mitigate the negative effects of the

dielectric substrate. But for very small and thin EBGs that have dielectric substrates, it may be necessary to include vias to realize the full potential of the improvement that the EBG will have on antenna performance.

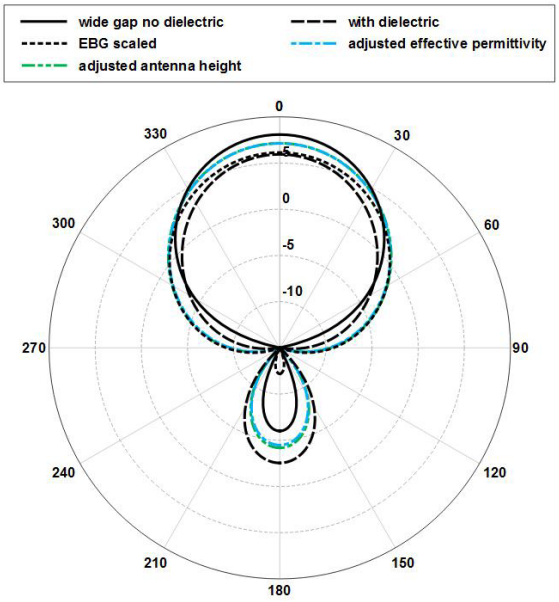

a)

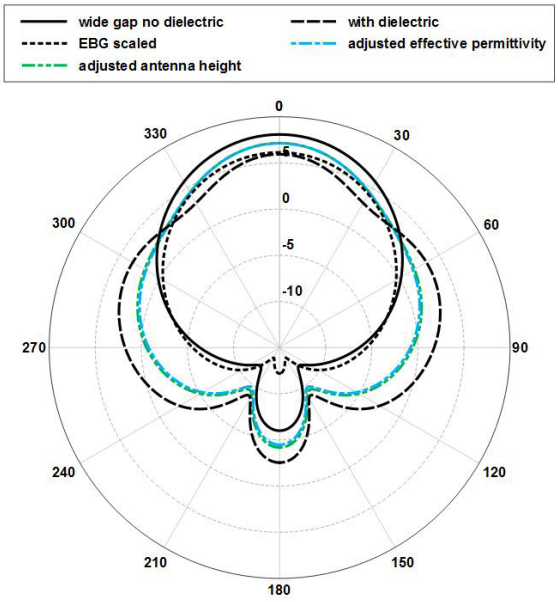

b)

Fig. 61 The realized gain patterns for the resonant (2.437 GHz) strip dipole in the presence of the wide-gap EBG with a dielectric substrate (relative permittivity 2.2). The EBG geometry and antenna height were adjusted to compensate for dielectric effects. a) E-plane and b) H-plane.

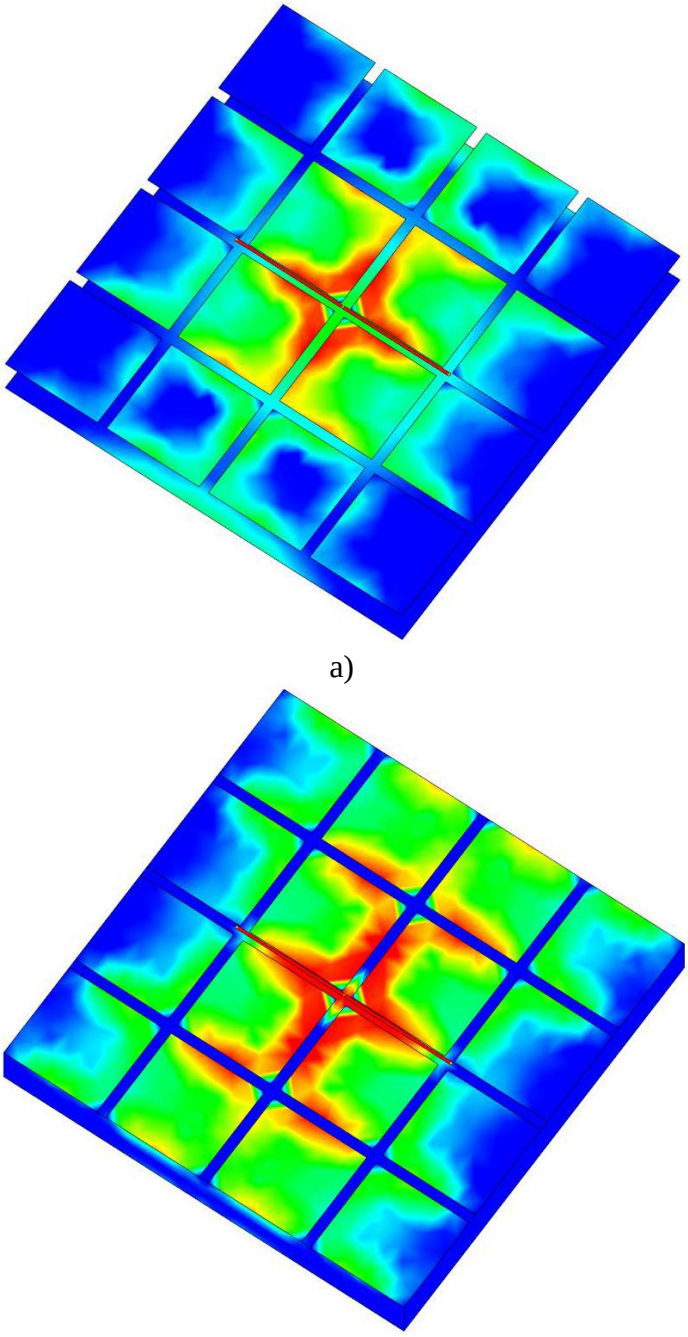

Fig. 62 The electric current distribution of the resonant strip dipole in the presence of the wide-gap EBG at the design frequency (2.437 GHz). a) Without a dielectric substrate and b) with a dielectric substrate.

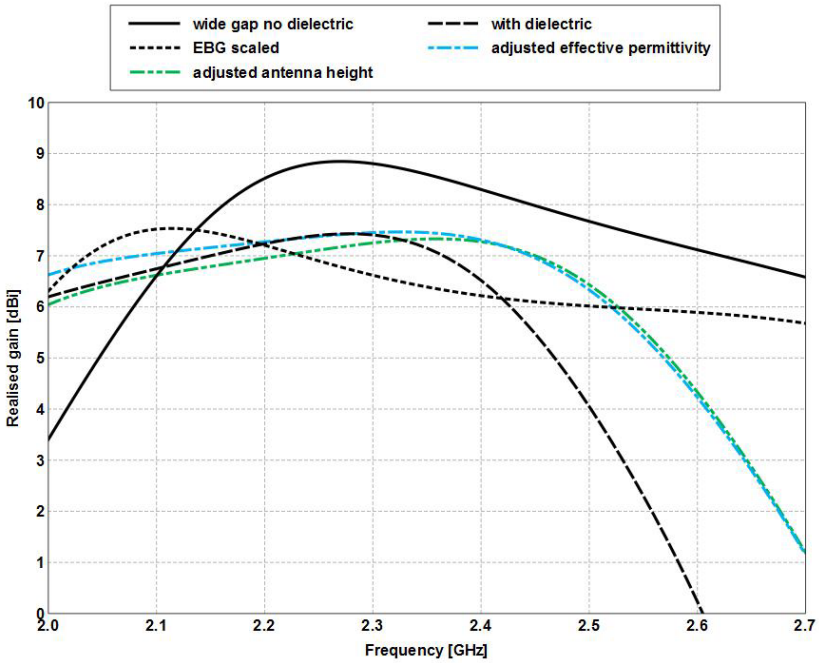

Fig. 63 The realized gain vs. frequency ($\theta = 90°$, $\phi = 0°$) for the resonant (2.437 GHz) strip dipole in the presence of the wide-gap EBG with a dielectric substrate (relative permittivity 2.2). The EBG geometry and antenna height were adjusted to compensate for dielectric effects.

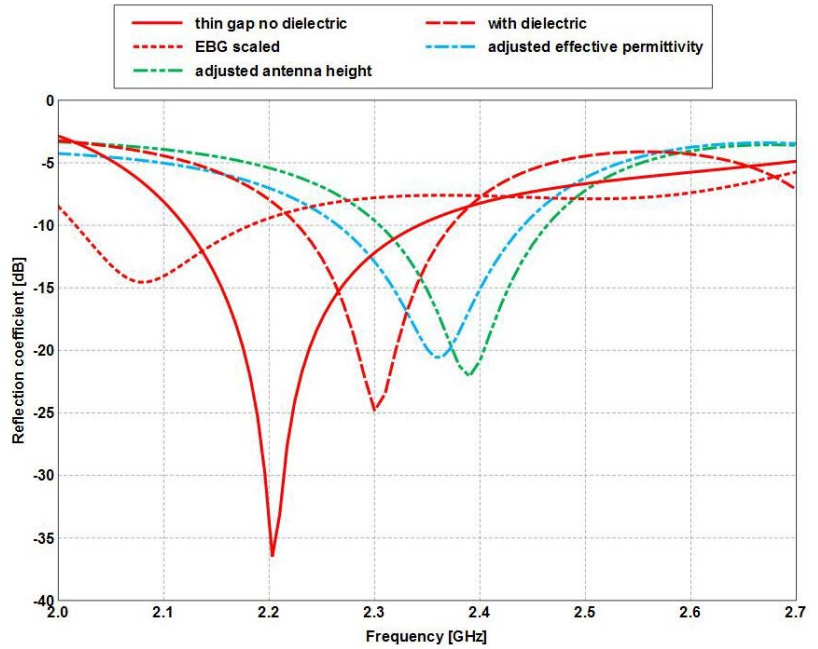

Fig. 64 The reflection coefficient for the resonant (2.437 GHz) strip dipole in the presence of the thin-gap EBG with a dielectric substrate (relative permittivity 2.2). The EBG geometry and antenna height were adjusted to compensate for dielectric effects.

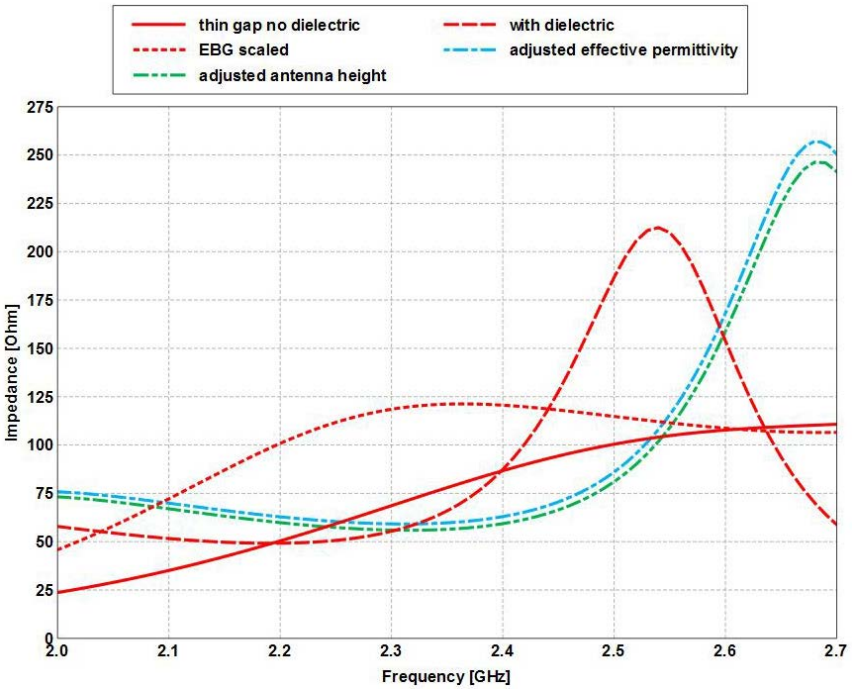

a)

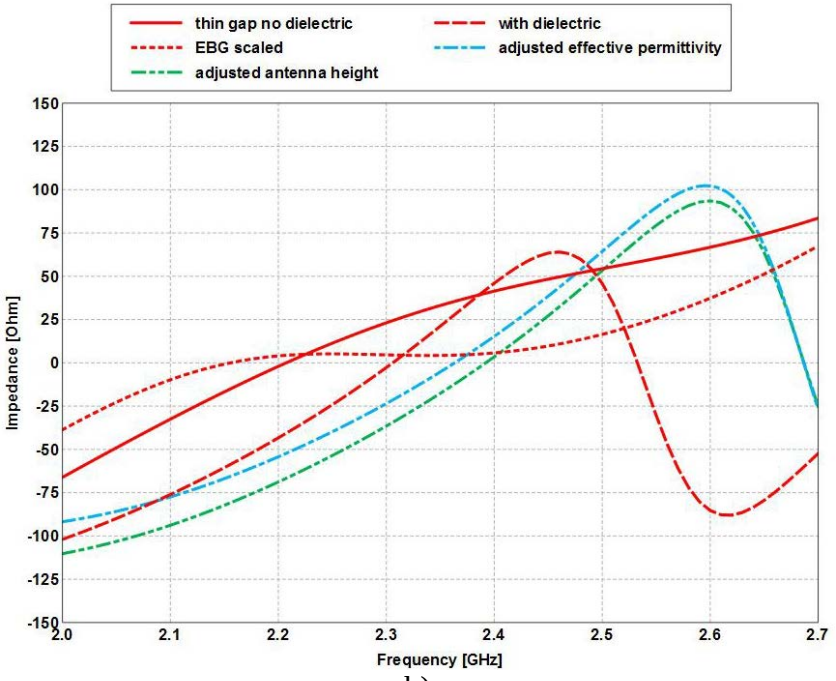

b)

Fig. 65 a) The input resistance for the resonant (2.437 GHz) strip dipole in the presence of the thin-gap EBG with a dielectric substrate (relative permittivity 2.2). The EBG geometry and antenna height were adjusted to compensate for dielectric effects. b) The input reactance for the resonant (2.437 GHz) strip dipole in the presence of the thin-gap EBG with a dielectric substrate (relative permittivity 2.2). The EBG geometry and antenna height were adjusted to compensate for dielectric effects.

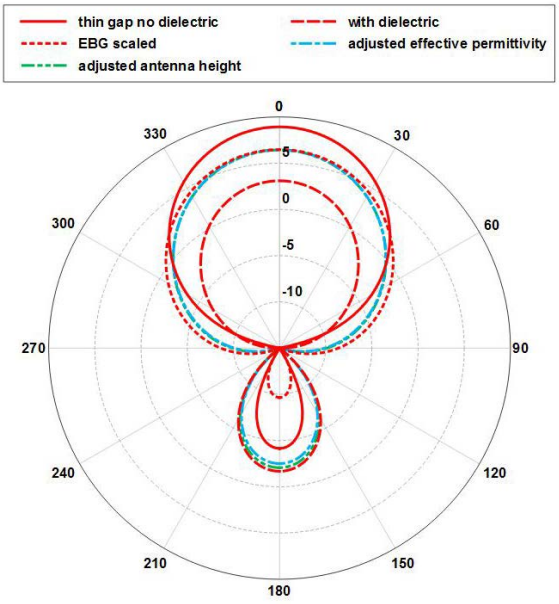

a)

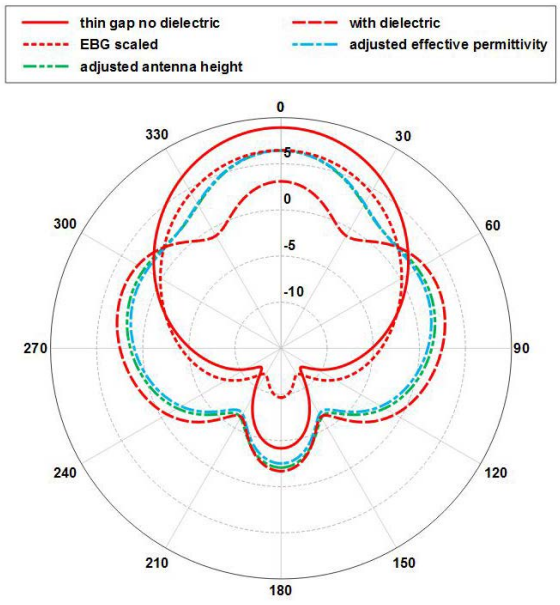

b)

Fig. 66 The realized gain patterns for the resonant (2.437 GHz) strip dipole in the presence of the thin-gap EBG with a dielectric substrate (relative permittivity 2.2). The EBG geometry and antenna height were adjusted to compensate for dielectric effects. a) E-plane and b) H-plane (right).

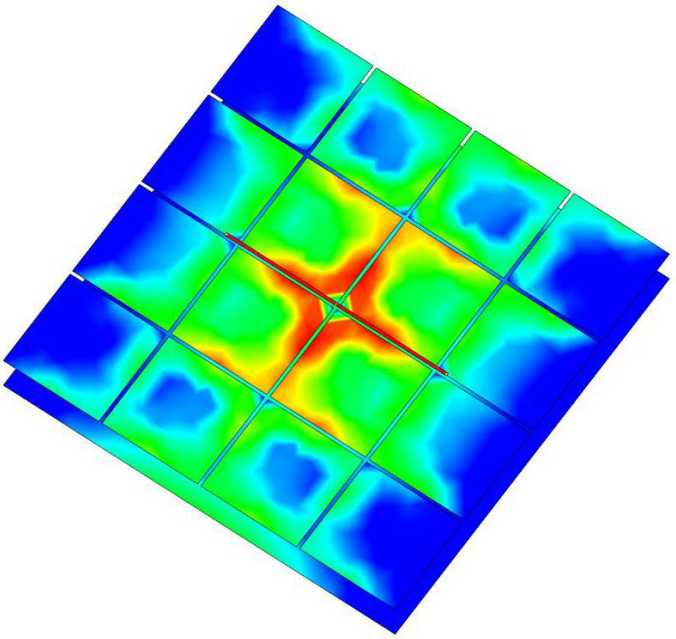

a)

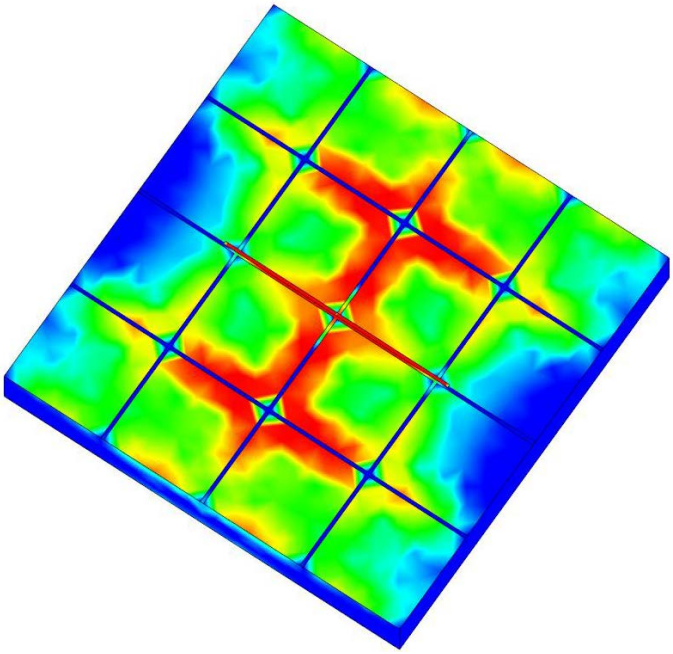

b)

Fig. 67 The electric current distributions of the resonant strip dipole in the presence of the thin-gap EBG at the design frequency (2.437 GHz). a) Without a dielectric substrate and b) with a dielectric substrate.

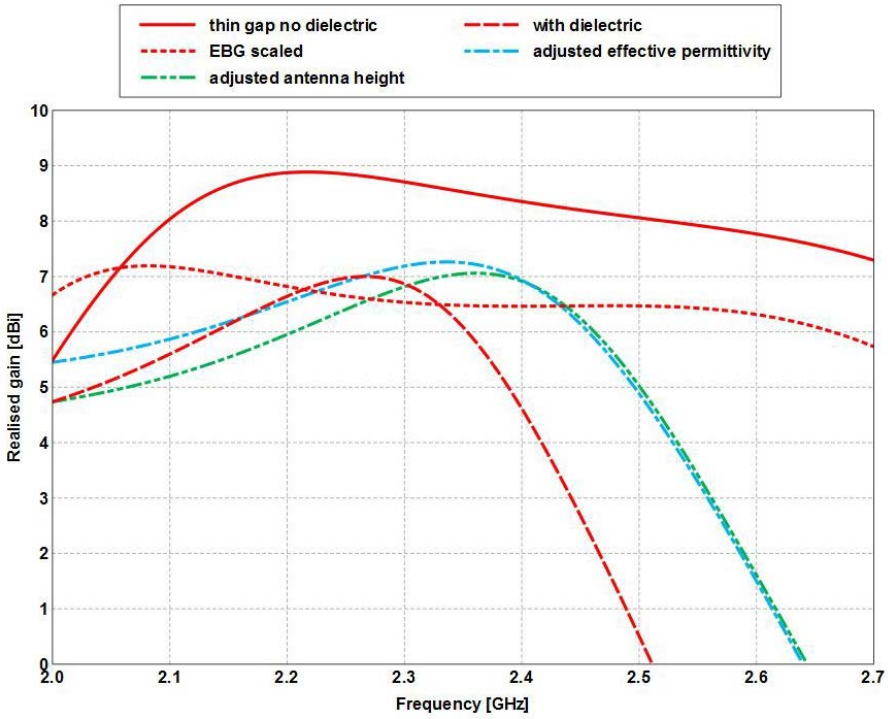

Fig. 68 The realized gain vs. frequency ($\theta = 90°$, $\phi = 0°$) for the resonant (2.437 GHz) strip dipole in the presence of the thin-gap EBG with a dielectric substrate (relative permittivity 2.2). The EBG geometry and antenna height were adjusted to compensate for dielectric effects.

6.3 EBG Modifications

Modifications can be made to an EBG either to improve performance and reduce size, or to compensate for dielectric effects. Like any modification, tradeoffs are to be considered, but sometimes the improvement may be worth the tradeoff. For this section, the wide-gap EBG designed in the previous 2 sections are used to demonstrate the impact of additional changes to an EBG. The first modification to consider is the addition of vias to help mitigate the negative effects from the dielectric substrate included with the wide-gap EBG example in the previous 2 sections. As previously discussed, the strip dipole excites an asymmetric current distribution on the EBG surface. The current distribution in Fig. 62 showed a larger current on the surface edges that are parallel to the strip dipole (H-plane). This current causes the pattern distortions in the H-plane, and worsens when a dielectric substrate is introduced. The inclusion of a dielectric substrate increases the coupling between the patches, thereby increasing the current on the outer edges and worsening the pattern distortion.

When vias are introduced (radius of $0.005\lambda_d$ where λ_d is the wavelength in the dielectric) the current on the surface of the EBG now have direct paths to ground. The fields within the substrate that cause the coupling are reduced in magnitude or

broken up by the vias, and the direct current paths allow for a more uniform current distribution (Fig. 69). The nulls in the strip dipole radiation pattern are located at $\theta = 90°$, $\phi = 90°$ and $\theta = 90°$, $\phi = 270°$. The current on the patches at these nulls is not uniform at all, and in fact, these patches contribute little to the radiation of the structure. The vias distribute more current on the patches in the nulls, effectively improving the aperture efficiency, increasing the realized gain, see Fig. 70. While the pattern is more directive, there is still distortion in the H-plane, and because the current distribution on the ground plane is more uniform, the radiation in the back lobe is increased as well, reducing the front to back ratio by a few decibels.

The vias also have a noticeable effect on the impedance match for the strip dipole. Because the patch coupling has been broken up by the vias, the EBG structure now appears more inductive, producing a greater frequency shift to lower frequencies in the strip dipole's reflection coefficient (Fig. 71). The dipole shows a reasonably wide impedance bandwidth when the vias are included, spanning nearly 300 MHz. To include the entire 802.11g/n Wi-Fi band requires the dipole to be shortened somewhat to shift its resonance to the required band. The improvement in impedance bandwidth comes from the smoother progression from capacitive loading to inductive loading in the reactance (Fig. 72). While the reactance maintains a similar shape at the higher frequencies after the inclusion of the vias, the shape of the reactance in the capacitive region shows a significant decrease, again attributed to the reduction in coupling between the patches.

The vias reduce the frequency range of the plateau in the resistance, cutting it in half (Fig. 73). This can be thought of as the vias reinforcing the pseudo-PEC like behavior at lower frequencies, where the direct path to the EBG ground shorts the dipole. Even though the vias improve the EBG's performance when a dielectric substrate is included, they do not completely mitigate the dielectric effects. Without the substrate, the strip dipole had a 6.5 dBi increase in realized gain, which is not completely regained when the vias are included (Fig. 74). However, the vias help to retain much of the wide realized gain bandwidth.

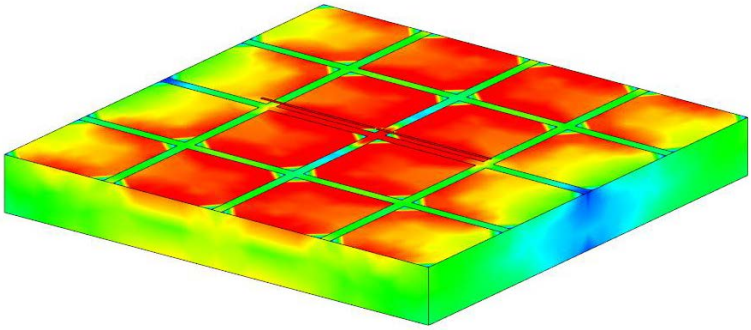

a)

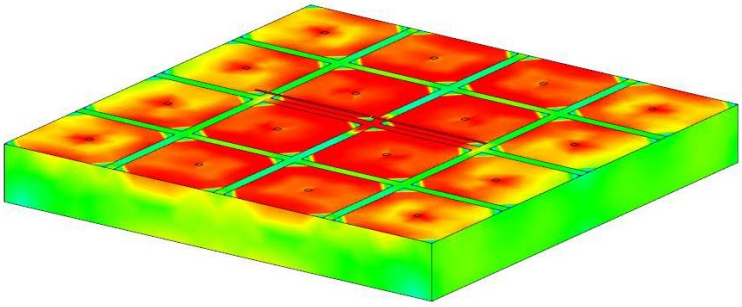

b)

Fig. 69 The electric current distributions for the strip dipole in the presence of the wide-gap EBG with a dielectric substrate at the design frequency of 2.437 GHz. a) Without vias and b) with vias.

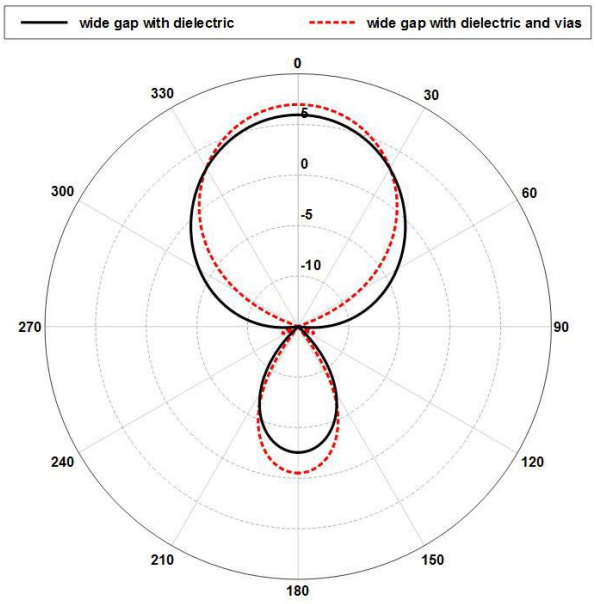

a)

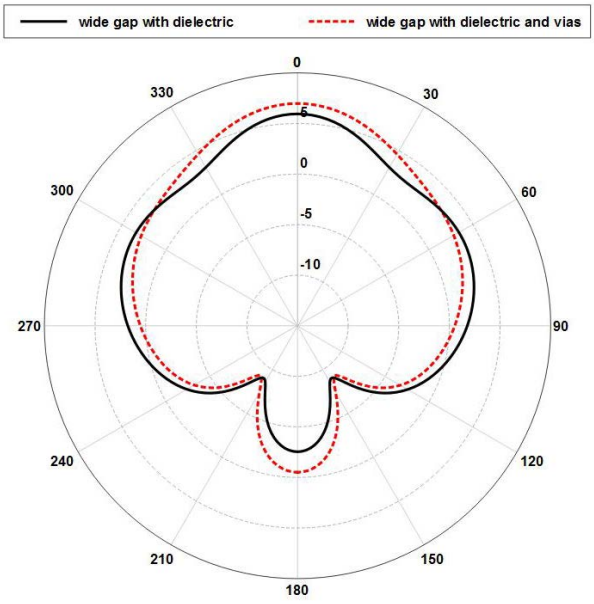

b)

Fig. 70 The realized gain patterns for the resonant (2.437 GHz) strip dipole in the presence of the wide-gap EBG including a dielectric substrate with vias and without vias. a) E-plane and b) and H-plane.

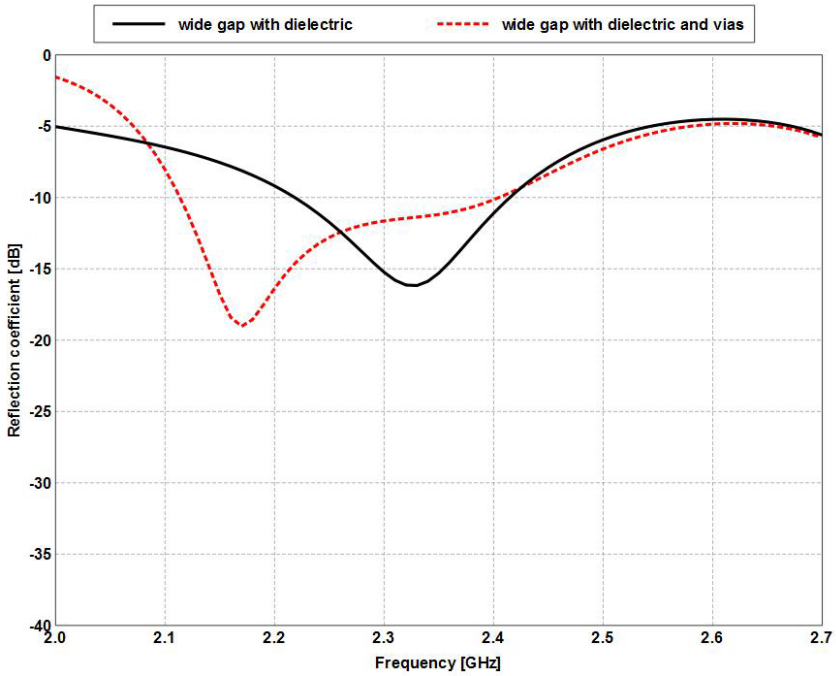

Fig. 71 The reflection coefficient for the resonant (2.437 GHz) strip dipole in the presence of the wide-gap EBG including a dielectric substrate with vias and without vias

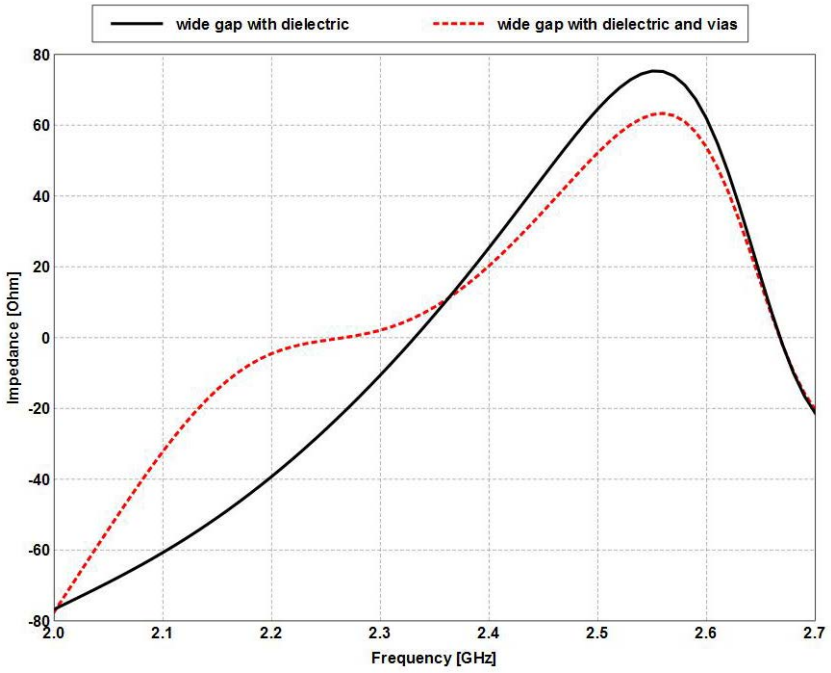

Fig. 72 The input reactance for the resonant (2.437 GHz) strip dipole in the presence of the wide-gap EBG including a dielectric substrate with vias and without vias

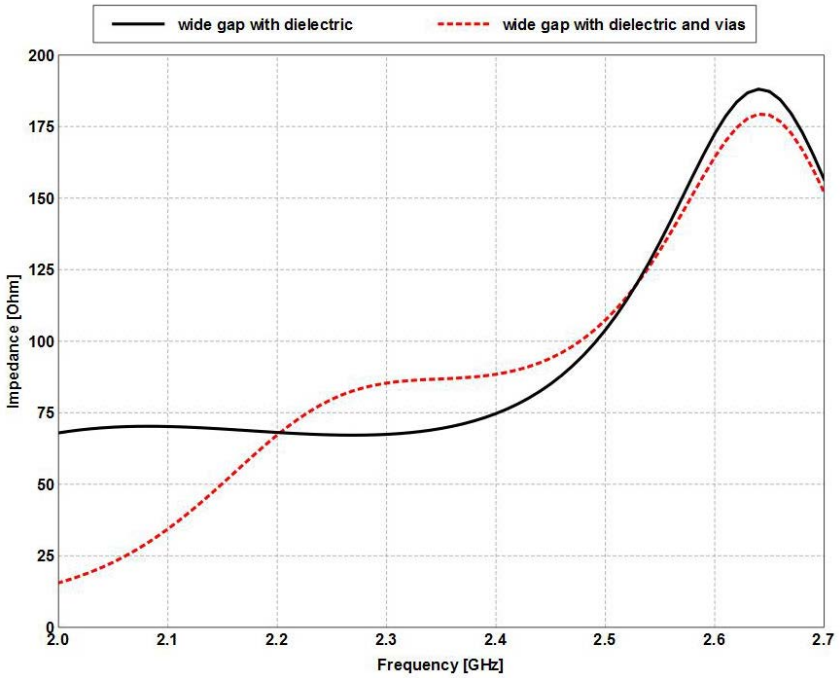

Fig. 73 The input resistance for the resonant (2.437 GHz) strip dipole in the presence of the wide-gap EBG including a dielectric substrate with vias and without vias

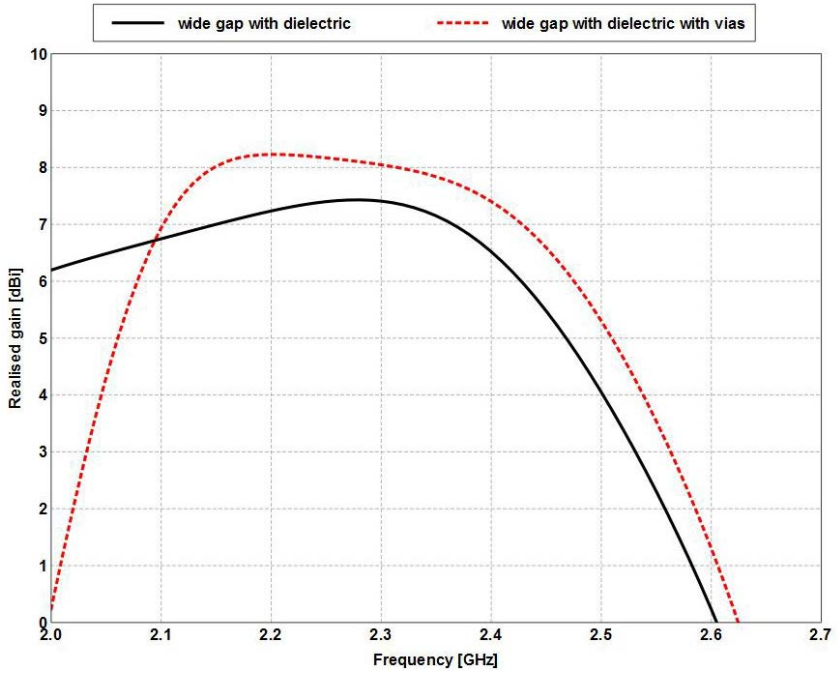

Fig. 74 The realized gain vs. frequency ($\theta = 90°$, $\phi = 0°$) for the resonant (2.437 GHz) strip dipole in the presence of the wide-gap EBG including a dielectric substrate with vias and without vias

Applying vias to the modified wide-gap EBG, where the EBG dimensions were scaled by 70% of the effective permittivity and the separation between the strip dipole and EBG surface was adjusted to compensate for the change in electrical length in the dielectric substrate, produced the expected current distribution, see Fig. 75. The current is more uniformly distributed on the surface of the EBG, effectively improving the aperture efficiency. Because of the reduced geometric size of the EBG, the current on the edges caused by the vias now produce side lobes about 15 dBi down from the main lobe in the E-plane, whereas before the vias, the side lobes were less than 25 dBi down. Geometrical modifications to the EBG helped to mitigate the pattern distortion in the H-plane, and including the vias improve the radiation pattern further even though they decrease the front to back ratio (Fig. 76).

The geometric modifications allowed the strip dipole-EBG structure to resonate at the design frequency without adjusting the length of the dipole, but the inclusion of the vias reduced the EBG capacitance, producing a more inductive load, thus requiring the dipole's length to be reduced in order to be resonate at the design frequency (Fig. 77). Scaling the strip dipole's length would also produce a much larger impedance bandwidth, as the plateau in the resistance is accompanied by a plateau in the reactance (Figs. 78 and 79). Reducing the dipole's length would shift the reactance such that both plateaus nearly line up, possibly producing a wide impedance bandwidth, but it may be necessary to adjust the separation between the strip dipole and EBG surface in order to better optimize the magnitude of the plateau in the resistance for a 50 Ω match. As expected, the vias improved the peak realized gain and realized gain bandwidth, by mitigating the dielectric effects (Fig, 80).

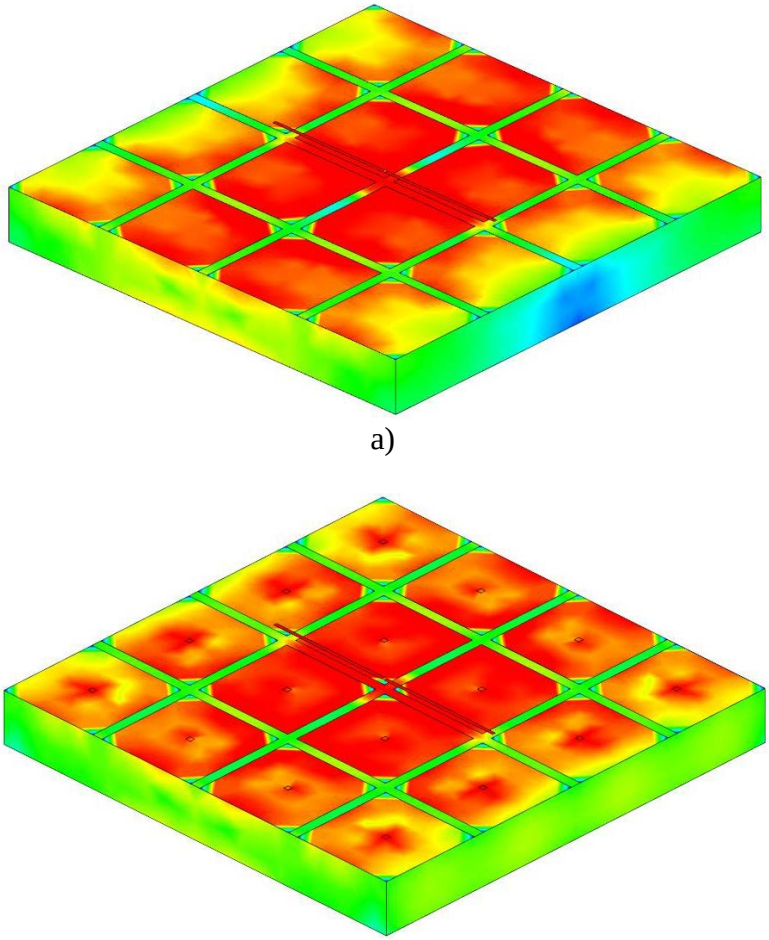

a)

b)

Fig. 75 The electric current distributions for the strip dipole in the presence of the wide-gap EBG with a dielectric substrate at the design frequency of 2.437 GHz. After the adjustments were made to scale the EBG and to scale the dipole height, vias were included to mitigate dielectric side effects. a) Without vias and b) with vias.

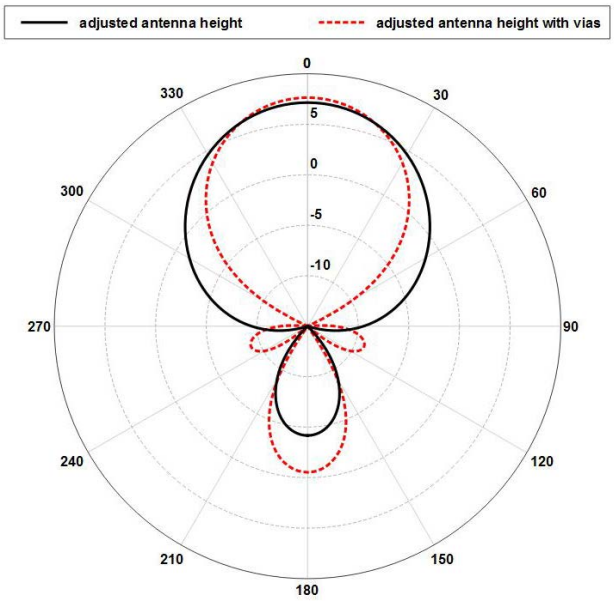

a)

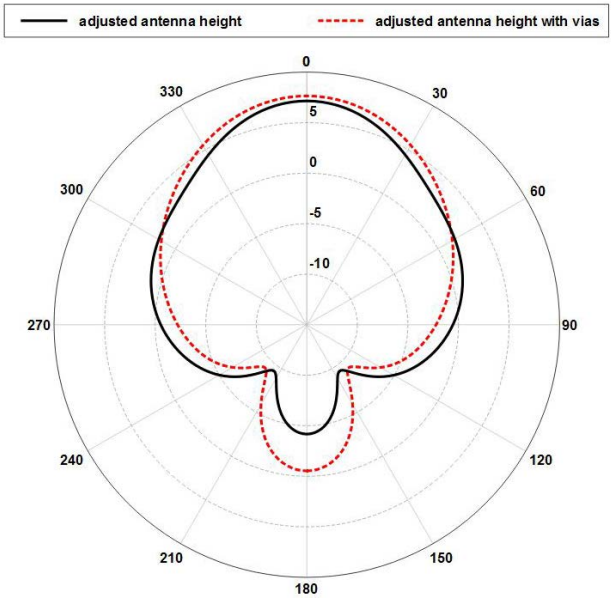

b)

Fig. 76 The realized gain patterns for the strip dipole in the presence of the wide-gap EBG with a dielectric substrate at the design frequency of 2.437 GHz. After the adjustments were made to scale the EBG and to scale the dipole height, vias were included to mitigate dielectric side effects. a) E-plane and b) H-plane.

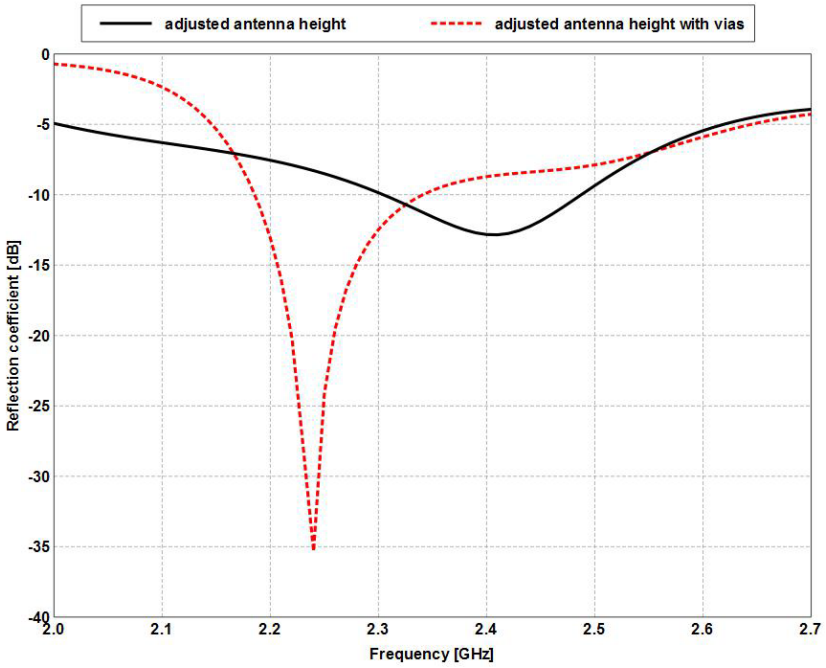

Fig. 77 The reflection coefficient for the strip dipole in the presence of the wide-gap EBG with a dielectric substrate at the design frequency of 2.437 GHz. After the adjustments were made to scale the EBG and to scale the dipole height, vias were included to mitigate dielectric side effects.

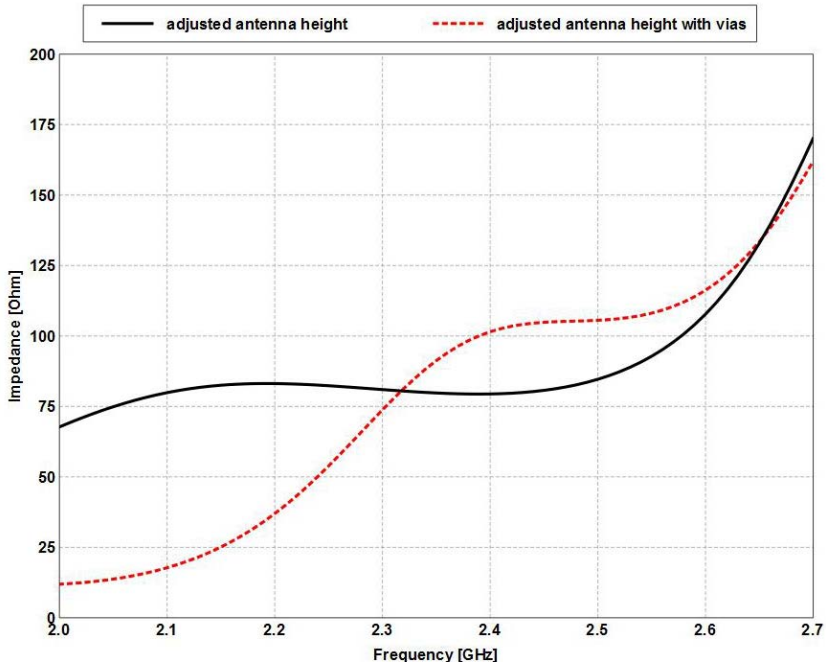

Fig. 78 The input resistance for the strip dipole in the presence of the wide-gap EBG with a dielectric substrate at the design frequency of 2.437 GHz. After the adjustments were made to scale the EBG and to scale the dipole height, vias were included to mitigate dielectric side effects.

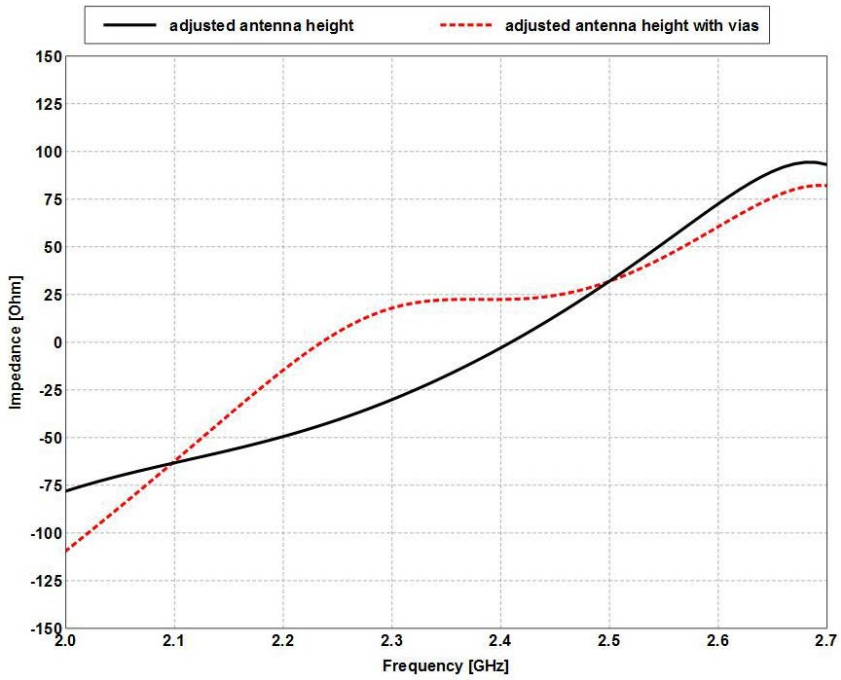

Fig. 79 The input reactance for the strip dipole in the presence of the wide-gap EBG with a dielectric substrate at the design frequency of 2.437 GHz. After the adjustments were made to scale the EBG and to scale the dipole height, vias were included to mitigate dielectric side effects.

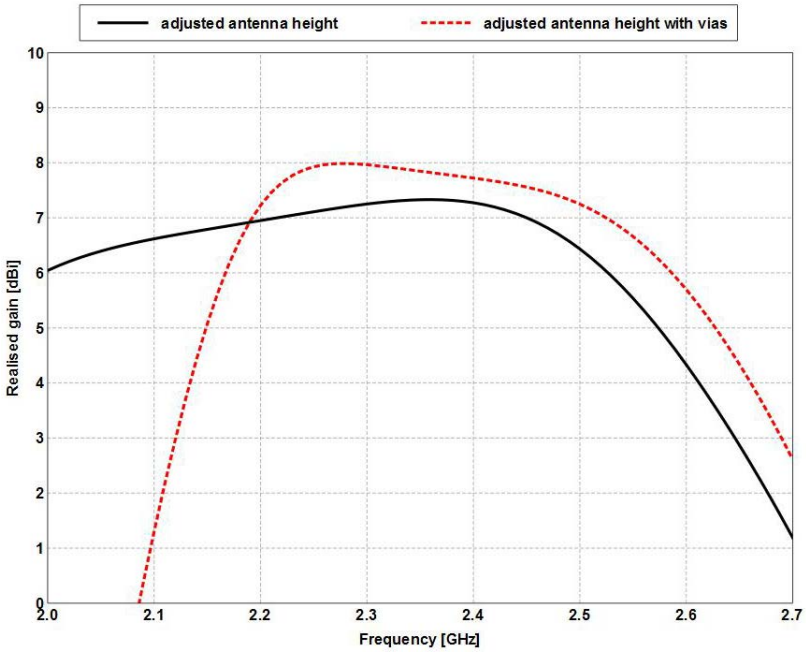

Fig. 80 The realized gain vs. frequency ($\theta = 90°$, $\phi = 0°$) for the strip dipole in the presence of the wide-gap EBG with a dielectric substrate at the design frequency of 2.437 GHz. After the adjustments were made to scale the EBG and to scale the dipole height, vias were included to mitigate dielectric side effects.

While the physical design parameters of an EBG tell an antenna engineer the dimensions of a single unit cell, there is little guidance on the importance of any particular arrangement or number of unit cells in the literature, which makes questionable whether or not EBG structures actually need any particular number of unit cells. Including an additional ring of unit cells has little impact on the strip dipole's reflection coefficient and impedance (Figs. 81 and 82). The EBG does not appear any more inductive or capacitive when additional unit cells are included, nor does the resistance change significantly. While there is a slight leftward shift in the reflection coefficient and the impedance bandwidth slightly increases, the biggest improvement comes in the realized gain and radiation patterns (Figs. 83 and 84). The peak realized gain improves by about 1 dB, and the back lobe is reduced by 2–3 dB as well. The modest improvement in gain is expected, as the aperture size has been increased. However, the physical area has increased by 43.8%, so adding additional unit cells may not be advantageous.

On the other hand, while adding additional unit cells may not be worth the increased EBG size, removing unit cells could be viable assuming that there are no drastic decreases in performance. Removing the outer ring of unit cells from the EBG would reduce the overall area by a factor of 4, making the EBG much smaller. The reflection coefficient (Fig. 85) demonstrates that the removal of the outer unit cells destroys the impedance match and makes the strip dipole-EBG structure effectively useless; however, the reduced performance is most likely due to the removal of the unit cells underneath the tips of the strip dipole.

Repeating the same simulation, but with the unit cells underneath the strip dipole tips replaced, results in a strip dipole-EBG structure that has half the physical area as the original while still maintaining a good impedance match (Fig. 86). The impedance bandwidth decreases by 20 MHz, but the bandwidth is still double that needed to cover the 802.11g/n band. There is also a slight leftward shift in the resonance, but it is negligible. Removing 2 rows of unit cells has little effect on the resistance and reactance of the structure below the design frequency, but above the design frequency, the effect becomes more important where both the input resistance and reactance increase more quickly for the reduced EBG structure (Fig. 87).

As expected, the realized gain is reduced by 1 to 1.5 dBi with the removal of the unit cells, and the slope of the realized gain versus frequency curve becomes a bit sharper near the peak thereby reducing the 1-dBi bandwidth by 13% (Fig. 88). The reduction in realized gain results in a more noticeable back lobe in the E-plane pattern, but the biggest impact is in the H-plane pattern where the sides of the pattern are now even more distorted than before. The difference between the bore sight realized gain and the sides of the H-plane pattern is now 7–8 dBi versus

13–14 dBi before the unit cells were removed (Fig. 89). However, these reductions in realized gain, –10-dB impedance bandwidth, and –1-dB gain bandwidth may be considered acceptable considering that the area of the EBG structure has been cut in half while still achieving a much more directive pattern compared to that of a lone strip dipole. The impedance and gain bandwidths can be further improved, of course, by reducing or increasing the strip dipole's length to shift the dipole back to the original design frequency

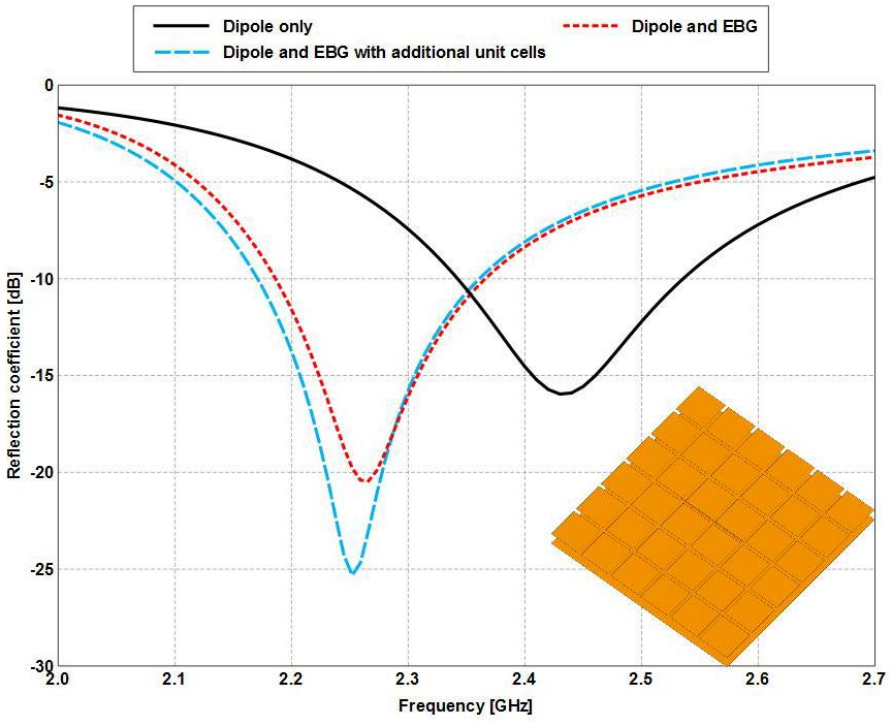

Fig. 81 The reflection coefficient for a resonant strip dipole in the presence of a wide-gap EBG with and without additional unit cells

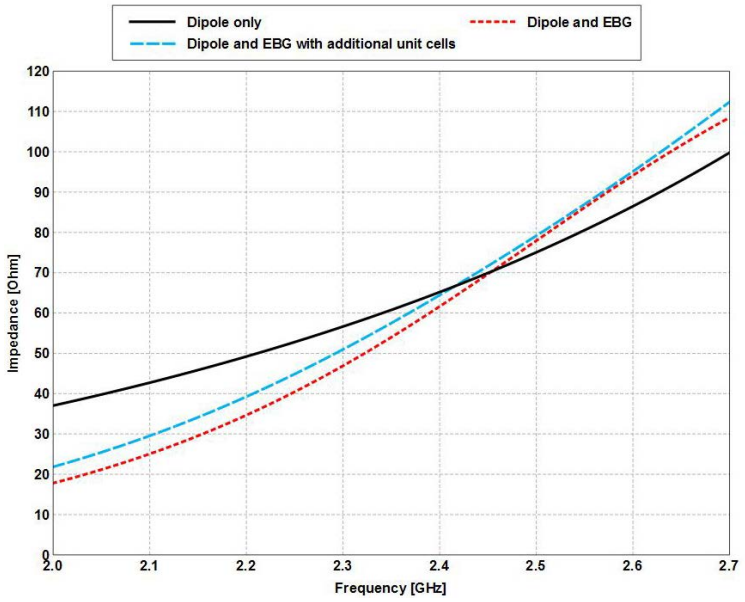

a)

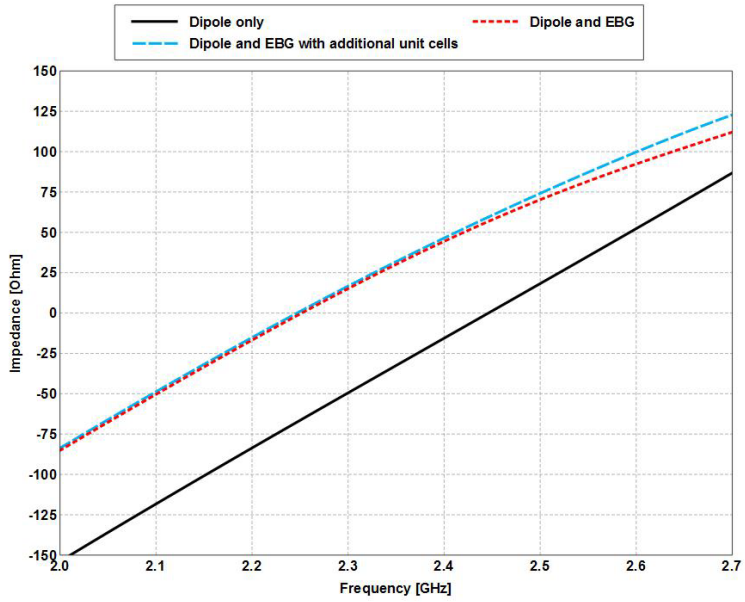

b)

Fig. 82 a) The input resistance and b) the input reactance for a resonant strip dipole in the presence of a wide-gap EBG with and without additional unit cells

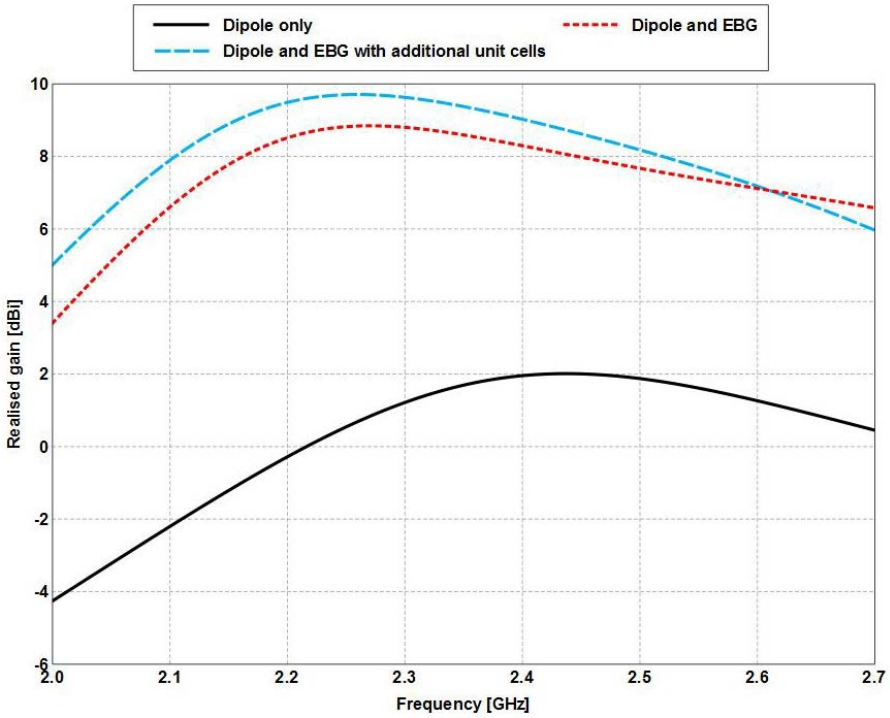

Fig. 83 The realized gain vs. frequency ($\theta = 90°$, $\phi = 0°$) for a resonant strip dipole in the presence of a wide-gap EBG with and without additional unit cells

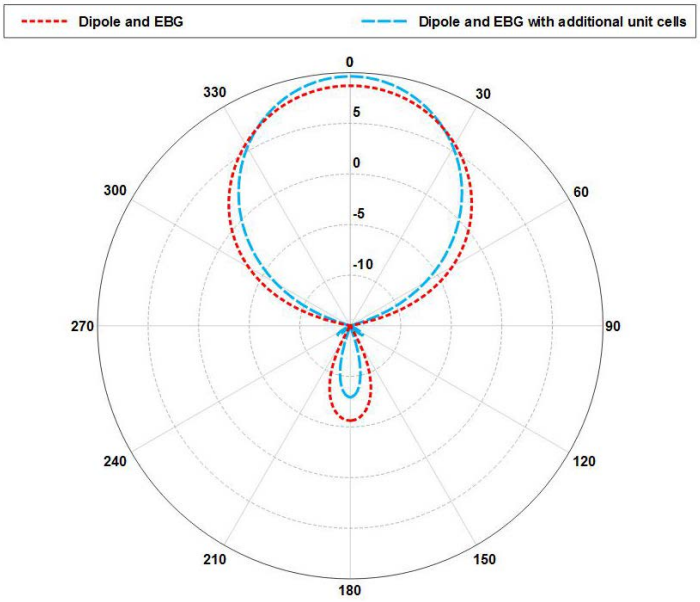

a)

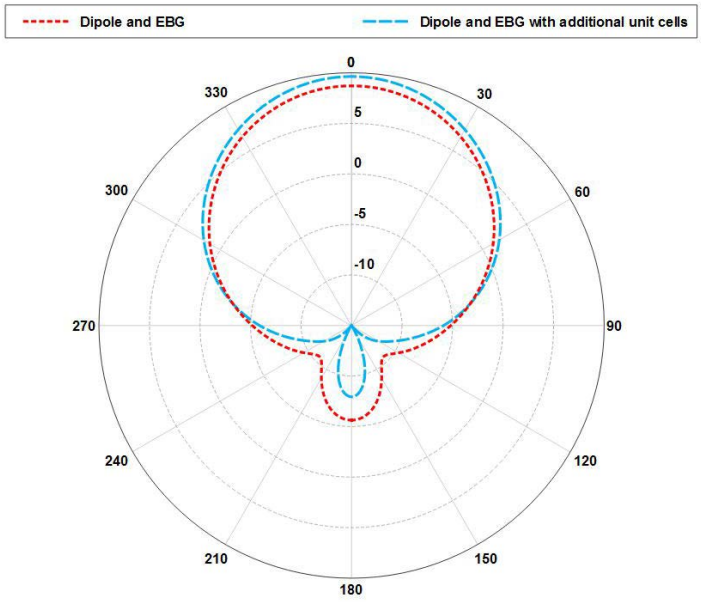

b)

Fig. 84 The realized gain patterns for a resonant strip dipole in the presence of a wide-gap EBG with and without additional unit cells. a) E-plane and b) H-plane.

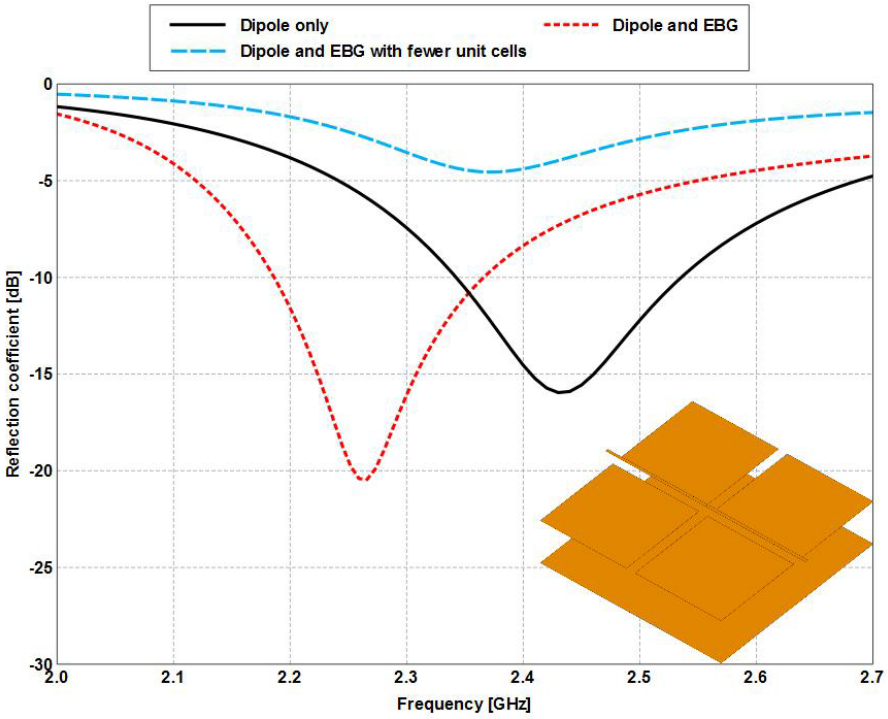

Fig. 85 The reflection coefficient for a resonant strip dipole in the presence of a wide-gap EBG with and without a ring of unit cells removed

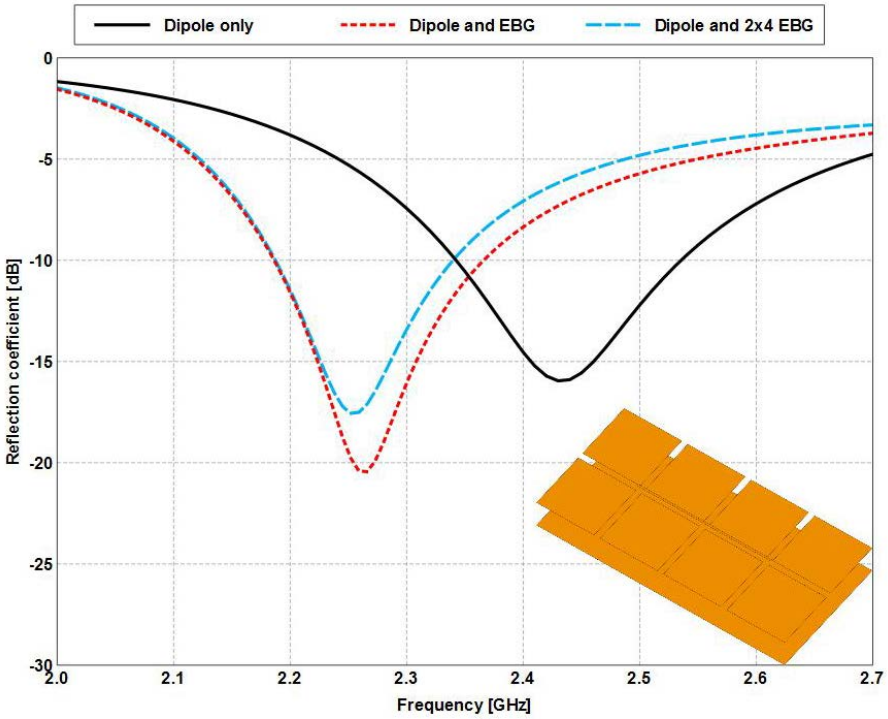

Fig. 86 The reflection coefficient for a resonant strip dipole in the presence of a wide-gap EBG with and without 2 rows of unit cells

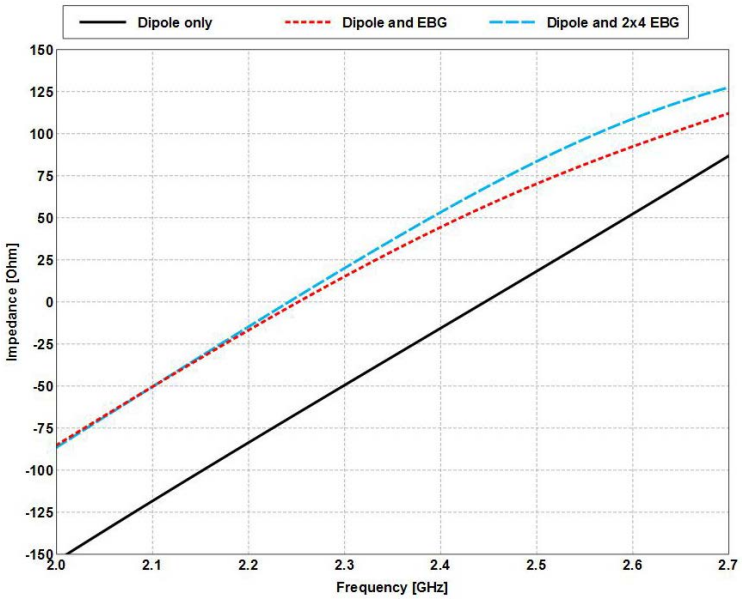

a)

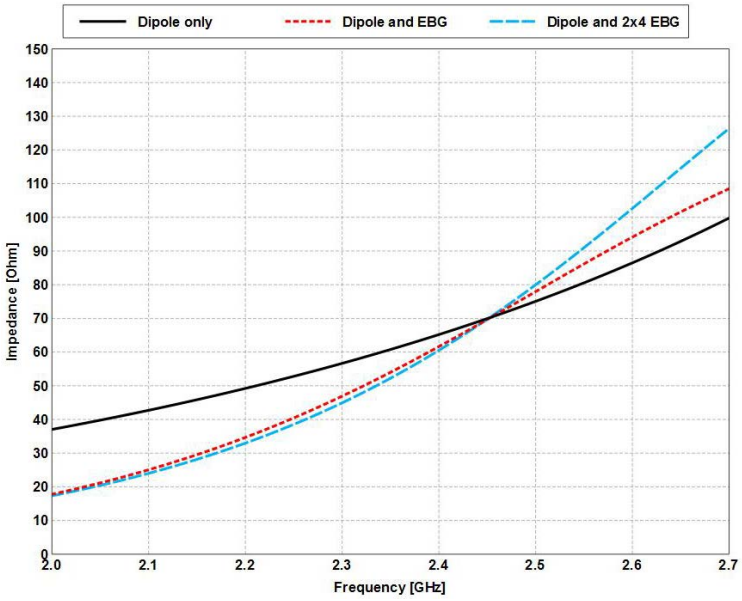

b)

Fig. 87 a) The input resistance and b) the input reactance for a resonant strip dipole in the presence of a wide-gap EBG with and without 2 rows of unit cells

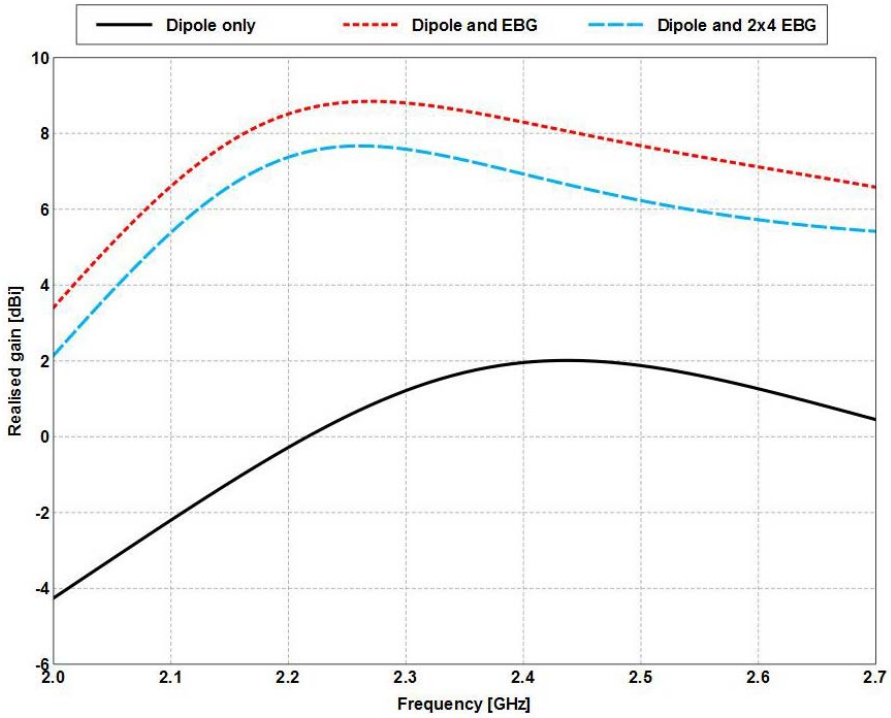

Fig. 88 The realized gain vs. frequency ($\theta = 90°$, $\phi = 0°$) for a resonant strip dipole in the presence of a wide-gap EBG with and without 2 rows of unit cells

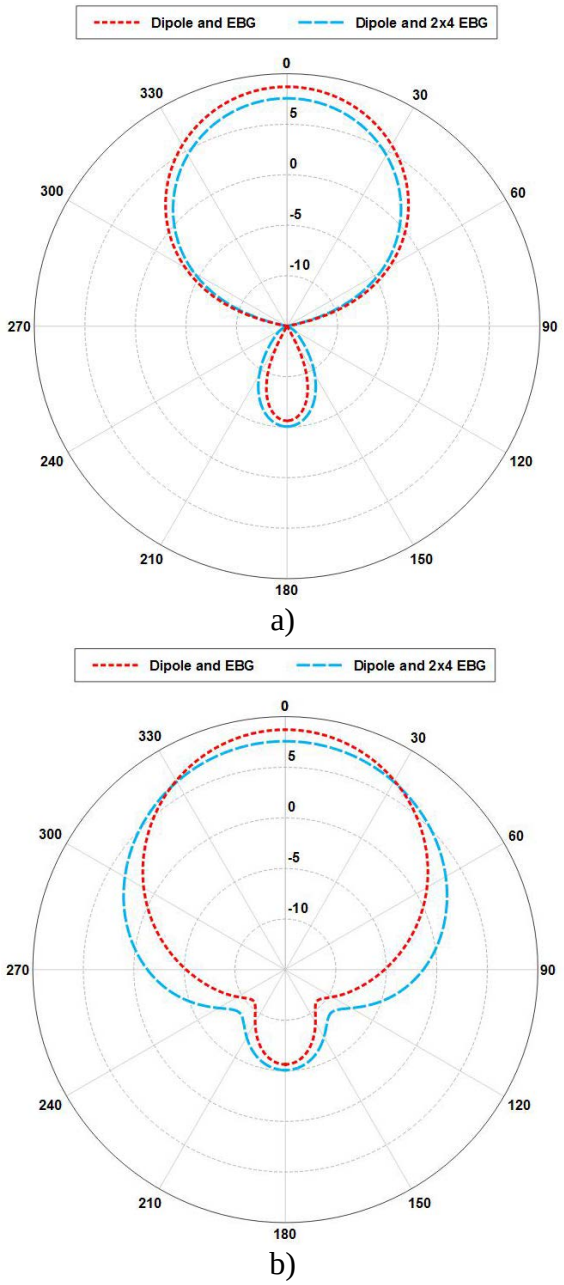

Fig. 89 Realized gain patterns for a resonant strip dipole in the presence of a wide-gap EBG with and without 2 rows of unit cells. a) E-plane and b) H-plane.

7. Conclusions

This technical report has presented a detailed summary of typical analytical and numerical models for EBG design. For applications in FSS and as a HIS, the use of the reflection coefficient phase is applicable, but for antenna applications it is not. An EBG will be placed a distance away from a particular antenna by fractions of a wavelength not several wavelengths. Such close proximity places the EBG in the

NF of the prospective antenna where the scattered fields have not traveled far enough to form the far field pattern. Characterizing an EBG by its impedance mismatch to free space neglects radiation from the structure itself, which is not the case for antenna applications where it is the interaction between the EBG and the antenna that improves the radiation pattern and realized gain. In addition, the close proximity to the prospective antenna loads the antenna, possibly improving its impedance bandwidth.

Typical analytical models such as the CM and TLM offer a rough start for EBG design, since they still only describe the EBG in terms of the reflection coefficient phase. The CM allows an antenna engineer to better understand the loading behavior of an EBG; however, the TLM was more consistent in agreement with numerical methods. IT, conversely, offers an analytical tool that includes the antenna, but is limited by frequency invariant phase and simple antenna structures. The typical numerical simulation method is to assume an infinitely repeating unit cell (which was designed using one of the analytical tools or some already published physical parameters) and calculate the reflection coefficient phase. The assumption of an infinite structure adds an additional nonrealistic property to the EBG analysis, further degrading any insight the results may offer for antenna applications. This report introduced looking at the phase of the scattered NFs as a substitute to the reflection coefficient phase.

For more complicated antennas, the scattered NFs can become difficult to interpret, so whether or not the phase is useful in these circumstances will require further investigation. For a simple strip dipole, however, the scattered-phase offered a simulated study of an antenna dependent finite EBG that showed different results when compared to the non-antenna dependent infinite EBG. The simulated scattered-phase was more informative regarding over what frequency range a strip dipole would be impedance matched when in the presence of an EBG to improve performance.

The loading behavior of the EBG was predominately inductive, which was expected from the CM where the intrinsic inductance was always much larger than the intrinsic capacitance. The amount that the strip dipoles resonance shifted was not linear, however, because there was a clear frequency range over which the inductive loading was greatest. The frequency range was associated with negative phase angles for the scattered-phase, and it was within this frequency range that the simulated strip dipole had the best performance. Within the negative phase regime, the strip dipole impedance bandwidth improved from a typical 8% bandwidth to near 12% (assuming a thin-gapped EBG). The peak realized gain improved by as much as 6.5 dBi and was still improved even when the strip dipole was not matched at all.

At lower frequencies, where the phase regime is positive, the strip dipole resistance is reduced resulting in a poor impedance bandwidth and realized gain. At higher frequencies, where the phase angles are greater than –90°, the H-plane cut of the strip dipole and EBG shows distortion, lowering the realized gain. The pattern becomes more distorted as the frequency increases eventually becoming a quadrupole pattern. This pattern distortion, even though a dielectric was not included, was due to the collection of current at the EBG edges parallel to the strip dipole.

The EBG edges that lie within the E-plane (orthogonal to the strip dipole) are in the nulls of the strip dipole, thereby resulting in the current on these edges to be small in comparison to the edges in the H-plane. The asymmetric current distribution results in an asymmetric radiation pattern. This behavior highlights edge effects that are not captured in any infinite structure analysis. Reducing the gap width on the EBG surface serves to improve the impedance bandwidth but increases the pattern distortion. Scaling the strip dipole's length to a lower resonant frequency can compensate for the pattern distortion, thereby improving the realized gain bandwidth.

The pattern distortion only worsens when a dielectric substrate is included. The relative permittivity increases the capacitance of the EBG structure reducing the inductive loading and increasing the amount of current on the EBG edges parallel to the strip dipole. Geometric modifications can be made to the EBG to scale its size, and adjustments must be made for the separation between the strip dipole and the EBG surface in order to compensate for the dielectric effects, but it is recommended to use thin dielectrics where possible.

Vias are an alternative to mitigate dielectric effects. Their presence reduces the coupling between the patches, producing less capacitance and a more inductive load, but the biggest impact is the more uniform current distribution brought about by direct paths for current to flow. Without vias, the strip dipole produces greater current on the EBG edges that are parallel to itself than on the EBG edges that are orthogonal. The direct current paths introduced by the vias, allow current to distribute more uniformly on the patches, thereby increasing the aperture efficiency and reducing the pattern distortion. However, vias are not necessary unless thick substrates or high-dielectric constants are used.

The frequency dependent behavior of the EBG phase suggests that at frequencies in the positive phase regime the EBG appears pseudo-PEC and in the negative phase regime appears pseud-AMC. For all of the EBG designs studied, the 90° ± 45° EBG bandwidth recommended in Yang and Rahmat-Samii (2003) was not appropriate. The 0° ± 45° EBG bandwidth, however, was much more accurate when

extracted from the scattered-phase when including the terminated strip dipole. The simulation results from this report may or may not be applicable to more complicated antenna structures, further investigation is necessary.

To design a basic EBG, this report found that the patch widths should be about $\frac{\lambda}{5}$. Some authors use smaller patches near $\frac{\lambda}{10}$, but in terms of the wavelength in the dielectric, the patch width is closer to $\frac{\lambda_d}{5}$. The gap width should be at least an order of magnitude smaller than the patch width and even smaller for further improvements in antenna impedance bandwidth. The thickness should be $\frac{\lambda_d}{10}$, where λ_d is the wavelength in the dielectric, with thinner substrates reducing the impedance bandwidth (Yang and Rahmat-Samii 2003).

These physical parameters are specific to a square patch EBG and are dependent on the wavelength in the dielectric, not the free space wavelength. It is typical to find design parameters for EBGs in the literature that base the physical features on the free space wavelength rather than the dielectric wavelength. This can be misleading, because it is expected that the design wavelength would correspond to the frequency where zero-phase occurs in the reflection-phase, but more often than not, the actual zero-phase occurs at a higher frequency. The number of unit cells to use depends on the application of the EBG. More unit cells result in a larger aperture, increasing the gain, but this will eventually saturate. Removing certain unit cells can greatly reduce the physical area of the EBG, but will also reduce the realized gain. Any modifications made to the EBG will be entirely dependent upon the application and desire of the antenna engineer.

The follow-up investigation to this report is to apply the EBG design parameters and analysis to an antipodal dipole through simulation and measurement. The antipodal structure was previously validated through measurements and showed good performance (McCormick 2014). The advantage of the antipodal structure is that it allows for the use of a microstrip feed that will prevent needing to feed the dipole through the EBG structure. The challenge will be the impact that the EBG surface will have on the microstrip feed, which will be loaded by the EBG inductance. Additional modifications may be necessary in order to optimize performance, but the goal is to achieve a low-profile antipodal dipole EBG structure that can be easily fed.

8. References

Abedin MF, Ali M. Effects of EBG reflection phase profiles on the input impedance and bandwidth of ultrathin directional dipoles. IEEE Trans. Ant. and Prop. November 2005;53(11).

Azad MZ, Ali M. Novel wideband directional dipole antenna on a mushroom like EBG structure. IEEE Trans. Ant. and Prop. May 2008; 56(5).

Best SR, Hanna DL. Design of a broadband dipole in close proximity to an EBG ground plane. IEEE Ant. and Prop. Magazine. Dec, 2008; 50:52–63.

Hansen RC. Effects of a high-impedance screen on a dipole antenna. IEEE Ant. and Wireless Prop. Letters. 2002;1.

Hayt Jr. WH Buck JA. Engineering electromagnetics. Eighth ed. New York: McGraw-Hill, pp. 146 and 152, 2006.

Kamadin K, Rahim MKA, Hall PS, Samsuri NA, Elias NA. Printed dipole with slot EBG structures with artificial magnetic conductor and band-notched behaviors. IEEE Int. RFM Conf. Seremban, Malaysia, Dec. 2011.

Kern DJ, Werner DH, Monorchio A, Lanuzza L, Wilhelm MJ. The design synthesis of multiband artificial magnetic conductors using high impedance frequency selective surfaces. IEEE Trans. Ant. and Prop. January 2005;53(1).

Luukkonen O, Simovski C, Granet G, Goussetis G, Lioubtchenko D, Räisänen AV, Tretyakov SA. Simple and accurate analytical model of planar grids and high-impedance surfaces comprising metal strips or patches. IEEE Trans. On Ant. and Prop., vol. 56, no. 6, June 2008.

McCormick Seth A. Planar dipole input resistance vs. trace thickness for different materials. Adelphi (MD): Army Research Laboratory (US); 2014 September. Report No.: ARL-TN-0634.

McMichael IT, Zaghloul AI, Mirotznik MS. A method for determining optimal EBG reflection phase for low profile dipole antennas. IEEE Trans. Ant. and Prop. May 2013;61(6).

Palreddy S, Zaghloul AI. Circuit analysis of electromagnetic band-gap (EBG) structures. URSI Electromagnetic Theory Symposium (EMTS), Hiroshima, Japan, May 2013.

Sievenpiper D, Zhang L, Broas RFJ, Alexopolous NG, Yablonovitch E. High-impedance electromagnetic surfaces with a forbidden frequency band. IEEE Trans. On Microwave Theory and Tech. Nov. 1999;47(11).

Volakis JL. Antenna engineering handbook. Fourth Ed. NewYork: McGraw-Hill, pp. 34.1–34.2, 2007.

Yang F, Rahmat-Samii Y. Reflection phase characterizations of the EBG ground plane for low profile wire antenna applications. IEEE Trans. Ant. and Prop. Oct. 2003;51(10).

List of Symbols, Abbreviations, and Acronyms

AMC	artificial magnetic conductor
CM	circuit model
CST	Computer Simulation Technology
EBG	electromagnetic band gap
E-field	electric field
FSS	frequency selective surface(s)
HFSS	high-frequency structural simulator
HIS	high-impedance surfaces
IT	Image Theory
MoM	method of moments
NEF	near electric field
NF	near field
PBC	periodic boundary condition(s)
PEC	perfect electric conductor(s)
PMC	perfect magnetic conductor
TDFD	time-domain finite-difference
TE	transverse electric
TLM	transmission line model
TM	transverse magnetic

1 (PDF) DEFENSE TECHNICAL INFORMATION CTR DTIC OCA

2 (PDF) DIRECTOR US ARMY RSRCH LAB RDRL CIO LL IMAL HRA MAIL & RECORDS MGMT

1 (PDF) GOVT PRINTG OFC A MALHOTRA

5 (PDF) US ARMY RSRCH LAB ATTN RDRL SER M S A MCCORMICK W O COBURN A ZAGHLOUL S WEISS E ADLER